



# ScuDo

Scuola di Dottorato ~ Doctoral School

WHAT YOU ARE, TAKES YOU FAR

Doctoral Dissertation

Doctoral Program in Mechanical Engineering (33<sup>th</sup> cycle)

# Analysis and Optimization of Variable Angle Tow Composites Through Unified Formulation

By

**Nasim Fallahi**

\*\*\*\*\*

**Supervisor(s):**

Prof. Erasmo Carrera

Prof. Alfonso Pagani

**Doctoral Examination Committee:**

Prof. Maria Cinefra

Prof. Calogero Orlando

Politecnico di Torino

2021

## **Declaration**

I hereby declare that, the contents and organization of this dissertation constitute my own original work and does not compromise in any way the rights of third parties, including those relating to the security of personal data.

Nasim Fallahi

2021

\* This dissertation is presented in partial fulfillment of the requirements for **Ph.D. degree** in the Graduate School of Politecnico di Torino (ScuDo).

Dedicate all the spiritual achievements of this thesis, which is very valuable to me, to those who loved me in all my pain, shed tears with me, and smiled deeply when I got up. Those who stood by me, inspiring and supporting me in Turin-Italy, so that I could survive in the hardest days of my life and move on.

---

Dedicated to:

My Dear Mother Mina Siahmansouri,

Professor Christina Bignardi,

Mrs. Angelillo Maria Grazia,

Mrs. Nilufar Tabatabaei,

Professor Alfonso Pagani,

My colleagues and friends Abbas, Iman, Stefano, Farhad, Maryam, Daniele

And dear Flavio

---

I would also like to thank myself for being with me in the hardships, standing alone and away from home, family and my land, working and motivating myself in all the hard moments to study, to learn and trying to do my best. I tried to grow in all the challenges, although the reward for this growth was the great pain I endured. I wish to transcend humanity beyond any achievement through the whole of my life.

---

## **Acknowledgements**

First and foremost, I would like to express my sincere appreciation to my advisor Prof. Erasmo Carrera for the immeasurable support of my PhD study and related research, for his patience, and tremendous knowledge. I could not have thought having a better advisor and mentor for my PhD study who influence not only my research program but also strengthening my character. I would like to thank also Professor Alfonso Pagani, for his kind support and assistance through my PhD program.

Besides my supervisors, I would like to thank the rest of my thesis committee: Prof. Maria Cinefra and Prof. Calogero Orlando, for their insightful comments and support, also for the precious questions which incited me to grow my research from different perspectives.

Beside of my PhD thesis, working in the international MUL2 research group allowed me to know my colleagues from different countries and culture which was so precious to me, I would like to thanks Manish, Andrea, Daniele, Riccardo, Ehsan, Didam, Daniel and all my colleagues through these three years. I received many affection, support and it let me enjoy drinking coffee, gathering for dinner, and for all those good moments which gave quality to my character I would like thanks all of them.

## Abstract

*The recent development of new manufacturing techniques of composite structures, for example additive manufacturing (AM) techniques, allows the designer to go beyond the classical design rules, thus finding innovative and more efficient solutions like the variable angle-tow (VAT) composites. Variable Angle Tow and have shown to improve structural performance by providing a better stiffness distribution. However, additional manufacturing constraints are involved compared to straight fibre laminates: mainly the maximum fibre steering curvature that can be achieved. Moreover, if a curvilinear fibre angle orientation in laminate is changed the form, depending buckling and vibration behaviour will be different. However, previous research has hinted numerically on free-vibration of VAT but further buckling improvements of variable stiffness laminates is incorporating additions, resulting in a variable thickness profile. In this thesis, the effect of the fibre orientation on the mechanical response of variable angle tow (VAT) panels is studied. A computationally efficient high-order one-dimensional model, obtained under the Carrera unified formulation (CUF) procedure, is applied. In particular, a layerwise approach is selected to predict the complex aspects that can arise in VAT panels. Buckling and free vibration analyses are presented, regarding various material properties, geometries, and boundary conditions, and the results are assessed with those taken by existing procedures. Considering the findings of the comparative analysis, numerous best design practices are suggested to increase the mechanical performances of VAT panels. In the next step, the Genetic Algorithm (GA) optimization method is performed to optimize critical buckling loads and natural frequencies of Variable Angle Tow (VAT) laminated composite plates. Optimization procedures of VAT plates are combined with the layerwise theory through one-dimensional (1D) Carrera Unified Formulation (CUF) models, to enhance the analysis effectiveness and the performance of the models. The stochastic GA system produces irregularities in the fibre angle orientation and effects on the performance of the structural system. Later, respecting the sample points*

*through the GA, the response surface is obtained to consider the convergence of results for the optimum design of the fibre orientation angle. The dynamic properties of simply supported square plates are investigated during undergoing buckling loads. Next, the results are compared with those observed using existing approaches. Finally, also different open-wall beam are reported through the free vibration problems by analysing the different boundary conditions and geometries.*

## Symbols

- $C_0^z$ : zig-zag and interlaminar continuity  
 $u_x, u_y, u_z$ : Displacement components  
 $x, y, z$ : Orthogonal Cartesian reference system  
 $\mathbf{B}, b$ : Differential Operator of the strain displacement relations  
 $B_2, B_3, B_4$ : Beam elements with two, three, four nodes  
 $E$ : Young's modulus  
 $F_\tau, F_s$ : Expansion functions  $G$ : Shear modulus  
 $i, j$ : Shape function indexes  
 $k$ : Layer index  
 $\mathbf{K}$ : Stiffness matrix  
 $k^{\tau sij}$ : Fundamental nucleus of stiffness matrix  
 $L_3, L_4, L_6, L_9, L_{16}$ : Lagrange cross-section elements with three, four, six, nine and sixteen nodes  
 $\zeta, \eta$ : Natural coordinate system  
 $\sigma$ : Stress vector  
 $\sigma_{xx}, \sigma_{yy}, \sigma_{zz}, \sigma_{xy}, \sigma_{xz}, \sigma_{yz}$ : Stress components  
 $\varepsilon$ : Strain vector  
 $\varepsilon_{xx}, \varepsilon_{yy}, \varepsilon_{zz}, \varepsilon_{xy}, \varepsilon_{xz}, \varepsilon_{yz}$ : Strain components  
 $\mathbf{C}$ : Matrix of elastic coefficients of material  
 $N_I, N_j$ : Shape functions  
 $N$ : Expansion order of  $F_\tau, F_s$   
 $\delta$ : Virtual variation  
 $V$ : Volume  
 $u_\tau$ : Generalized displacement vector  
 $q$ : nodal unknown  
 $C_{22}, C_{66}, C_{44}, C_{23}$ : Stiffness coefficients  
 $L_{int}$ : Work of internal forces  
 $K_\sigma^0$ : Geometrical stiffness matrix  
 $L_{ine}$ : Work of inertial forces  
 $n$ : Total number of possible outcomes in probability distribution process  
 $\rho$ : Density of material  
 $\ddot{u}$ : Acceleration vector  
 $X$ : Random variables  
 $\bar{x}$ : Mean value

$s^2$ : Sample variance

$s$ : Standard deviation

$P$ : Load

$L$ : Length of beam

$h$ : Beam height

$I$ : Inertia moment

$b_0, b_1, b_{ij}$ : Regression coefficient

**-Acronyms:**

$a, b$ : upper and lower interval of PDF

BC: Boundary Condition

CDF: Cumulative Distribution Function

CLT: Classical Laminate Theory

CUF: Carrera Unified Formulation (CUF)

CS: Constant stiffness

DOE: Design of Experiment

DOF: Degree of Freedom

1D/2D/3D: One/Two/Three- Dimensional

EBBT: Euler Bernoulli Beam Theory

ESL: Equivalent Single Layer

FEM: Finite Element Model

FN: Fundamental nucleus

FRP: Fiber-reinforced Polymer

HLE: Hierarchical Lagrange Expansion

HSDT: Higher-Order Shear Deformation Theories

IC: Interlaminar Continuity

LE: Lagrange Expansion

LHS: Latin Hypercube Sampling

LW: Layerwise theory

MC: Monte Carlo

PDF: Probability Density Function

PVD: Principle of Virtual Displacement

RA: Regression Analysis

RS: Response Surface

TBT: Timoshenko Beam Theory

TE: Taylor Expansion



VAT: Variable Angle Tow

ZZ: Zig-Zag theory

# Contents

<b>List of Figures</b>	<b>xiii</b>
<b>List of Tables</b>	<b>xix</b>
<b>1 Introduction</b>	<b>1</b>
1.1 Overview . . . . .	1
1.2 Problem Statement . . . . .	2
1.3 Objective of the Research Project . . . . .	3
1.4 Outline . . . . .	3
<b>2 Multi-Layered Beam Structures: Classical Models and Unified Formulation</b>	<b>5</b>
2.1 Introduction . . . . .	5
2.2 Theories of multi-layered structures: Displacement-Based Formulation	6
2.2.1 Theory of Equivalent Single Layer . . . . .	7
2.2.2 Layerwise Theory . . . . .	7
2.2.3 Zig-Zag Theory . . . . .	8
2.3 One Dimensional Carrera Unified Formulation (CUF) . . . . .	9
2.3.1 Taylor Series Expansion . . . . .	11
2.3.2 Lagrange Expansion . . . . .	12
2.4 Finite Element Formulation of 1D CUF framework . . . . .	15

---

2.4.1	Preliminaries . . . . .	15
2.5	Weak Formulation and Governing Equation . . . . .	17
2.6	Numerical implementation of the VAT concept . . . . .	20
2.6.1	Linearized buckling equations . . . . .	21
2.6.2	Free Vibration Equations . . . . .	22
2.7	Conclusion . . . . .	23
<b>3</b>	<b>Stochastic Analysis</b>	<b>24</b>
3.1	Introduction . . . . .	24
3.2	Monte Carlo Method . . . . .	24
3.3	Random Sampling Method . . . . .	25
3.3.1	Probability Distribution . . . . .	27
3.3.2	Description of Probability Density Function (PDF) . . . . .	28
3.4	Cumulative Probability Distribution function (CPD) . . . . .	29
3.4.1	Normal Distribution of Random Sampling . . . . .	29
3.4.2	Latin Hypercube Sampling Method . . . . .	30
3.5	Surrogate Model . . . . .	32
3.5.1	Response Surface . . . . .	32
3.5.2	Artificial Neural Network (ANN) . . . . .	33
3.6	Conclusion . . . . .	39
<b>4</b>	<b>Numerical Results of VAT</b>	<b>40</b>
4.1	Introduction . . . . .	40
4.1.1	VAT laminate equation . . . . .	41
4.1.2	Buckling Analysis . . . . .	42
4.1.3	Pre-buckling and buckling analyses of a sixteen-layer VAT plate . . . . .	46
4.1.4	Free Vibration Analysis . . . . .	52

---

4.2	Conclusion . . . . .	56
<b>5</b>	<b>Optimization of VAT structures</b>	<b>57</b>
5.1	Introduction . . . . .	57
5.2	Optimization of Variable Angle Tow . . . . .	59
5.2.1	Direct search stochastic methods . . . . .	59
5.2.2	Buckling Analysis . . . . .	61
5.2.3	Free Vibration . . . . .	69
5.3	Conclusion . . . . .	72
<b>6</b>	<b>Isotropic Thin-Walled open-cross-section beams</b>	<b>74</b>
6.1	Introduction . . . . .	74
6.2	Linear vibration . . . . .	75
6.3	Free Vibration . . . . .	76
6.3.1	CUF and Chen's methods Evaluation . . . . .	77
6.3.2	Mono-symmetric C-shaped cross-section beam . . . . .	79
6.3.3	Tee-shaped mono-symmetric cross-section beam . . . . .	87
6.3.4	Arbitrary non-symmetric cross-section beams . . . . .	91
6.3.5	Doubly clamped T-shaped thin walled beam . . . . .	100
6.3.6	Cantilever T-shaped beam . . . . .	102
6.3.7	Cantilever C-shaped- open walled beam . . . . .	102
6.3.8	Doubly clamped T-shaped cross-section . . . . .	103
6.4	Conclusion . . . . .	105
	<b>References</b>	<b>107</b>
	<b>Appendix A Validation of Variable Angle Tow Composites</b>	<b>117</b>

# List of Figures

2.1	Observation of the given displacement field in global, local and $C_z^0$ requirements [1]. . . . .	6
2.2	Scheme of Layerwise approach . . . . .	8
2.3	A generic beam Cartesian system . . . . .	10
2.4	Cross-section function $F_\tau$ with various polynomial order . . . . .	12
2.5	Three-, six-, four-, nine-, Sixteen- node Lagrange element in actual geometry . . . . .	12
2.6	CUF LE elements in actual and normalized coordinate systems . . . . .	13
2.7	1D beam model where y is the along the beam axis, and cross-section lay on x, z plane through thickness. . . . .	17
2.8	Two, three, four-node bar. . . . .	18
2.9	Assembly of stiffness matrix in a beam model from the fundamental nucleus. . . . .	19
2.10	VAT definition by Gaussian points . . . . .	21
3.1	Monte Carlo-sample point . . . . .	26
3.2	Example of probability of a die. . . . .	27
3.3	A probability distribution expressed in cumulative form . . . . .	29
3.4	Normal distribution for E by 1000000 random sampling points . . . . .	30
3.5	Latin hypercube sampling for one dimension- Only one sample per stratification . . . . .	31

3.6	Latin hypercube sampling for two dimensions- Only one sample in each row and each column . . . . .	31
3.7	Comparison of artificial intelligence, machine learning, deep learning and neural network. . . . .	34
3.8	One artificial neural network within the function of activation. . . . .	35
3.9	Neural network definition diagram, $x_1, x_2$ example of inputs, $wh_1, wh_2, wh_3$ example of weights. . . . .	36
4.1	Variable angle tow, $T_0$ and $T_1$ . . . . .	42
4.2	Boundary condition of a single VAT laminate ( $< 75^\circ   15^\circ >$ ). . . . .	42
4.3	Refined elements over the cross-section. . . . .	43
4.4	Refined elements through the beam with L9 expansion over the cross-section. . . . .	43
4.5	Refined elements through the beam with L16 expansion over the cross-section. . . . .	44
4.6	First critical buckling load vs. DOF, based on the refinement of the beam elements. . . . .	45
4.7	Second critical buckling load vs. DOF, based on the refinement of the beam element. . . . .	45
4.8	SSSS boundary condition (B.C.) of the plate. . . . .	46
4.9	Critical buckling load in the first six modes vs. the natural logarithm of the DOF for 10, 15, and 20 beam elements. . . . .	47
4.10	First six critical buckling mode shapes under different $T_1$ . . . . .	51
4.11	First six critical buckling mode shapes under different $T_1$ values vs. number of modes. . . . .	51
4.12	Four-edge plates subjected to four different B.Cs, case 1 (SSSS), case 2 (SSSS-I), case 3 (CCCC) and case 4 (CFCF). . . . .	52
4.13	Sensitivity of the first six frequencies under case 1 B.C. for different fiber orientations $T_1$ . . . . .	53

---

4.14	Sensitivity of the first six frequencies under case 2 B.C. for different fiber orientations $T_1$ . . . . .	54
4.15	Sensitivity of the first six frequencies under case 3 B.C. for different fiber orientations $T_1$ . . . . .	55
4.16	Sensitivity of the first six frequency under case 4 B.C. for different fiber orientations $T_1$ . . . . .	55
5.1	Flowchart of Genetic algorithm procedure (MATLAB) in combination with CUF approach (FORTRAN). . . . .	60
5.2	1D CUF cross-section refinement with 10B3 effect on the buckling load in $VAT_1$ in contrast with FEM and degree of freedom number. .	61
5.3	1D CUF beam element refinement with 160L9 effect on the buckling load in $VAT_1$ in contrast with FEM and degree of freedom number. .	62
5.4	Comparison between different layup design with the optimum result.	63
5.5	The first buckling modes in different laminates. . . . .	64
5.6	The first five first buckling modes of optimum VAT laminates. . . .	64
5.7	Distribution of variables and first critical buckling load, $T_0$ - $T_1$ , First buckling load- $T_0$ and First buckling load- $T_1$ . . . . .	65
5.8	Contour plots and response surfaces based on GA and LHS for $T_0$ , $T_1$ which denotes variables and first critical buckling load as the response. . . . .	65
5.9	Comparison between different fit ANN algorithm based on the number of hidden layer for VAT problem. . . . .	68
5.10	Regression plot in the three subdivision: i) training, ii) testing and ii) all. The bubbles represent the perfect fit between the two values ( $R^2 = 1$ ), the coloured solid lines show the real correlation between the computed output and the initial target. . . . .	68
5.11	Errors distribution concerning the training, and test sets. . . . .	69
5.12	Comparison between different layup design with the optimum result for dynamic analysis. . . . .	70

5.13	The first natural frequency modes of laminates in different layup design. . . . .	70
5.14	The first five natural frequency modes. . . . .	71
5.15	Distribution of variables and first natural frequency, $T_0$ - $T_1$ , First natural frequency- $T_0$ and First natural frequency- $T_1$ . . . . .	71
5.16	Contour plot and response surface showing effects of variables (fiber orientation angles) during GA procedure in free vibration problem. .	72
6.1	Boundary conditions: free-free (BC1), doubly clamped beam (BC2) and Cantilever beam (BC3). . . . .	77
6.2	Beams with arbitrary cross section. . . . .	78
6.3	Mode shapes of frequency in 3D FEM in Abaqus, Beam 1, BC1. . .	80
6.4	Mode shapes of frequency in CUF, Beam 1, BC1. . . . .	81
6.5	1D CUF model with various discretization in beam 1 (a) over the cross sections and (b) along the beam. . . . .	82
6.6	Mesh study and convergence analysis of CUF model respect to 3D solid FEM in Abaqus. . . . .	82
6.7	Modal shapes in Beam 1 and BC2– quadratic element within Abaqus	84
6.8	Modal shapes in Beam 1 and BC2– quadratic element within CUF framework. . . . .	85
6.9	Modal shapes in Beam 1 and BC3– quadratic element within Abaqus.	86
6.10	Modal shapes in Beam 1 and BC3– quadratic element within CUF framework. . . . .	87
6.11	1D CUF model discretization in beam 2 (a) over the cross sections and (b) through the beam. . . . .	88
6.12	Modal shapes in Beam 2 and BC2– quadratic element within Abaqus	88
6.13	Modal shapes in Beam 2 and BC2– quadratic element within CUF framework. . . . .	89
6.14	Modal shapes in Beam 2 and BC3– quadratic element within Abaqus.	90



---

6.15	Modal shapes in Beam 2 and BC3– quadratic element within CUF framework (15L9-13B3). . . . .	91
6.16	1D CUF model discretization in beam 3 (a) over the cross sections and (b) through the beam. . . . .	92
6.17	Modal shapes in Beam 3 and BC2– quadratic element within Abaqus. . . . .	93
6.18	Modal shapes in Beam 3 and BC2– quadratic element within CUF framework. . . . .	94
6.19	Modal shapes in Beam 3 and BC3– quadratic element within Abaqus . . . . .	95
6.20	Modal shapes in Beam 3 and BC3– quadratic element within CUF framework.. . . . .	96
6.21	1D CUF model discretization in beam 4 (a) over the cross sections and (b) through the beam. . . . .	96
6.22	Modal shapes in Beam 4 and BC2– quadratic element within 3D solid in Abaqus. . . . .	97
6.23	Modal shapes in Beam 4 and BC2– quadratic element within CUF framework. . . . .	98
6.24	Modal shapes in Beam 4 with BC3– 3D solid FEM in Abaqus with quadratic element. . . . .	99
6.25	Modal shapes in Beam 4 and BC3– quadratic element within CUF framework. . . . .	100
6.26	T-shaped cross-section thin-walled beam. . . . .	101
6.27	Modal shapes in Doubly-clamped T-shaped beam– Abaqus. . . . .	101
6.28	Modal shapes in Doubly-clamped T-shaped beam– CUF framework. . . . .	102
6.29	Modal shapes in T-shaped cross-section- 3D solid Abaqus. . . . .	102
6.30	C-shaped thin-walled beam. . . . .	103
6.31	Modal shapes in U-shaped cantilever– CUF framework. . . . .	104
6.32	Modal shapes in C-shaped Doubly-clamped cross-section– CUF framework. . . . .	105
A.1	Lamination of first ply (Lamina a) and second lamination (Lamina b) . . . . .	118

A.2	Frequency modes for laminate a with three layers under CCCC-thick plate. . . . .	122
A.3	Frequency modes for laminate b with three layers under CCCC-thick plate. . . . .	122
A.4	Frequency modes for laminate b with three layers under CCCC-thin plate. . . . .	123
A.5	Frequency modes for laminate b with three layers under CCCC-thin plate. . . . .	123
A.6	Meshed thick plate with 180 elements in cross-section. . . . .	125
A.7	First 5 modal shapes of the CCCC 3-layer thick plate (Laminate a). .	125
A.8	First 5 modal shapes of the CCCC 3-layer thick plate (Laminate b). .	125
A.9	Meshed thick plate with 180 elements in cross-section. . . . .	126
A.10	First 5 modal shapes of the CCCC 3-layer thick plate (Laminate a). .	126
A.11	First 5 modal shapes of the CCCC 3-layer thick plate (Laminate b). .	126
A.12	First 9 frequency modes in different number of beam elements (y and x) and nodes per thickness (z) in thin plate . . . . .	127
A.13	First 9 frequency modes in different number of beam elements (y and x) and nodes per thickness (z) in thin plate . . . . .	128
A.14	First 9 frequency modes in different number of beam elements (y and x) and nodes per thickness (z) in thick plate . . . . .	129
A.15	First 9 frequency modes in different number of beam elements (y and x) and nodes per thickness (z) in thick plate . . . . .	130

# List of Tables

4.1	Linear elastic buckling estimates according to the number of elements through the beam and cross-section. . . . .	44
4.2	Buckling mode shapes in the SSSS B.C., as obtained using the CUF and FEM approaches, for $[\langle 60^\circ   15^\circ \rangle \langle -60^\circ   -15^\circ \rangle / \langle -60^\circ   -15^\circ \rangle \langle 60^\circ   15^\circ \rangle]_4$ . . . . .	47
4.3	Different lay-up designs for the laminate. . . . .	48
4.4	Pre-buckling displacement and stress distribution for seven different designs of VAT fiber orientation angles under the SSSS B.C. . . . .	49
4.5	First six critical buckling mode shapes under the SSSS B.C. based on six different lay-up designs. . . . .	50
4.6	First six natural frequencies for case 1- SSSS. . . . .	53
4.7	First six natural frequencies for case 2- SSSS-I. . . . .	54
4.8	First six natural frequencies for case 3- CCCC. . . . .	54
4.9	First six natural frequencies for case 4- CFCF. . . . .	55
5.1	Reference laminate lay-up designs in contrast with optimum VAT plate. . . . .	62
5.2	Reference laminate lay-up designs in contrast with optimum VAT plate. . . . .	70
6.1	The geometry of beam and properties of material. . . . .	79
6.2	First frequencies (Hz) for Beam 1 BC1. . . . .	80

6.3	References for Beam 1 BC2 with quadratic elements. . . . .	83
6.4	Natural frequencies of the C-shape cross-section beam with doubly clamped boundary condition through CUF framework, Beam 1-BC2. . . . .	83
6.5	Mesh study for Beam 1 BC3 with quadratic elements by different references. . . . .	86
6.6	Natural frequencies of the C-shape cross-section cantilever beam through CUF framework, Beam 1-BC3. . . . .	86
6.7	Reference study for Beam 2 BC2 with LEs on the cross section (L9). . . . .	88
6.8	Mesh study for Beam 2 BC2 with LEs on the cross section (L9). . . . .	88
6.9	References study for Beam 2 BC3 with quadratic elements. . . . .	89
6.10	Mesh study for Beam 2 BC3 with quadratic elements. . . . .	90
6.11	Reference study for Beam 3 BC2 with quadratic element. . . . .	92
6.12	Convergence analysis in Beam 3 BC2 with quadratic element. . . . .	92
6.13	Reference study for Beam 3 BC3 with LEs on the cross section (L9). . . . .	94
6.14	Mesh study for Beam 3 BC3 with LEs on the cross section (L9). . . . .	95
6.15	Reference study for Beam 4 BC2 with quadratic elements. . . . .	97
6.16	Convergence study in Beam 4 BC2– quadratic elements in CUF framework. . . . .	97
6.17	Reference solutions in Beam 4 BC3 with quadratic element. . . . .	98
6.18	Convergence analysis in Beam 4 BC3– quadratic element in CUF model. . . . .	99
6.19	Doubly clamped T-shaped beam– Convergence analysis. . . . .	101
6.20	Analytical solution for eigenvalues respect to CUF framework in C-shaped cantilever cross-section- RTO: Rotational Terms Omitted, RTI: Rotational Terms Included. . . . .	103
6.21	Analytical natural frequencies respect to CUF procedure in C-shaped doubly-clamped cross-section. . . . .	104
A.1	VAT plates under clamped boundary condition-free vibration analysis. . . . .	119

---

A.2	Convergence analysis for linear natural frequencies [Hz] for clamped VSCL plates. . . . .	119
A.3	Linear natural frequencies [Hz] for clamped VSCL plates. . . . .	120
A.4	Convergence analysis in VAT plates under clamped boundary condition-free vibration analysis. . . . .	120
A.5	Convergence analysis in VAT plates under clamped boundary condition-free vibration analysis.. . . .	121
A.6	Convergence analysis in VAT plates under clamped boundary condition-free vibration analysis.. . . .	121
A.7	Convergence analysis in VAT plates under clamped boundary condition-free vibration analysis.. . . .	124
A.8	Goodness of fit from Curve Fitting solution by interpolant with the method of thin-plate spline. . . . .	124

# Chapter 1

## Introduction

### 1.1 Overview

Over the last decades, Fibre-Reinforced Polymer (FRP) composite materials become well known as fast-growing area and favoured materials for construction of aircraft and spacecraft, automotive, marine, sports and in civil infrastructures [2, 3]. The FRP composite materials introduce numerous advantages in contrast to the metallic structures in terms of weight decrease and enhanced structural performance. In aerospace structure design, stability is the most critical factor, therefore all the probable loading conditions on various parts of the structure have to be analysed to produce a safer design. Also, the recent evolution of new composite construction and manufacturing techniques, for example the machines of automated fibre placement, makes it possible to go beyond classical design rules, so the designer is looking for innovative and more efficient solutions than the classic straight fibre settings. The use of automated fibre placement technology created a novel level of composite materials which is called Variable Angle Tow (VAT) composites (see [4–6]). Such structures achieved a great influence since they allow the designer to tailor a structure to show the most desirable static and dynamic response under the designated loads. In recent years, the use of VAT panels in aerospace applications increased. The continuous variation of the stiffness properties, obtained by curvilinear fibre path, provides considerable advantages in comparison with the conventional composite, in terms of buckling and dynamic properties which presented by [7–9].

## 1.2 Problem Statement

The analysis and modelling of such anisotropic structures represent a challenging issue for scientists. The Classical Laminated Theory (CLT) was first adopted for this aim. For instance, Leissa et al. [7] used the Ritz method and the theory of thin plates to confirm the improvement of buckling load and the fundamental frequency of 38% and 21%, respectively. Olmedo and Gurdal [10] showed an 80% improvement in VAT composite buckling loads. [11] used the highly efficient Riley-Ritz theory as a traditional finite element model. Most of the literary works such as [12–15] deal with the buckling behaviour of VAT panels performed with numerical, semi-analytical and analytical methods that mostly use CLT. Besides, [16, 17] used the CLT for the dynamic analysis of panels with variable stiffness properties. The Ritz method can be used as an efficient and versatile method for the variable stiffness doubly curved shell structures in free vibrations and linear transient analysis, see [18]. In general, the Finite Element Method (FEM) is the most well-known numerical method for accurate analysis of composite structures. This method is detailed enough, although, in a repetitive step in the design of such structures, 3D FEM is slow and high-priced due to the need for mesh and high computational costs. Refined finite element techniques may be applied to decrease computational costs without compromising accuracy. A comprehensive approach that can be applied to extract refined finite element models was presented by [19].

The Carrera Unified Formulation (CUF) introduced for 1D beam models and 2D plates and shells by going beyond from different classical theories obstacles. CUF has employed the notation which is condensed and providing the 3D displacement field over the cross-section of beam structure and over the thickness of thickness in plate and shells. A different function of expansion are used in CUF within the formulas; these expansions that can be employed are polynomial, harmonic, and exponential. In CUF the weak form of governing equations is achieved by FEM. In the CUF framework, any desired order of cross-section can be used independently from the properties of the problem. Giunta et al. [20] employed the 1D CUF models which show an outstanding computational cost reduction in contrast with 3D solid FEM. In other words, using CUF, a 1D FEM can be applied for analyzing complex 3D structures. A comprehensive review of whole 1D models can be found in [20]. There is a vast literature on the subject of CUF models, [21–25], and in the form of 1D beam [26–29].

## 1.3 Objective of the Research Project

The main aim of this research project is to analysis the VAT composite structures through the 1D beam in CUF framework to develop a fit optimization method over different types of structural analysis. Specific aspects of the present research to address the above objective are:

- 1D CUF Modeling and analysis of VAT in different geometries to be investigated in different boundary condition for buckling and vibration behaviour of VAT.
- In the next step as the main goal of the current thesis, Genetic Algorithm (GA) is chosen to fit buckling and vibration analysis and then Latin Hypercube Sampling method is used to be compared with the results those obtained by GA stochastic sample generation.
- One more objective of this thesis was to evaluate the open cross-section thin-wall beam structure in vibration analysis. A comprehensive study has done on boundary conditions, beam length and effect of the geometry of open cross-section under the natural frequencies.

## 1.4 Outline

Formation of the current thesis is classified in six chapters that concisely present as following:

CHAPTER 1 introduced an overview for PhD thesis.

CHAPTER 2 is concentrated on the primary and principal theories and beam models in both classical and unified formulation and mostly focused on multi-layered structures.

CHAPTER 3 describes different sample generation methods and all necessary definition of stochastic analysis.

CHAPTER 4 addressed to the results from variable angle tow composites under different boundary conditions, geometries, materials which investigated in different types of analysis.

CHAPTER 5 is focused on the optimization procedure for variable angle two in two different analysis such as buckling and free vibration analysis. In this chapter, the



CUF method is linked with a Genetic Algorithm to achieve the optimum outcomes for the highest first buckling load and highest first natural frequency.

CHAPTER 6 is the final part of this study which present the vibration behaviour in the thin-wall beam which is modelled in the CUF framework in comparison with different references.

## **Chapter 2**

# **Multi-Layered Beam Structures: Classical Models and Unified Formulation**

### **2.1 Introduction**

In recent decades, the development of mathematical models capable of accurately describing the behaviour of multilayer composites has become increasingly important. First, the potentials of the classical approaches used for mechanical models of metallic structures were investigated. Despite, the classical models do not take into account some specific kinematic and mechanical aspects of composite materials, for example, transverse deformation and the maximum shear and normal stresses on the mechanical behaviour of composites. For this reason, researchers tried to obtain new theories for the precise definition of composite materials to improve their understanding and predicting their mechanical behaviour.

This chapter shortly describes the 1D refined models applied within the thesis study. 1D CUF model is formulated in the finite element model in terms of fundamental nuclei and by using the Principle of Virtual Displacement (PVD). The abilities of 1D CUF beam models are distinguished within numerical models dealing with structural analysis of composite panels. This chapter is the core for solving various kinds of the problem through the thesis.

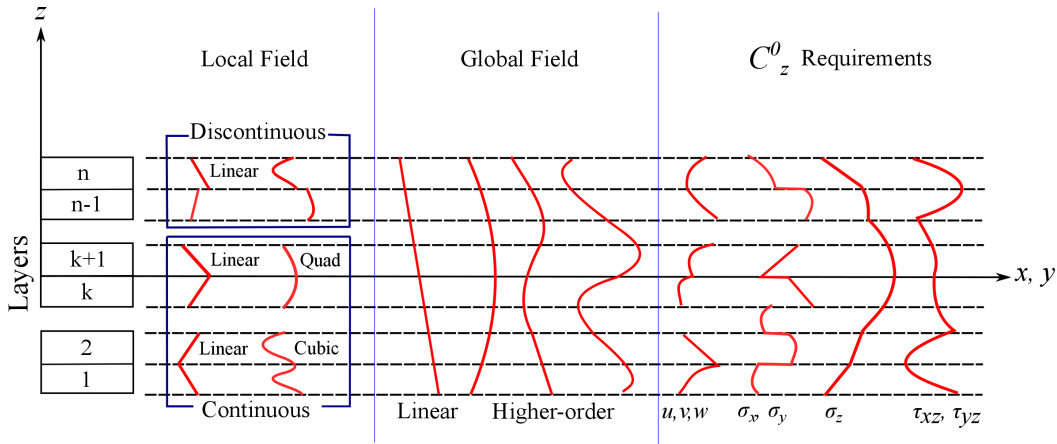


Fig. 2.1 Observation of the given displacement field in global, local and  $C_z^0$  requirements [1].

## 2.2 Theories of multi-layered structures: Displacement-Based Formulation

For structural analyzing of composite materials, we are faced with many features and challenges. These challenges arise due to the anisotropic and heterogeneous nature of composite materials. Besides, there are some requirements for defining the continuity of displacement and transverse stresses through the thickness, that is called  $C_z^0$  requirements. For evaluating the behaviour of composite structures, two main categories exist:

- The theories with displacement base
- The theories with the mixed formulation

Equivalent single layer (ESL) theory is the most common hypothesis based on the displacement theories which consists of three approaches: classical laminate theory (CLT), Zig-Zag theory (ZZ) and Layerwise (LW) approach [1]. In Figure 2.1, the displacement field express by polynomial function while other types of function can be used, for instance, exponential, trigonometric and hyperbolic for expansion of displacement-based theories [1].

### 2.2.1 Theory of Equivalent Single Layer

For modelling of composite structures, classical plate theories are the first hypothesis which was used for composite structures. In these type of theories, the behaviour of global transverse effect was evaluated independently from layers number and the displacement field assumption continuously within the thickness. Moreover, the laminates considered like one single layer. These assumption can be considered as ESL theories [1, 30].

$$\begin{aligned}
 u(x, y, z) &= u_0(x, y) - \frac{dw}{dx}z \\
 v(x, y, z) &= v_0(x, y) - \frac{dw}{dy}z \\
 w(x, y, z) &= w_0(x, y)
 \end{aligned} \tag{2.1}$$

CLT deficiency refers to the assumption that the transverse shear is zero. Therefore, the Reissner and Mindlin [31, 32] can be used for overcoming this limitation which developed the formulation of plates. Consequently, several pieces of the research proposed the displacement theories by higher-order polynomials, which can call Higher-Order Shear Deformation Theories (HSDT) that the generic form of that express by:

$$\begin{aligned}
 u(x, y, z) &= \sum_{i=0}^m u_i(x, y)z^i \\
 v(x, y, z) &= \sum_{i=0}^m v_i(x, y)z^i \\
 w(x, y, z) &= \sum_{i=0}^m w_i(x, y)z^i
 \end{aligned} \tag{2.2}$$

### 2.2.2 Layerwise Theory

In classical Bernoulli-Euler and Timoshenko (first-order shear deformation) beam theories, it is assumed that the cross-section plane remains plane after deformation. This hypothesis is accurate enough for isotropic and layered composite beams

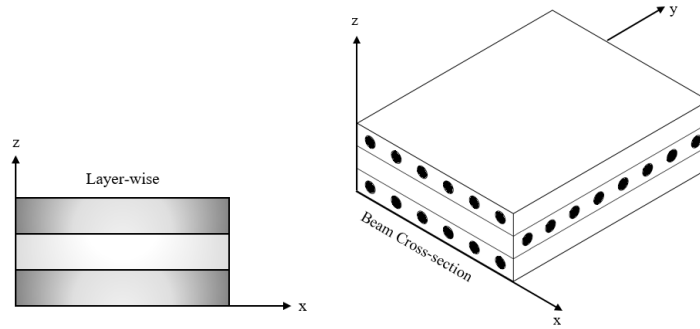


Fig. 2.2 Scheme of Layerwise approach

with similar stiffnesses in plies while it drives to serious contrasts with the actual state of stresses in laminated beams when one or more layers have quite different stiffnesses [33]. Following the approach, third-order layerwise theory can express by displacement field in a generalized form as [34, 35]:

$$\begin{aligned}
 u^k(x, y, z) &= u_0^k(x, y) + u_1^k(x, y)z + u_2(x, y)z^2 + u_3(x, y)z^3 \\
 v^k(x, y, z) &= v_0^k(x, y) + v_1^k(x, y)z + v_2(x, y)z^2 + v_3(x, y)z^3 \\
 w^k(x, y, z) &= w_0^k(x, y) + w_1^k(x, y)z + w_2(x, y)z^2 + w_3(x, y)z^3
 \end{aligned} \tag{2.3}$$

Displacement field based on Eq. 2.3 possess four variables in each component, and in common, there are  $12n$  variables for a laminate with  $n$  layers. In fact, layerwise theory presents an expansion of local displacement field for each layer of materials. Therefore, the layerwise theories describe both zig-zag displacement computation and transverse stresses which are continues within the thickness. As a result, layerwise theory can provide an accurate behavioural prediction of the composite laminates. Nonetheless, it presents some penalties such as high computational cost.

### 2.2.3 Zig-Zag Theory

A comprehensive historical review on layerwise theories which were focused on the zig-zag theories is presented by Carrera [36]. This study highlighted the prior research by Lekhnitskii [37], Ambartsumian [38] and Reissner [32]. Zig-Zag theories

provided a displacement field which is continued in the direction of plate thickness and it is known as Interlaminar (IC) of transverse stresses at each layer interface.

The geometry of the plate and the shell are taken into account, even if in some cases the beams are also considered. Models in which the number of displacement variables is kept independent of the number of constituent layers are the most controversial. Attention is limited to those plate and shell theories that are based on the so-called method of hypotheses or the axiomatic approach in which hypotheses for displacement and/or transverse stresses are introduced, a complete review can be found in Carrera in 2003 [36].

Different 2D modelling of multilayered plates and shells such as Cauchy-Poisson-Kirchhoff-Love thin plate/shell theory, or Reissner-Mindlin theory [31, 32] not appropriate to describe the reproduce piecewise continues displacement and transverse stress field through-thickness direction in multilayered structures. These two effects introduced by the acronym  $C_z^0$ -a requirement which shows that the displacements and transverse stresses must be  $C_z^0$ -continue functions in the thickness direction, along  $z$ -coordinate. Piecewise of transverse stress and displacement field is often described in the open literature as ZZ And IC, respectively.

$$\begin{aligned} u^k(x, y, z) &= u_0^k(x, y) + u_1^k(x, y)z + u_2(x, y)z^2 + u_3(x, y)z^3 \\ v^k(x, y, z) &= v_0^k(x, y) + v_1^k(x, y)z + v_2(x, y)z^2 + v_3(x, y)z^3 \\ w^k(x, y, z) &= w_0(x, y) \end{aligned} \quad (2.4)$$

## 2.3 One Dimensional Carrera Unified Formulation (CUF)

In the 1D model of Carrera Unified Formulation (CUF) approach, the unknown variables turn to the beam axial coordinate as one of the coordinates. The axial coordinate in CUF framework is along the  $y$  axis and cross-section coordinates lay on the  $xz$ -coordinates which shows by a plane of  $\Omega$  in Figure 2.3. A generalized three-dimensional displacement vector can be presented as:

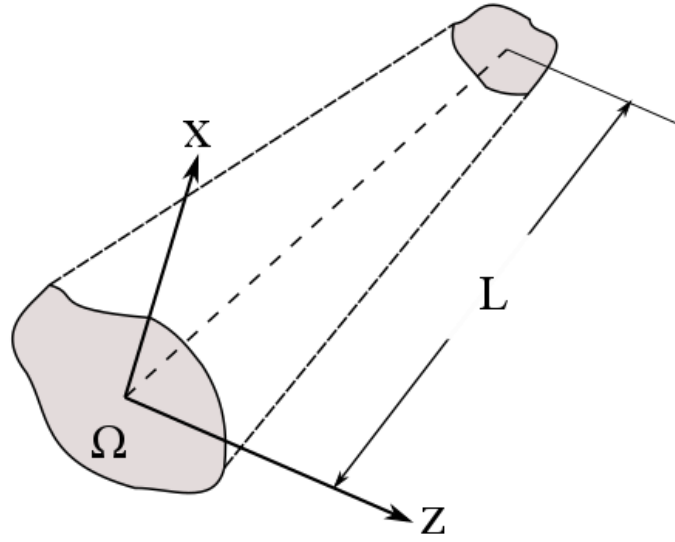


Fig. 2.3 A generic beam Cartesian system

$$u(x, y, z) = \{u_x \quad u_y \quad u_z\}^T \quad (2.5)$$

where  $u$  is a displacement vector and  $T$  is a transposition. In CUF as a hierarchical system, the structural theories defined by the cross-section expansion function, as following:

$$u(x, y, z) = F_\tau(x, z)u_\tau(y) \quad \tau = 1, 2, \dots, M \quad (2.6)$$

where  $F_\tau(x, z)$  is the expansion function of cross-section,  $u_\tau(y)$  denotes the generalized displacement vector and  $M$  is the number of terms in expansion function.  $F_\tau$  in terms of  $M$  can remain arbitrary in classical beam model like Euler Bernoulli Beam Theory (EBBT) or Timoshenko Beam Theory (TBT) Different classes of basis function can be used as an instance: polynomial, harmonic, trigonometric or exponential expansion. In the framework of 1D CUF beam model, three kinds of expansion functions are commonly employed: (i) Taylor Expansion (TE), (ii) Lagrange Expansion (LE) and (iii) Hierarchical Lagrange Expansion (HLE) [39]. TE and LE function expansions are widely used through the current thesis which is explained in detail by the next section.

### 2.3.1 Taylor Series Expansion

$$\begin{aligned}
F_1 &= 1, \\
F_2 &= x, \quad F_3 = z, \\
F_4 &= x^2, \quad F_5 = xz, \quad F_6 = z^2 \\
F_7 &= x^3, \quad F_8 = x^2z, \quad F_9 = xz^2, \quad F_{10} = z^3
\end{aligned} \tag{2.7}$$

in which the polynomial expansions are taken from Pascal's triangle. Classical beam theories (CBT) such as EBBT and TBT can be introduced by the first order of Taylor expansion (TE1). Displacement field for EBBT built based on:

$$\begin{aligned}
u_x &= u_{x1} \\
u_y &= u_{y1} - \frac{\partial u_{x1}}{\partial u_y} x - \frac{\partial u_{z1}}{\partial u_y} z \\
u_z &= u_{z1}
\end{aligned} \tag{2.8}$$

From the mathematic point, EBBT displacement field can be written in the form of Maclaurin series expansion where a zero-order approximation is used for the in-plane components and  $N$ -order=1 is adopted for axial displacement, and by kinematic consideration, the relations between unknown can be driven. Then, the displacement of the TBT theory with five unknown presents:

$$\begin{aligned}
u_x(x, y, z) &= u_{x1}(y) \\
u_y(x, y, z) &= u_{y1}(y) + \phi_z(y)x + \phi_x(y)z \\
u_z(x, y, z) &= u_{z1}(y)
\end{aligned} \tag{2.9}$$

For more detail on the formulation of EBBT and TBT, see [20].



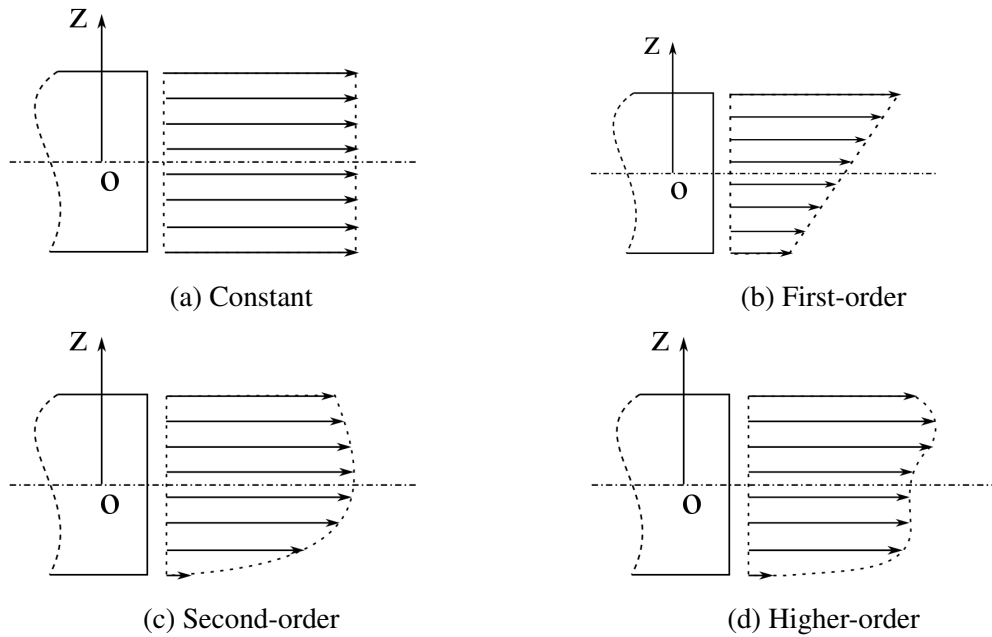


Fig. 2.4 Cross-section function  $F_\tau$  with various polynomial order

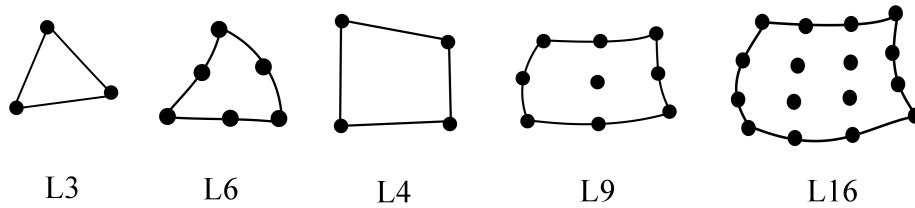


Fig. 2.5 Three-, six-, four-, nine-, Sixteen- node Lagrange element in actual geometry

### 2.3.2 Lagrange Expansion

The Lagrange expansion in 1D modes is introduced as LE models that can be expressed by Lagrange-type polynomial. LE has more advantages than TE models, including the physical meaning of Lagrange models, and uses a different approach and exploited the isogeometric parameters. The cross-sections can be discretized by employing different types of Lagrange elements. For instance linear three-node (denotes as L3), bi-linear four-point (L4), quadratic nine-point (L9) and cubic sixteen-point (L16) elements Different coordinate systems are shown for 9L9 elements in Figure. 2.5.

Furthermore, an example of L9 element in actual and natural coordinate system is shown in Figure. 2.6. The coordinate transformation from an arbitrary cross-section

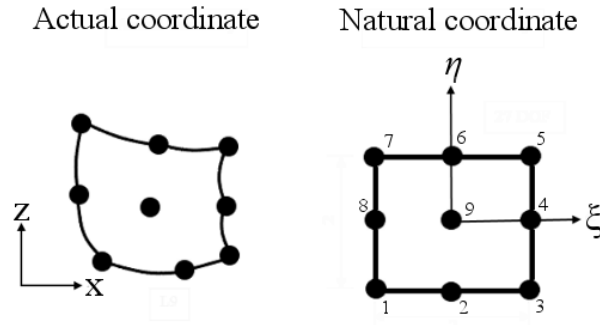


Fig. 2.6 CUF LE elements in actual and normalized coordinate systems

coincides with  $F_\tau$  expansion function refers to coordinates of  $(x, z)$  to the natural square  $(\zeta, \eta)$ , for detailed information refer to [40].

Therefore, in the natural coordinate system  $(\zeta, \eta)$ , the Lagrange polynomial expansion is expressed for quadrilateral Lagrange polynomial with four-point ( $L4$ ):

$$F_\tau(\zeta, \eta) = \frac{1}{4}(1 + \zeta\zeta_\tau)(1 + \eta\eta_\tau) \quad \tau = 1, 2, 3, 4 \quad (2.10)$$

where  $-1 \leq \zeta \leq 1$  and  $-1 \leq \eta \leq 1$  whereas  $\zeta_\tau$  and  $\eta_\tau$  are natural coordinates of  $\tau^{th}$  Lagrange point of the element. The second set refers to  $L9$ :

$$\begin{aligned} F_\tau(\zeta, \eta) &= \frac{1}{4}(\zeta^2 + \zeta\zeta_\tau)(\eta^2 + \eta\eta_\tau) & \tau = 1, 3, 5, 7 \\ F_\tau(\zeta, \eta) &= \frac{1}{2}\eta_\tau^2(\eta^2 - \eta\eta_\tau)(1 - \zeta^2) + \frac{1}{2}\zeta_\tau^2(\zeta^2 - \zeta\zeta_\tau)(1 - \eta^2) & \tau = 2, 4, 6, 8 \\ F_\tau(\zeta, \eta) &= (1 - \zeta^2)(1 - \eta^2) & \tau = 9 \end{aligned} \quad (2.11)$$

Furthermore, the polynomials for  $L16$  are written by [19]:

$$F_{\tau_{JK}}(\zeta, \eta) = L_J(\zeta)L_K(\eta) \quad J, K = 1, 2, 3, 4 \quad (2.12)$$

where  $L_J$  and  $L_K$  are calculated as following:

$$\begin{aligned} L_1(\zeta) &= \frac{1}{16}(\zeta - 1)(1 - 9\zeta^2) & L_2(\zeta) &= \frac{9}{16}(1 - \zeta^2)(1 - 3\zeta) \\ L_3(\zeta) &= \frac{9}{16}(1 - \zeta^2)(1 + 3\zeta) & L_4(\zeta) &= \frac{1}{16}(1 + \zeta)(9\zeta^2 - 1) \end{aligned}$$

The displacement field for  $L4$  cross-section element can be express respectively as:

$$\begin{aligned} u_x &= F_1u_{x1} + F_2u_{x2} + F_3u_{x3} + F_4u_{x4} \\ u_y &= F_1u_{y1} + F_2u_{y2} + F_3u_{y3} + F_4u_{y4} \\ u_z &= F_1u_{z1} + F_2u_{z2} + F_3u_{z3} + F_4u_{z4} \end{aligned} \quad (2.13)$$

where  $F_1, F_2, \dots, F_4$  are based on the four Lagrange polynomials on the cross-section coordinate, and  $u_{x1}, u_{x2}, \dots, u_{x4}$  are 12 unknown displacement variables along y-axis and express pure displacement components at each point of the  $L4$  and respectively for  $L9$  displacement field with 27 unknown displacement variables is written as:

$$\begin{aligned} u_x &= F_1u_{x1} + F_2u_{x2} + \dots + F_9u_{x9} \\ u_y &= F_1u_{y1} + F_2u_{y2} + \dots + F_9u_{y9} \\ u_z &= F_1u_{z1} + F_2u_{z2} + \dots + F_9u_{z9} \end{aligned} \quad (2.14)$$

and finally for  $L16$  with 48 unknown displacement variables is written as::

$$\begin{aligned} u_x &= F_1u_{x1} + F_2u_{x2} + \dots + F_{16}u_{x16} \\ u_y &= F_1u_{y1} + F_2u_{y2} + \dots + F_{16}u_{y16} \\ u_z &= F_1u_{z1} + F_2u_{z2} + \dots + F_{16}u_{z16} \end{aligned} \quad (2.15)$$

## 2.4 Finite Element Formulation of 1D CUF framework

### 2.4.1 Preliminaries

The stress and strain vectors can be defined as:

$$\begin{aligned}\boldsymbol{\sigma} &= \{\sigma_{xx} \quad \sigma_{yy} \quad \sigma_{zz} \quad \sigma_{yz} \quad \sigma_{xz} \quad \sigma_{xy}\}^T, \\ \boldsymbol{\varepsilon} &= \{\varepsilon_{xx} \quad \varepsilon_{yy} \quad \varepsilon_{zz} \quad \varepsilon_{yz} \quad \varepsilon_{xz} \quad \varepsilon_{xy}\}^T\end{aligned}\quad (2.16)$$

where where  $\boldsymbol{\varepsilon}$  is strain and is define using a linear differential operator  $\mathbf{b}$  which is a  $6 \times 3$ , see [19]:

$$\boldsymbol{\varepsilon} = \mathbf{b}\mathbf{u} \quad (2.17)$$

And based on Hook's law, the stress vector is expressed as:

$$\boldsymbol{\sigma} = \mathbf{C}\boldsymbol{\varepsilon} \quad (2.18)$$

Here,  $\mathbf{C}$  is the matrix of the elastic coefficients of the material, that can be investigated as a variable of the space coordinate which can be varied for VAT panels, which will be explained in detail at the end of the current chapter. Then finite element method is adopted along  $y$ -axis for the discretization of the structure with the generalized displacement vector, which is approximated by:

$$\mathbf{u}(x, y, z) = F_\tau(x, z)N_i\mathbf{q}_\tau i \quad i = 1, 2, \dots, K \quad (2.19)$$

where index  $i$  refers to the number of nodes of the beam element,  $N_i(y)$  denotes shape function,  $\mathbf{q}_\tau i$  stands for nodal unknowns, and  $K$  is the nodes number on the element. Figure 2.7 illustrates the shape function along  $y$  coordinate as the beam axis and a expansion of  $F_\tau(x, z)$  over the cross-section ( $xz$ -plane) through a 1D CUF

finite element model. It should be noticed that the shape function of  $N_i$  stands independently from the  $F_\tau$  which refers to expansion function. Besides, a Lagrange polynomial which is standardly employed as the shape functions. In this thesis, three different 1D finite elements are used: (i) two-nodes (B2), three-nodes (B3) and four-nodes (B4), can be adapted to present the displacement in the form of a linear, a quadratic and a cubic interpolation through the beam direction, respectively. The shape function of B2, B3 and B4 elements in a natural system can express respectively, as follows:

*B2 :*

$$\begin{aligned} N_1(\zeta) &= \frac{1}{2}(1 - \zeta) \\ N_2(\zeta) &= \frac{1}{2}(1 + \zeta) \\ \zeta_1 &= -1 \quad \zeta_2 = 1 \end{aligned} \tag{2.20}$$

*B3 :*

$$\begin{aligned} N_1(\zeta) &= \frac{1}{2}\zeta(1 - \zeta) \\ N_2(\zeta) &= (1 + \zeta)(1 - \zeta) \\ N_3(\zeta) &= \frac{1}{2}\zeta(1 + \zeta) \\ \zeta_1 &= -1 \quad \zeta_2 = 0 \quad \zeta_3 = 1 \end{aligned} \tag{2.21}$$

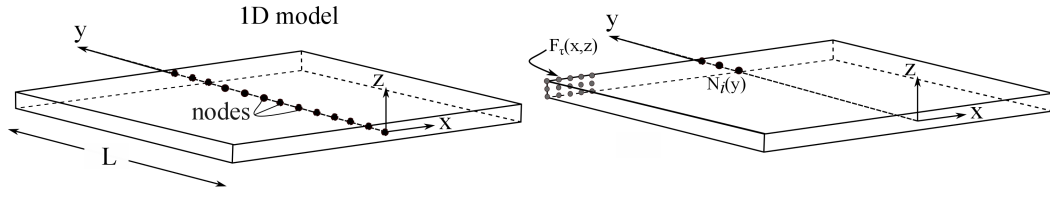


Fig. 2.7 1D beam model where  $y$  is the along the beam axis, and cross-section lay on  $x, z$  plane through thickness.

B4 :

$$\begin{aligned}
 N_1(\zeta) &= -\frac{9}{16}\left(\zeta + \frac{1}{3}\right)\left(\zeta - \frac{1}{3}\right)(\zeta - 1) \\
 N_2(\zeta) &= \frac{27}{16}(\zeta + 1)\left(\zeta - \frac{1}{3}\right)(\zeta - 1) \\
 N_3(\zeta) &= -\frac{27}{16}(\zeta + 1)\left(\zeta + \frac{1}{3}\right)(\zeta - 1) \\
 N_4(\zeta) &= \frac{9}{16}(\zeta + 1)\left(\zeta + \frac{1}{3}\right)\left(\zeta - \frac{1}{3}\right)
 \end{aligned} \tag{2.22}$$

$$\zeta_1 = -1 \quad \zeta_2 = -1/3 \quad \zeta_3 = 1/3 \quad \zeta_4 = 1$$

Figure 2.8, shows the distribution of the nodes and shape functions in natural coordinate.

## 2.5 Weak Formulation and Governing Equation

Based on principal virtual displacement (PVD), virtual internal work can be written as follows:

$$\delta L_{int} = \int_V \delta \boldsymbol{\varepsilon}^T \boldsymbol{\sigma} dV \tag{2.23}$$

where  $L_{int}$  refers to strain energy,  $V$  is the volume of the element,  $\boldsymbol{\sigma}$  is the stress vector, and  $\delta \boldsymbol{\varepsilon}$  is the virtual variation of strain, which is presented as:

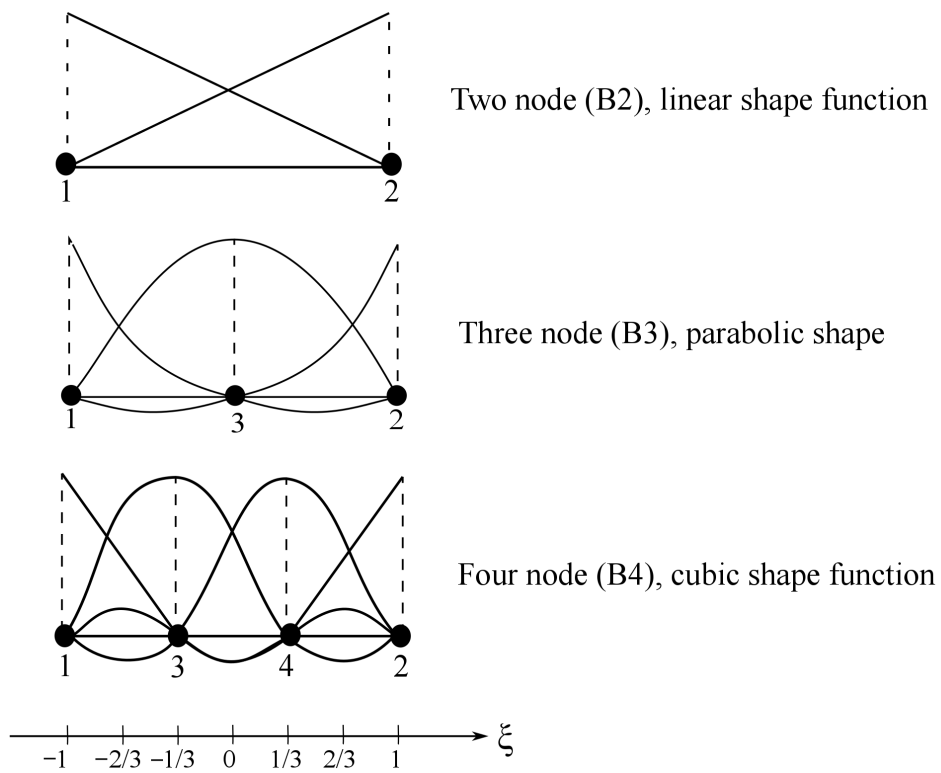


Fig. 2.8 Two, three, four-node bar.

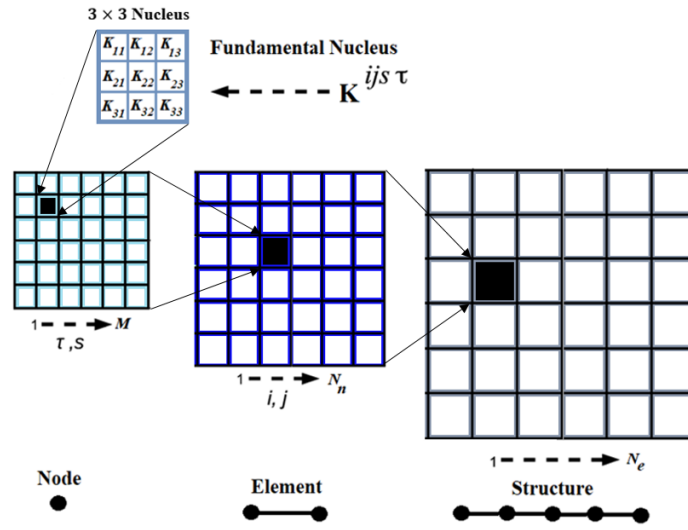


Fig. 2.9 Assembly of stiffness matrix in a beam model from the fundamental nucleus.

$$\delta \mathcal{E} = b \delta u = b(F_s(x, z) N_j(y)) \delta q_{s,j} \quad (2.24)$$

where  $\mathbf{b}$  is differential operator of the strain-displacements relations,  $j$  and  $s$  present the shape function and expansion function indexes, respectively;  $F_s$  is expansion function over  $x$ - $z$  coordinates of cross-section,  $N_j$  stands for  $j$ -th shape function and  $\delta q_{s,j}$  is the virtual variation nodal unknown. Equation 9 can, then, be written as follows:

$$\begin{aligned} \delta L_{int} &= \delta q_{s,j}^T \int_V \underbrace{b^T N_j(y) F_s(x, z) C b F_\tau(x, z) N_i(y) dV}_{\text{Fundamental Nucleus}} q_{\tau i} \\ &= \delta q_{s,j}^T \mathbf{k}^{\tau s i j} q_{\tau i} \end{aligned} \quad (2.25)$$

where  $\mathbf{k}^{\tau s i j}$  is CUF *Fundamental Nucleus* (FN) of the matrix  $\mathbf{k}$ , see Figure. 2.9. The FN is a  $3 \times 3$  matrix which represent the basic building block that can be expanded by using the indexes to obtain the element stiffness matrix of any arbitrary refined beam model [41].



## 2.6 Numerical implementation of the VAT concept

Depending on the path function in VAT composites, each layer offers point-by-point continuous angle variations with different values. In the case of VAT, FN components use volume integrals. For the sake of brevity, only two terms of the FN are given below; Others can be achieved by permutations [19]:

$$\begin{aligned}
 k_{xx}^{\tau sij} &= \int_V C_{22} F_{\tau,x} F_{s,x} N_i N_j dV + \int_V C_{66} F_{\tau,z} F_{s,z} N_i N_j dV \\
 &\quad + \int_V C_{44} F_{\tau} F_s N_{i,y} N_{j,y} dV; \\
 k_{xy}^{\tau sij} &= \int_V C_{23} F_{\tau} F_{s,x} N_{i,y} N_j dV + \int_V C_{44} F_{\tau,x} F_s N_i N_{j,y} dV; \quad (2.26)
 \end{aligned}$$

In this matter, stiffness coefficients  $\mathbf{C}$  vary within the computational domain; hence, these coefficients must remain inside the integral of the FN.

In overall, while using finite elements, integrals can be obtained by implementing the well-known Gauss–Legendre formula. The integral form of the function is evaluated in the  $(\eta, \zeta)$  domain by considering a natural system (for more details, please see Carrera et al. [19]). In the VAT structure, each fibre path can be defined as an arbitrary function, and the fibres follow a curvilinear pattern. Hence, each position corresponds to a different stiffness value. Moreover, in the VAT composite, the lamination angle should be accurately represented in the entire domain of the plate, in which  $\mathbf{C}$  is no longer constant. In this study, the integral can be introduced in the unique form of the volume, as presented in Eq. 2.26. In this application, the Gauss integration technique is used, and the material coefficients in the VAT composite can be evaluated in a specific Gauss point. Accordingly, in the CUF framework, the real values of the lamination angle at each Gauss point are considered. Furthermore, the use of the 1D CUF beam model guarantees a smoother approximation of the component stiffness in contrast with that taken using the finite element method; for more features, please note to [19]. Figure. 2.10 depicts a simplified example of the VAT concerning the Gauss points for four nodes; in the opposite, nine Gaussian points were used in the present research.

In the VAT structure, each fibre path can be described as an arbitrary function, and the fibres serve a curvilinear pattern. Hence, in the plate domain,  $\mathbf{C}$  is no longer

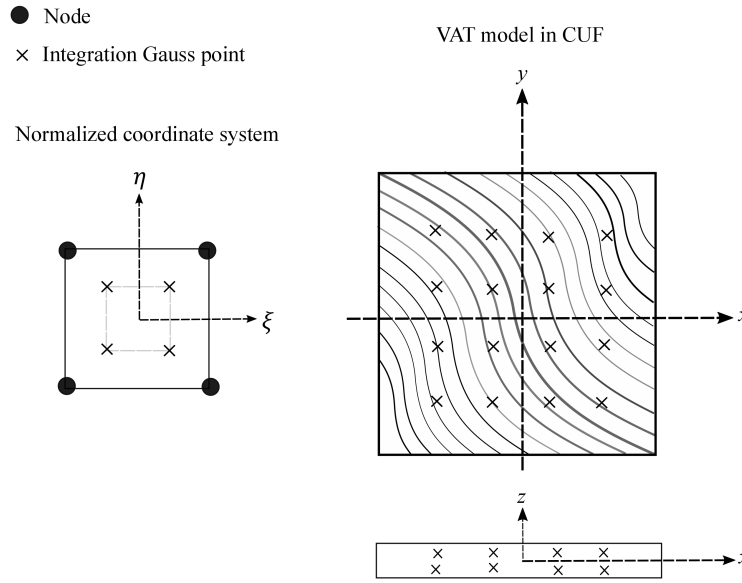


Fig. 2.10 VAT definition by Gaussian points

constant. Therefore, integrals can be presented in a unique form from Eq.2.26–based volume.

### 2.6.1 Linearized buckling equations

For VAT composites in buckling problem, the *Tangent stiffness matrix* is conferred in terms of CUF and FEM approximations, for more further aspect see [19]. In this illustration, the stable buckling problems can be addressed in linearized form as the virtual variation of the internal strain energy  $\delta(\delta L_{int})$ :

$$\delta(\delta L_{int}) \approx \delta \mathbf{q}_{\tau i}^T \mathbf{k}^{\tau s i j} \delta \mathbf{q}_{s j} + \int_V \delta(\delta \boldsymbol{\varepsilon})^T \boldsymbol{\sigma}^0 dV \quad (2.27)$$

where  $\delta(\delta L_{int})$  is calculated regarding the sum of the linear stiffness and virtual variation work associated with the initial stresses  $\boldsymbol{\sigma}^0$ . Consequently, by applying the CUF formulation in Eq. (7) and FEM in Eqs. (10) and (16), the following formulation can be obtained based on the Green–Lagrange nonlinear strain and displacement relations (notice to Carrera et al. [19]):

$$\delta(\delta L_{int}) \approx \delta \mathbf{q}_{\tau i}^T \mathbf{k}^{\tau s i j} \delta \mathbf{q}_{s j} + \delta \mathbf{q}_{\tau i}^T \mathbf{k}_{\sigma^0}^{\tau s i j} \delta \mathbf{q}_{s j} = \delta \mathbf{q}_{\tau i}^T (\mathbf{k}^{\tau s i j} + \mathbf{k}_{\sigma^0}^{\tau s i j}) \delta \mathbf{q}_{s j} \quad (2.28)$$

where  $\mathbf{k}^{\tau s i j}$  the same as in Eq. 2.26, and a new  $\mathbf{k}_{\sigma^0}^{\tau s i j}$  appears in the form of a diagonal matrix, which is investigated as the FN of the geometrical stiffness matrix and is expressed for the buckling case as follows:

$$\begin{aligned} \mathbf{k}_{\sigma^0}^{\tau s i j} = & \left( \int_V \sigma_{xx}^0 F_{\tau,x} F_{s,x} N_i N_j dV + \int_V \sigma_{yy}^0 F_{\tau} F_s N_{i,y} N_{j,x} dV + \int_V \sigma_{zz}^0 F_{\tau,s} F_{s,z} N_i N_j dV \right. \\ & + \int_V \sigma_{xy}^0 F_{\tau,x} F_s N_i N_{j,y} dV + \int_V \sigma_{xy}^0 F_{\tau,x} F_{s,x} N_{i,y} N_j dV + \int_V \sigma_{xy}^0 F_{\tau,x} F_{s,z} N_i N_j dV \\ & \left. + \int_V \sigma_{xz}^0 F_{\tau,s} F_{s,x} N_i N_j dV + \int_V \sigma_{yz}^0 F_{\tau,z} F_s N_{i,y} N_{j,y} dV + \int_V \sigma_{xy}^0 F_{\tau} F_{s,z} N_{i,y} N_j dV \right) I \end{aligned} \quad (2.29)$$

Meanwhile Eq. 2.29, the stress tensor is defined by the 9 components corresponding to a  $3 \times 3$  identity matrix  $I$ . Furthermore, depending on shape function ( $N_i$ ) and function  $F_{\tau}$  over the cross-section, any desired beam model can be available in the CUF framework. Eventually, the global matrices are assembled in the classical FEM. The critical buckling loads are circumscribed as those initial stress states  $\sigma^0$ , that define the tangent stiffness matrix singular; i.e.,  $|K + K_{\sigma^0}^0| = 0$ , see [41].

## 2.6.2 Free Vibration Equations

For free vibration in the frame of the 1D CUF beam model, the same approach can be written based on specified Eqs. 2.19, 2.23, 2.24, and Eq. 2.25. Following that, the work performed by the inertial forces presents the fundamental nucleus of the Mass matrix [41]. The virtual variation of the work-based internal loading can be expressed as follows:

$$\delta L_{ine} = \int_V \rho \ddot{u} \delta u^T dV \quad (2.30)$$

Where  $\rho$  stands as the material density, and  $\ddot{u}$  show the acceleration vector.

## 2.7 Conclusion

Current chapter well explained the 1D higher-order beam model which is applied through the analysis of beam structure in the present thesis. This 1D model achieved by CUF framework which is a hierarchical formulation and can be used in the different form of structures such as beam, plate and shell. Moreover, it showed that the CUF governing equation are taken based on the fundamental nucleus definition by using PVD. 1D CUF model is obtained three-dimensional displacement field which can reduce the computational costs.

# Chapter 3

## Stochastic Analysis

### 3.1 Introduction

Sampling is the process by which values are randomly drawn from input probability distributions. Therefore, choosing a sampling method directly affects both the quality of results and the length of simulation time. Each iteration is one simulation with  $N$  random samples. The current chapter explains what is Monte Carlo (MC) and how it can be implemented, and the problem of Monte Carlo sampling method. Then Latin Hypercube Sampling (LHS) is considered as alleviating the problem and how correlation in LHS can be introduced.

### 3.2 Monte Carlo Method

In general, MC methods refers to a large group of computational algorithm which is based on the repeating random sampling to achieve the numerical results fo a given mathematical model. Monte Carlo is an inherent random sampling. The basic premise is to use randomness to solve problems that can be decisive. Usually in three problem classes the MC can be used: (1) optimization, (2) numerical integration and (3) equalization generation of probability distributions [42]. Monte Carlo methods can solve any problem with a possible interpretation. Based on the number of factors involved, simulation can be complex but in general Monte Carlo can be worked in some simple defined steps:

- Identification of the transfer equation  
Transfer equation can be an engineering formula or it can be based on the created model by a Design Of Experiment (DOE) or Regression Analysis (RA).
- Definition of every input parameters  
For every factor in the transfer equation, the distribution of data should be determined. Each input can follow different distribution such as Normal Distribution, triangle, uniform distribution or any other types of distribution.
- Create random data  
To obtain a valid simulation, large and random data points should be created for each input. This data points investigate and simulate the behaviour of each parameter which would be seen over a long time.
- Analyze and simulate the output process  
By transferring the random data set to the selected equation, the outcome can be calculated. By running enough large quantity of input data, the final model can be predicted for the reliable decision over time, based on the variation of each input.

MC method can be used to all of the deterministic or stochastic problems which deterministic algorithms or analytical methods can not be profitably applied for them [43]. MC especially can be used for studying the system which characterizes by a large number of degrees of freedom.

After all discussion about MC, it is proper to remember that one of the problems of MC is that the values in the outer ranges of distribution are not represented in the samples and therefore, the impact of these data on the results can not be included in the simulation of the output. To overcome this problem, a large number of samples is needed. Furthermore, the new sample points which are generated in the MC method, are not considering the previously generated sample points.

### **3.3 Random Sampling Method**

After all discussion about MC, it is proper to remember that one of the problems of MC is that the values in the outer ranges of distribution are not represented. A part

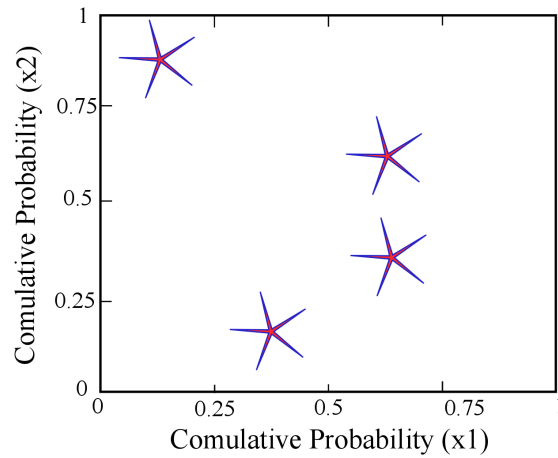


Fig. 3.1 Monte Carlo-sample point

of the sampling technique refers to Random sampling in which each sample present an equal probability of being chosen. A chose random sample proposed to be an unbiased representation of the total population. If for any reason, the sample does not present population, the variation is called a sampling error. Random sampling is known as one of the most simple forms of collecting data from the total population. Regarding the random sampling method it is necessary to define some aspects:

- **Sample Space** List all possible results of an experiment. Each possible result of such an experiment is presented by a single point in the sample space. The elements (or members) of the sample space can be thought of as all the different probabilities that may occur.
- **Probability** Provides a probability description of the quantitative of occurrence.
- **Realization or Observation** Realization, or the observed value of a random variable, is the value that is observed (what happened). Realization is indicated in lower case (to distinguish them from random variables).
- **Event** An event in a set of results of an experiments. Each subset of the a sample space is an event.
- **Random variable** A random variable can be a function of the X parameter defined from a sample space to a measurable space.

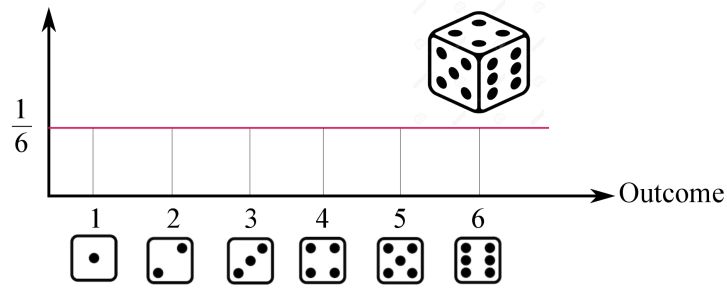


Fig. 3.2 Example of probability of a die.

Random variables come in two categories. They can be discrete or continuous. In a discrete random variable, the outcome of a random process can only take place with exact values and for continuous one, the outcomes come with continuous value as an output.

In the current thesis, discrete random variables are used in the samples and therefore, the impact of these data on the results can not be included in the simulation of the output. To overcome this problem, a large number of samples is needed. Furthermore, the new sample points which are generated in the MC method, are not considering the previously generated sample points.

### 3.3.1 Probability Distribution

The concept of a probability distribution is vitally important and play a key role in the sampling methods. In the previous part, the importance of a random variable is explained in some sort of function mapping results to real values, as well as how probabilities relate to these results. A simple example can be for a die, where the outcomes are equally like to happen, where the outcomes can either be a number between 1 to 6. In this case, the probability associated with each outcome ( $\frac{1}{n}$ ), where  $n$  stands for the total number of possible outcomes, see Figure. 3.2. Since each result has a related probability, this probability can be considered values versus the possible outcome values. In statistics, this is what we call probability distribution.



### 3.3.2 Description of Probability Density Function (PDF)

The concept of PDF (Probability Density Function) and CDF (Cumulative Distribution Function) are the important definitions to be introduced. PDF is a function which is described with two different parameters, a mean value and a standard deviation. When a function like normal distribution defines as a continuous probability distribution, this function call Probability Density Function or PDF. PDF is used for continuous random variables and the other function which is used for discrete random variables call Probability Mass Function. PDF is used to calculate the probability of a random variable within an interval:

$$P(a \leq X \leq b) = \int_a^b PDF(x)dx \quad (3.1)$$

$x \approx D$  is as a mathematical notation which mean  $X$  as random variable has the probability distribution  $D$ . In statistic, three concepts definition are very important, which are the sample mean, sample variance and sample standard deviation which are introduced respectively:

$$\bar{x} = \frac{x_1 + x_2 + \dots + x_n}{n} = \frac{\sum_{i=1}^n x_i}{n} \quad (3.2)$$

where  $\bar{x}$  is the mean value,  $x_1, \dots, x_n$  are the samples value, and  $n$  is the total number of sample points.

$$s^2 = \frac{\sum_{i=1}^n (x_i - \bar{x})^2}{n - 1} \quad (3.3)$$

where  $s^2$  is sample variance;

$$s^2 = \frac{\sum_{i=1}^n (x_i - \bar{x})^2}{n - 1} = \sqrt{\left( \frac{n \sum_{i=1}^n x_i^2 - (\sum_{i=1}^n x_i)^2}{n(n - 1)} \right)} \quad (3.4)$$

The square root of variance known as standard deviation  $s$ .

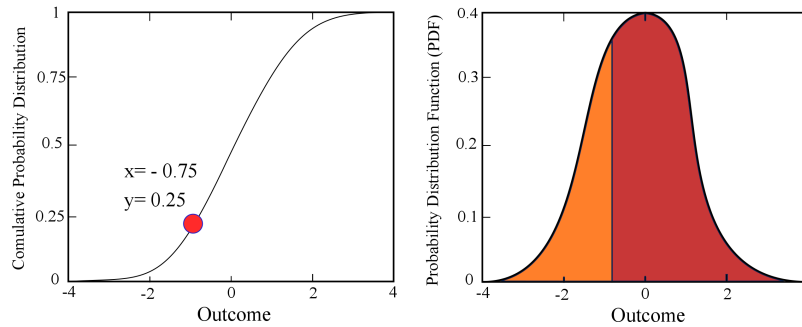


Fig. 3.3 A probability distribution expressed in cumulative form

### 3.4 Cumulative Probability Distribution function (CPD)

Any probability distribution may be expressed in a cumulative form which is one of the key concept. when there is Probability distribution function as an example normal distribution function, it can be represented in the form of cumulative distribution. In Figure. 3.3, an example of presenting data is shown. As an instance, when  $x = 0.75$  and  $y = 0.25$ , means 25% of the numbers of are below of  $-0.75$  and 75% of the numbers are upper than  $-0.75$ , which can present the meaning of cumulative probability function.

#### 3.4.1 Normal Distribution of Random Sampling

For an simple exam deflection of a beam defined as:

$$\delta = \frac{PL^3}{3EI} = \frac{4PL^3}{Ebh^3} \quad (3.5)$$

where  $\delta$  is the deflection of the beam,  $P$  is load,  $L$  is the length of the beam  $E$  stands as elasticity modulus and  $h$  is the beam height and  $I$  is inertia moment for rectangular cross-section beams that can be calculated as:

$$\mathbf{I} = \frac{bh^3}{12} \quad (3.6)$$

For a simple exam: For calculating the result (deflection) based on the Elasticity modulus, or/and length as the variables input, other parameters are supposed to be constant values to a better understanding of relationships between them. With MC

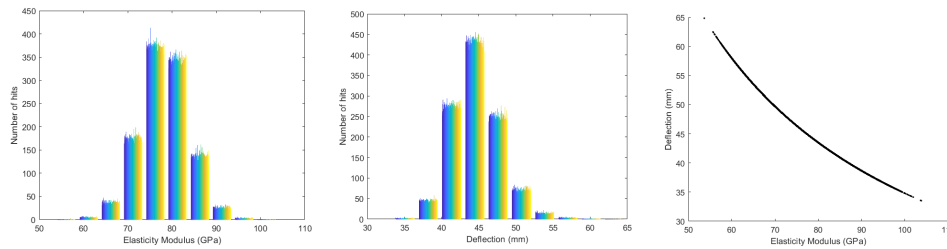


Fig. 3.4 Normal distribution for E by 1000000 random sampling points

method accurate stochastic results can be obtained through an accurate sampling of the input parameter. In the example of deflection of a beam, module elasticity is selected for generating normal distribution for sampling as one of the input data and other parameter had fixed values.  $P = 100$  N,  $L = 2$  m,  $a = 0.2$  m,  $b = 0.02$  m, and E distributed normally to show its effect on the deflection results, see Figure 3.4, where the number of hits can be present as PDFs.

### 3.4.2 Latin Hypercube Sampling Method

The LHS is one of the ways to generate random samples of the values of the parameters. LHS is widely used in MC simulation, due to drastically reducing the number of necessary runs to achieve reasonably accurate results [44]. LHS is based on the Latin square design, which presents a single sample in each row and column, and a hypercube refers to a cube with more than three-dimension. From multiple dimension and multiple hyperplanes, Latin square can be extended. The most important reason for using LHS is due to saving processing time through Monte Carlo running [45]. The purpose of LHS is to recreate the input distribution with fewer samples. The simple steps for doing LHS can follow:

- The key factor in this method is stratification of the input probability distribution.
- Stratification divides the cumulative curve into equal intervals.
- A sample is then randomly taken from each interval or stratification.

The example of LHS is bring for one dimension and two dimensions as shown in Figure.3.5 and Figure. 3.6, respectively.

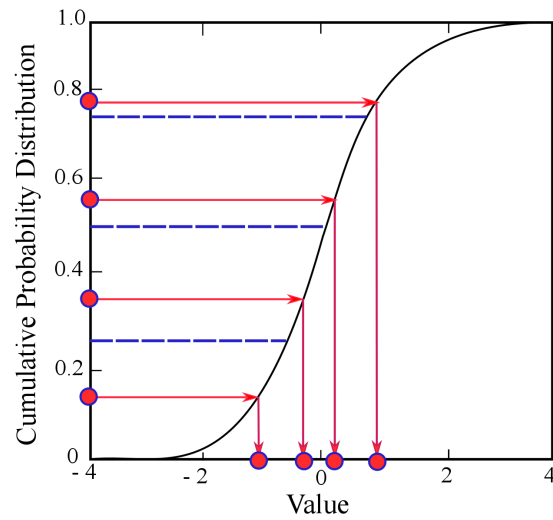


Fig. 3.5 Latin hypercube sampling for one dimension- Only one sample per stratification

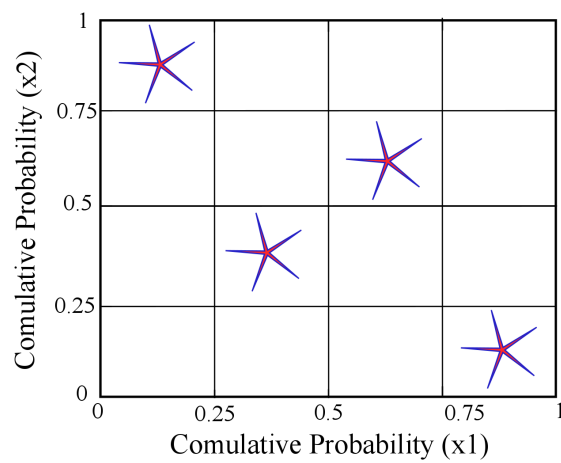


Fig. 3.6 Latin hypercube sampling for two dimensions- Only one sample in each row and each column

In the circumstances of statistical sampling, a square grid including sample position is Latin Square if and only if there is only one sample in each row and each column.

LHS can define for any arbitrary dimensions, whereby each sample is only in one in each-axis, aligned hyperplane containing it. MC can call as a memoryless sampling due to not taking into account the previous sample point while LHS remembered in which row and column sample point was taken (memory).

## 3.5 Surrogate Model

An surrogate model is an engineering method used when the desired result is easily measured directly, so an outcome model is used instead. Most engineering design problems require experimental testing and/ or simulation to evaluate design objective function and design constraints as a function of design variables. A model is constructed based on modelling the response of simulator to a limited number of intelligently chosen data points. When only a single design variable is involved, the process is known as curve fitting. The most popular surrogate models are polynomial

The most popular polynomial surrogate model that are used in current thesis are response surface (RS) and artificial neural network (ANN) which will explained in detail in next section and chapters 5.

- Response Surface (RS) and Artificial Neural Network (ANN)

In the current thesis Response Surface and Artificial Neural Network are used through analysis of composite structures, see chapter 5.

### 3.5.1 Response Surface

For enhancing the Monte Carlo Response surface can be obtained by polynomial approximation based on:

- Taylor's series expansion.
- Newton's series expansion.

Here, in this report, Newton's Series are using for calculation of RS. By Random exploration of RS, the output can be achieved.

To enhance the performance of MC method to reduce its high computational costs, MC can be coupled with RS. Statistically, RS express the relationship between different variables in connection with one or more outcome variables [46]. RS shows the approximation of system outputs in terms of some favourite inputs. Output data collection can be done by random RS exploration. There are several methods for calculating RS: polynomial regression, Surrogate model, radial basis functions, and the Kriging method. As an example, for a approximation of the true input-output function, second order polynomial models can be typically used in the from [47]:

$$y = b_0 + \sum_{j=1}^k b_j X_j + \sum_{j=1}^k \sum_{i=1}^k b_{ij} X_i X_j \quad (3.7)$$

where  $b_0$ ,  $b_j$  and  $b_{ij}$  are the regression coefficients with  $i, j = 1, 2, \dots, k$  and  $X_i$  are the  $k$  input variables.

Besides, in current research RS is combined with LHS method as well, which will explain in detail in chapters 5.

### 3.5.2 Artificial Neural Network (ANN)

When the problem is faced with large amount of results, Artificial Neural Network (ANN) can be considered as a appropriate technique to conduct the describing the correlation between different parameters from each other. ANN does not need any prior knowledge about the form of function, NN describes the final dependencies between the parameters. In this study, we will define and explain the NN approach, how it is created, used, and validated. We will then apply this technique as a post-processing method to the database created through GA optimization of VAT in buckling analysis, to show the accuracy of optimization results in Chapter 5.

#### Neural network and machine learning

In general, it can be said that NN includes machine learning algorithms, which lead to the classification of input data and the provision of optimal output. This is why NN can be considered as part of the machine learning process. In addition, Deep

learning (DL) is referring to the depth of layers in a NN. A NN with more than three layers would be inclusive of the inputs and outputs can be investigated as a deep learning algorithm. A deep learning model would require more data points to improve its accuracy while a machine learning models need fewer data provided the underlying data structure. In fact, deep learning is used in the problem with high complexity. Finally, artificial intelligence (AI) is the broadest term used to classify machines that mimic human intelligence, see Figure 3.7. AI is applied for predicting, automating, and optimizing tasks that humans have historically done, such as decision making, and translation.

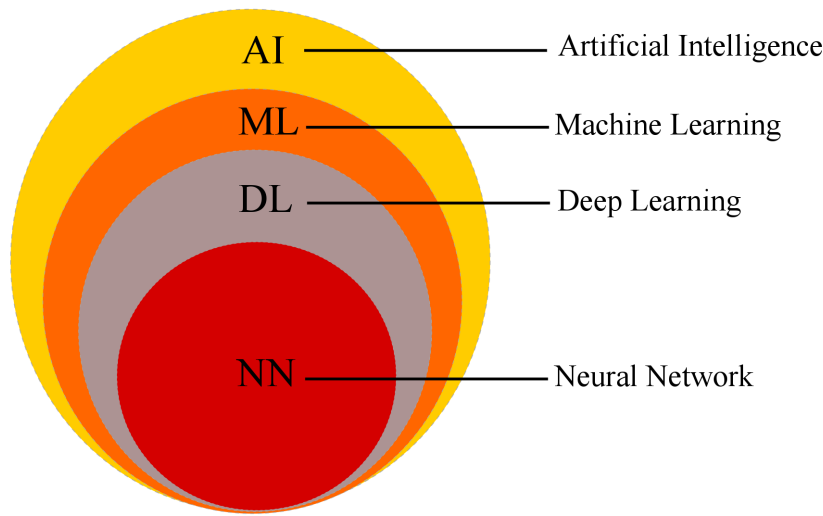


Fig. 3.7 Comparison of artificial intelligence, machine learning, deep learning and neural network.

The supervised training concept describes a nonlinear variant of classical statistical modelling approaches. A neuron forms one NN single unit. This notation is a nonlinear parametric algebraic function with finite values determined by [48]:

$$o_j = \varphi\left(\sum_{i=0}^n w_{ij}x_i\right) = \varphi(w_{oj} + \sum_{i=0}^n w_{ij}x_i) \quad (3.8)$$

where  $o_j$  is the output of  $j^{th}$  neuron. This formulation is presented as the artificial neuron which is formed of the elements described in Figure 3.8 which are:

The input values  $(x_1, x_2, \dots, x_n)$ , which can be the input parameters for the evaluated neuron or the output of other neurons in the same NN,  $n$  stands as the inputs number, for example,  $i = 0$ ,  $x_0$  input is given a value +1 with  $w_{oj}$  as weight

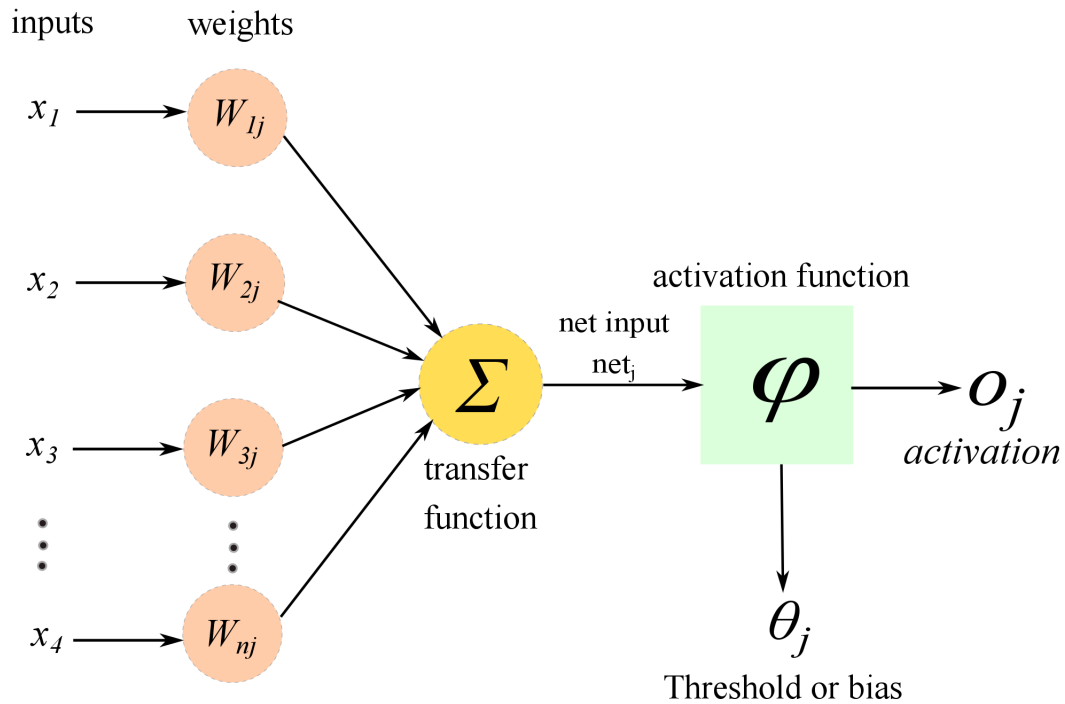


Fig. 3.8 One artificial neural network within the function of activation.

and  $b$  noted for bias. Transfer function is  $\Sigma$  which is a linear combination of sum up the inputs of  $x_{ij}$  and weighted with the parameter of  $w_{ij}$ . Moreover,  $\varphi$  is an activation function which can be a linear or non-linear function which transforms the weighted input in the neuron to the output (response). And finally,  $o_j$  refers to the overall activity of  $j^{th}$  neuron respect to its level of activation [48]. Finally,  $o_j$  refers to  $j^{th}$  neurons that is the entire activity related to its activation level [48].

There are three different layers which are related to a simple ANN design that can be defined as input layers, hidden layers and also output layers. The input values get some weight and bias and make the data as a piece of valuable information. Then, the information will modify by an activation function from every hidden and output layers until the final output reached, see Figure 3.9.

### Creating the ANN

For creating an optimal ANN, different parameters are required to be selected. For example, ANN type, the paradigm of learning, algorithms of training and also



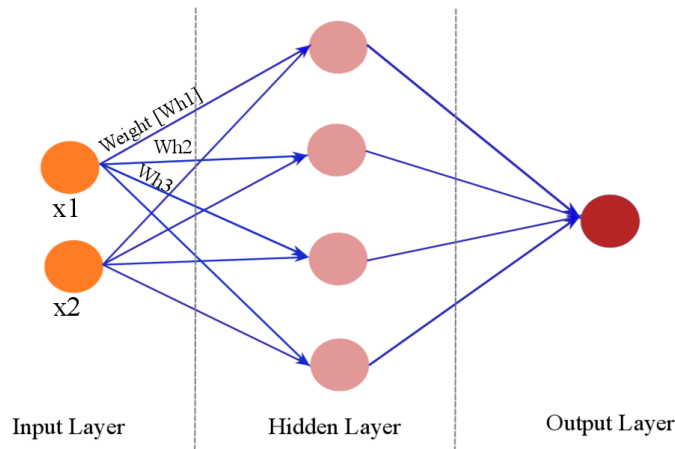


Fig. 3.9 Neural network definition diagram,  $x_1$ ,  $x_2$  example of inputs,  $wh_1$ ,  $wh_2$ ,  $wh_3$  example of weights.

the hidden number of neurons should be recognized. Moreover, it is appropriate to normalize the dataset of samples by using the formulation of maximum and minimum values [48].

### Neural network learning methods:

#### I. Supervised learning

Also called classification, humans provide their categorized information to the neural network as a collection of data. In this case, the NN is expected to find the output relationship and the input data. Supervised NN is trained to produce desired outputs in response to sample inputs, making them particularly well suited for modelling and controlling dynamic systems, classifying noisy data, and predicting future events.

#### II. Unsupervised learning

In unsupervised learning, also known as clustering, the goal is to find common ground. In this method, there is no specific characteristic for identifying similarities. Most of the data in the world are unlabeled data.

### Normalizing

One of the most important parameters that directly effect on the efficiency of neural network training and accelerating the process, refers to normalization. The aim is to include both inputs (I) and outputs or target (T) in one range between  $-1$  and  $+1$  using following equations [48]:

$$I_n = 2 \times \frac{I - I_{min}}{I_{max} - I_{min}} - 1; \quad T_n = 2 \times \frac{T - T_{min}}{T_{max} - T_{min}} - 1 \quad (3.9)$$

where  $I_n$  and  $T_n$  are normalized input and target, respectively. Furthermore,  $I_{min}$  and  $I_{max}$ ,  $T_{min}$  and  $T_{max}$  are respectively the minimum and maximum values for the input  $I_n$  and the target  $T_n$ .

### Choice of the number of hidden neurons

Akaike's information criterion (AIC) can calculate the optimal hidden layer number based on the model quality with a statistical formulation [49]:

$$AIC = L \cdot \ln(MSE) + 2 \cdot m \quad (3.10)$$

In the Eq. 3.10,  $L$  stands for sample number which is considered in the training phase,  $m$  express for synapse weight through the network that can calculate easily by the sum of input and output multiple with the hidden neurons. It can also count as the ANN DOF. In the next step, it is mandatory to calculate the mean square error (MSE). The weight of synapses and bias of them in ANN can be obtain using error minimizing [50]:

$$MSE = \frac{1}{L} \sum_{l=1}^L (d_l - y_l)^2 \quad (3.11)$$

where  $d_l$  denotes as value of normalized target and  $y_l$  stands as normalized generated output for the sample number 1. In describing the AIC with lower value indicate the better model of ANN, for more details, see [51–53]. Furthermore, the optimal hidden neuron number can be obtained from optimal performance corresponding to the minimum value of Root Mean Squared Error (RMSE), that is

the MSE standard deviation [48]:

$$RMSE = \sqrt{MSE} = \sqrt{\frac{1}{L} \sum_{l=1}^L (d_l - y_l)^2} \quad (3.12)$$

### Training algorithms

Then, a training process will act progressively for the reduction of the total error of the network using the iteratively modifying the weights.

### Coefficient of determination

For evaluating the performance of the ANN model and minimizing the error, the value of targets is compared with the generated results in the neural network. Usually, some statistical parameters are used for measuring the model reliability and also validating of that model. In this case, the MSE and determination coefficient is called  $R^2$ . Therefore, in the next step, the regression plot is obtained to show the correlation between outputs and target three aims consideration:

- The more  $R^2$  is near to 1 a better fitted model can be achieved.
- Regression plot can help for train and test of every model of neural construction.
- The output values, calculated through the training and testing process.
- Set can be correlated with the values of the target.
- The bubbles lines represent the best possible fit  $R^2$ .
- The solid lines shows the real correlation between the computed output and initial target.

The detailed current research related to the coefficient of determination will discuss in the following section.

## 3.6 Conclusion

This chapter described the different sampling methods which can use through evaluation of structural analysis in CUF framework. First MC method introduced which inherent random sampling. This method can be used to solve math and physics problems when other solutions encounter problems and obstacles. MC was able to use in optimization, numerical integration and equalization generation of probability distributions. Furthermore, random sampling explained in detail, probability distribution and probability density function as well. At the final subsection, Latin hypercube is introduced to show how it can reduce the computational cost. Besides, RS introduced to enhance the capability of MC and LHS. Finally, the ANN also described in particular based on the ANN sequence which is used in current thesis.

# Chapter 4

## Numerical Results of VAT

### 4.1 Introduction

Composite materials are presented as the lightweight design flexibility or tailoring materials for desired demands in the laminate stacking sequence aerospace industries. The benefits of composite materials are to provide high strength and high stiffness regard to the weight, identified fatigue strength, wear, and corrosion resistance provided with the high performance and reliability [54], [55]. Buckling analysis is one of the significant behaviour which can reach to the required resistance with constant stiffness (CS) fibre angles through the thickness of each layer in the conventional composites, while via the generation of a new class of composites known as variable stiffness (VS) pointed as laminate tailoring, with embrace the curvilinear fibre paths to the spatially, and hence vary in-plane stiffness, buckling response can manifest significantly betterment [4], [56], in compared with CS counterpart. The stiffness variation propose in discrete model such as Patch design or introducing continues fiber path curvilinear which described as VAT laminates [57], [58], [59], [60]. Setoodeh et al. [61] showed that in-plane loads and buckling resistance in the stiff zone with greater satisfied, and not in the critical zone can present higher buckling load adequately in VAT plates based on finite element models [5]. Lopes et al [62], illustrate the advantages of variable stiffness composite in compressive buckling and failure modes of the first ply by taking advantage of finite element models as the numerical simulation.

Stability analysis of simply-supported rectangular plates under non-uniform uniaxial compression using rigorous and approximate plane stress solutions [63]. Buckling introduced together with the significant failure in the thin-walled structure and thin plates [64], [65], [66]. A classical finite element can not grantee continuity and smooths of the variable angle tow fibres with the presumption of them straight. Following by discretization of the fibres, a large number of elements and even higher by using refined mesh size, which may influence on the buckling analysis results by providing a wide variety of error including higher computational time due to higher Degree of Freedom (DOF) [67]. For buckling analysis in an aerospace application, Carrera Unified Formulation can introduce as a capable higher-order beam model (1D) to represent displacement as regards arbitrary unknown over the cross-section by Taylor-like expansion with a generic  $N$ -the order which obtained [68], [69] or Lagrange-like polynomial expansion by expressing [41] for linear buckling analysis. In anisotropic composite materials, refined 1D CUF beam organise to display as Component-wise [70],[71] or layer-wise model [21], to achieve better solution in contrast with commercial code for classical beam, plates and solid [72]. Lately, the CUF procedure successfully employed to perform free vibration analysis of VAT structures by Viglietti et al. [73], [74] and [75]. This chapter present linear buckling and vibration analysis which modelled for variable stiffness composite by 1D CUF beam model, for a thin plate with sixteen layers and then the results will be compared with FEM to show the capability of CUF for decreasing the DOF, computational time with well presented the continuity of variable stiffness fibre and accurate model.

### 4.1.1 VAT laminate equation

The linear variation of the fiber orientation angle in the VAT composites can be designed based on the curvilinear fiber path that linearly varies along the beam axis ( $y$ ):

$$\theta(y) = 2(T_1 - T_0) \frac{|y|}{a} + T_0 \quad (4.1)$$

where  $\theta(y)$  shows the fiber orientation angle which is varied along the  $y$ -axis.  $T_0$  stands for the fiber orientation angle in the center of the plate  $x = 0$  and  $T_1$  is the fiber orientation angle at the edges,  $x = \pm \frac{a}{2}$ .  $a$  presents the wide of the VAT panels, see Figure 4.1.

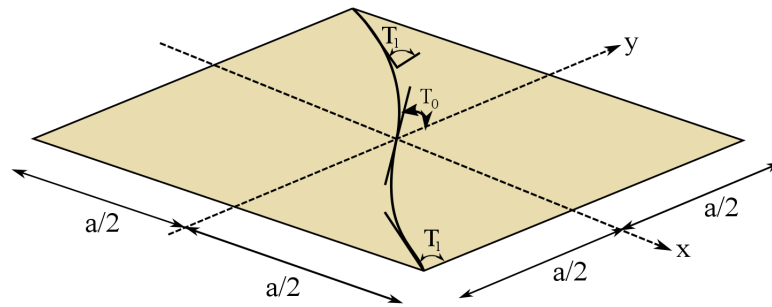


Fig. 4.1 Variable angle tow,  $T_0$  and  $T_1$ .

### 4.1.2 Buckling Analysis

The convergence analysis is used for one layer of the VAT plate in the CUF procedure considering various kinematics and beam elements. Eventually, the outcomes are validated using the FE model, which is a built-in Nastran model. The properties of the square VAT lamina are as follows:  $E_1 = 50$  GPa,  $E_2 = E_3 = 10$  GPa,  $G_{12} = G_{13} = G_{23} = 5$  GPa,  $\nu_{12} = 0.25$ , with a thickness of 0.02 m and equal length and wide of  $a = b = 1$  m. The linear fiber orientation distribution  $\langle T_0 | T_1 \rangle = \langle 75^\circ | 15^\circ \rangle$  exposed to the boundary condition is as illustrate in Figure 4.2.

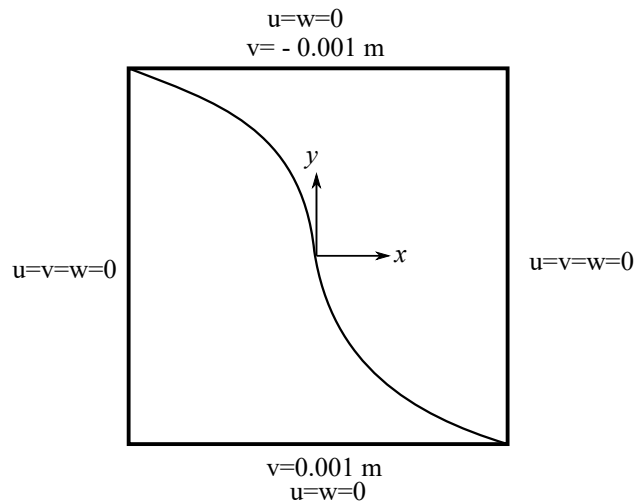


Fig. 4.2 Boundary condition of a single VAT laminate ( $\langle 75^\circ | 15^\circ \rangle$ ).

Based on the studied CUF model,  $B3$  beam elements are used along the beam axis ( $y$ ) with two different polynomial expansions  $L9$  and  $L16$  to allow the beam kinematics approximation on the cross-section ( $xz$ -coordinates). First, to investigate the convergence of the models, refinement is performed along the  $z$ -direction with

$n_z^* = (1, 3, 6, 9)$  considering the  $L9$  Lagrange polynomial expansions on the cross-section. In this example, the number of elements in the  $x$  and  $y$  directions ( $10B3$ ) was fixed on the symmetric square plate (see Figure 4.3). In the following step, refinement was given along the beam axis with  $n_y^* = (5, 7, 10, 15, 20, 30) B3$ . This refinement was performed considering both the  $L9$  and  $L16$  expansions on the cross-section, to demonstrate the sensitivity of the results, as shown in Figures 4.4 and 4.5, respectively. Table 4.1 reviews the results achieved for the first and second critical

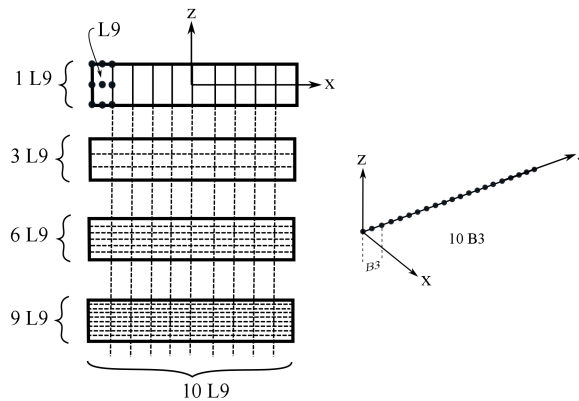


Fig. 4.3 Refined elements over the cross-section.

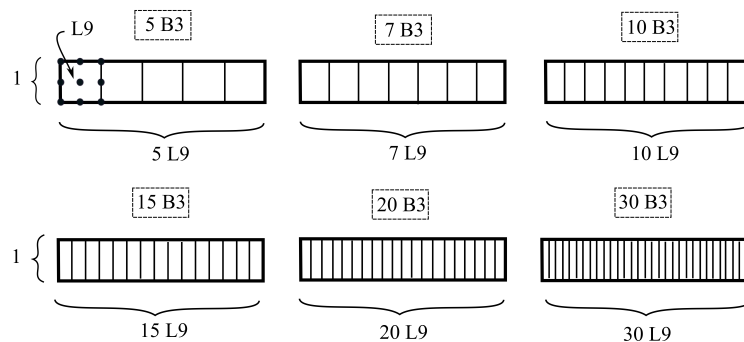


Fig. 4.4 Refined elements through the beam with  $L9$  expansion over the cross-section.

buckling loads for the models, which designate the convergence of the intended CUF approach with a significantly lower number of DOF as compared to those in the Nastran results (see Figures 4.6 and 4.7). Moreover, the results show that the CUF model with  $L9$  polynomial expansions and  $10B3$  beam elements can converge adequately compared to the Nastran model. Consequently, this approach can be employed for additional modelling.



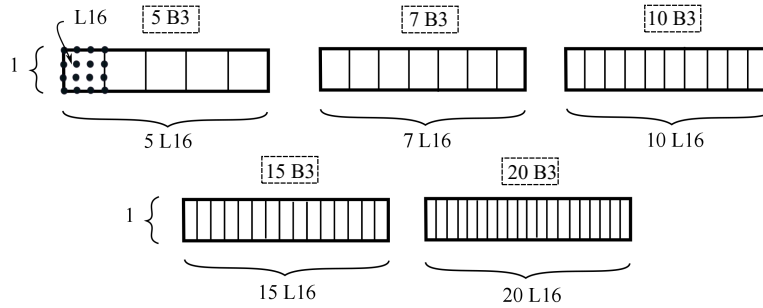


Fig. 4.5 Refined elements through the beam with L16 expansion over the cross-section.

	DOF	1st Critical Load	2nd Critical Load	$n_z^*$	$n_x^* = n_y^*$
	61206	1.92 N	2.04 N	-	-
Nastran	242406	1.85 N	2.02 N	-	-
	964806	1.85 N	2.02 N	-	-
	3969	1.91 N	2.04 N	1	10
	9261	1.90 N	2.03 N	3	10
CUF L9	17199	1.90 N	2.03 N	6	10
	25137	1.90 N	2.03 N	9	10
	1089	2.13 N	2.57 N	1	5
	2025	1.98 N	2.18 N	1	7
	3969	1.91 N	2.04 N	1	10
CUF L9	8649	1.87 N	1.98 N	1	15
	15129	1.86 N	1.97 N	1	20
	2112	1.97 N	2.48 N	1	5
	3960	1.92 N	2.14 N	1	7
CUF L16	7812	1.88 N	2.02 N	1	10
	17112	1.86 N	1.97 N	1	15
	30012	1.85 N	1.96 N	1	20

$n_z^*$  number of elements through the thickness  
 $n_x^*$  number of elements along the width  
 $n_y^*$  number of elements along the beam axis

Table 4.1 Linear elastic buckling estimates according to the number of elements through the beam and cross-section.

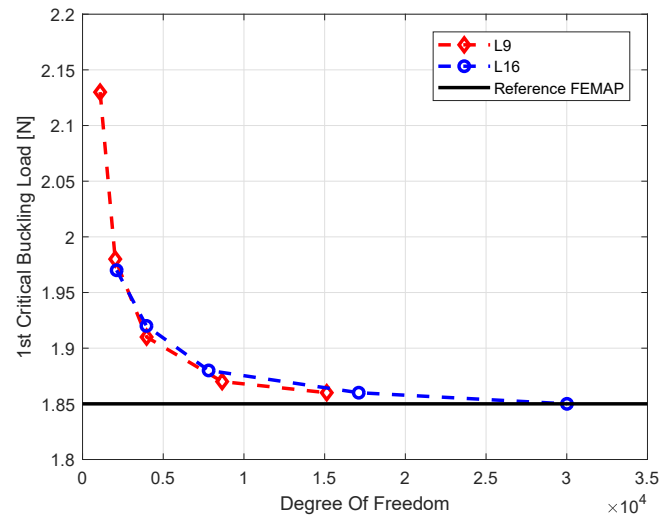


Fig. 4.6 First critical buckling load vs. DOF, based on the refinement of the beam elements.

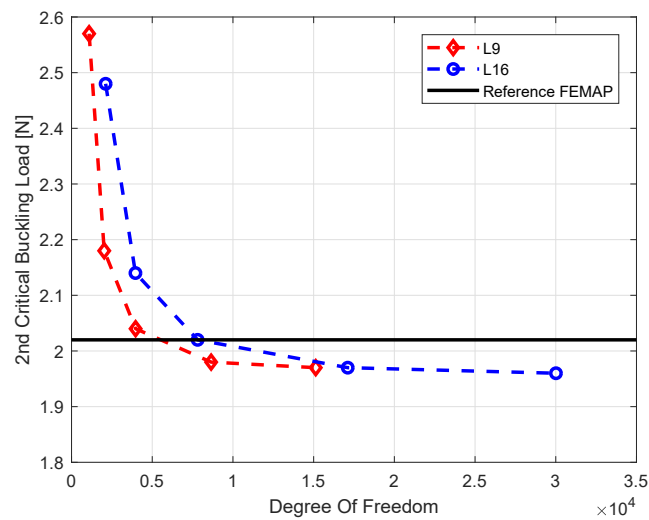


Fig. 4.7 Second critical buckling load vs. DOF, based on the refinement of the beam element.

### 4.1.3 Pre-buckling and buckling analyses of a sixteen-layer VAT plate

As explained in the coming sections, the CUF framework was used to model the VAT composites for buckling problems, and the results were verified using the ABAQUS model detailed in [67]. A 16-ply balanced symmetric square plate with a length of  $a = 254$  mm was designed with a fiber angle orientation of  $[\langle T_0|T_1 \rangle \langle -T_0|-T_1 \rangle / \langle -T_0|-T_1 \rangle \langle T_0|T_1 \rangle]_4$  under a pure compression load, as shown in Figure 4.8. The lamina properties are set as follows:  $E_1 = 181$  GPa,  $E_2 = 10.270$  GPa,  $G_{12} = G_{13} = 7.170$  GPa,  $G_{23} = 3.780$  GPa,  $\nu_{12} = 0.28$ , and ply thickness of 0.15 mm. The boundary condition (B.C.) corresponds to a fully simply supported (SSSS) configuration, and the fibre path represents the curvilinear function as displayed in equation 4.1. The CUF approach is used with 10B3, 15B3, and 20B3

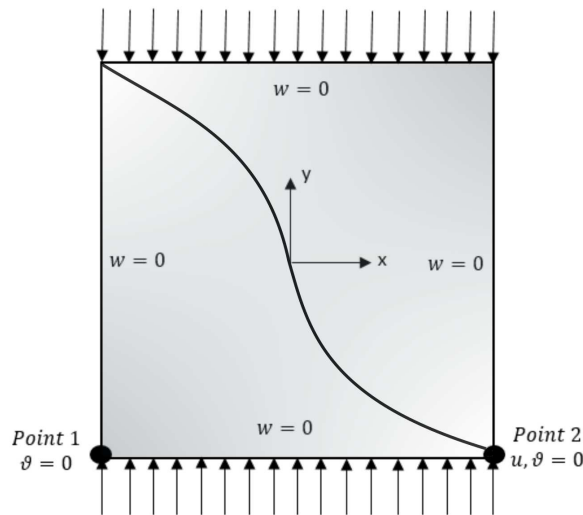


Fig. 4.8 SSSS boundary condition (B.C.) of the plate.

beam elements corresponding to 160, 240 and 320  $L9$  elements, respectively, within the cross-section to compare the FEM approach employing the quadratic element [67]. As described in Table 4.2, the CUF model converged with a significantly lower number of DOFs compared to that for the FEM model. It could be noted that the CUF model can obtain such accuracy using only a small number of DOFs. The different numbers of beam elements based on the CUF models for the first six buckling modes are shown in Figure 4.9. Besides, it can be noted that refining the elements along the beam axis promotes the convergence of the buckling load results.

In addition, a pre-buckling analysis was presented to determine the non-uniform

Beam Element	DOF	Mode 1		Mode 2		Mode 3		Mode 4		Mode 5	
Ref. [67] (ABAQUS)	387205	$F_{cr1} = 13.62$	$kN$	$F_{cr2} = 21.62$	$kN$	$F_{cr3} = 35.40$	$kN$	$F_{cr4} = 54.46$	$kN$	$F_{cr5} = 56.01$	$kN$
CUF 10B3	43659	$F_{cr1} = 13.78$	$kN$	$F_{cr2} = 22.03$	$kN$	$F_{cr3} = 37.67kN$		$F_{cr4} = 55.24$	$kN$	$F_{cr5} = 60.57$	$kN$
CUF 15B3	95139	$F_{cr1} = 13.61$	$kN$	$F_{cr2} = 21.69$	$kN$	$F_{cr3} = 35.94$	$kN$	$F_{cr4} = 54.51$	$kN$	$F_{cr5} = 57.65$	$kN$
CUF 20B3	166419	$F_{cr1} = 13.67$	$kN$	$F_{cr2} = 21.68$	$kN$	$F_{cr3} = 35.69$	$kN$	$F_{cr4} = 54.60$	$kN$	$F_{cr5} = 56.69$	$kN$

Table 4.2 Buckling mode shapes in the SSSS B.C., as obtained using the CUF and FEM approaches, for  $[\langle 60^\circ | 15^\circ \rangle \langle -60^\circ | -15^\circ \rangle / \langle -60^\circ | -15^\circ \rangle \langle 60^\circ | 15^\circ \rangle]_4$ .

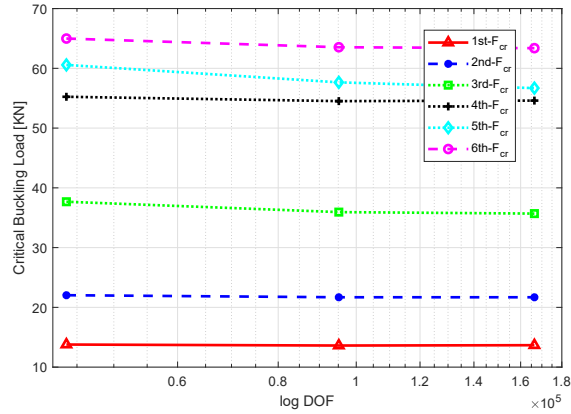


Fig. 4.9 Critical buckling load in the first six modes vs. the natural logarithm of the DOF for 10, 15, and 20 beam elements.

stress distribution and the effect of the in-plane load on the buckling behaviour of the VAT composite plates. Afterwards, the pre-buckling and buckling analyses were performed respecting stacking sequences. Here,  $T_0$  is a fixed angle, and  $T_1$  grows from  $0^\circ$  to  $90^\circ$  in steps of  $\pi/12$ , as described in Table 4.3. In these instances, the beam elements are fixed on 10B3.

In particular, the results for the displacement and stress vary with changes in the fibre orientation on the edge of the laminates. Under the SSSS B.C., by raising  $T_1$  from  $0^\circ$  to  $90^\circ$ , the magnitude of maximum displacement displays a decreasing oscillation on the edges and the smallest maximum amplitude corresponds to lay-up 4, as shown in Table 4.4. The most optimal design of the VAT corresponds to the one in which a stress resultant ( $\sigma_{xx}$ ,  $\sigma_{yy}$ ) was redistributed away from the central

Lamination scheme	Lay-up design
	$[\langle T_0 T_1 \rangle \langle -T_0 -T_1 \rangle / \langle -T_0 -T_1 \rangle \langle T_0 T_1 \rangle]_4$
Lay-up 1	$[\langle 60^\circ 0^\circ \rangle \langle -60^\circ 0^\circ \rangle / \langle -60^\circ 0^\circ \rangle \langle 60^\circ 0^\circ \rangle]_4$
Lay-up 2	$[\langle 60^\circ 15^\circ \rangle \langle -60^\circ -15^\circ \rangle / \langle -60^\circ -15^\circ \rangle \langle 60^\circ 15^\circ \rangle]_4$
Lay-up 3	$[\langle 60^\circ 30^\circ \rangle \langle -60^\circ -30^\circ \rangle / \langle -60^\circ -30^\circ \rangle \langle 60^\circ 30^\circ \rangle]_4$
Lay-up 4	$[\langle 60^\circ 45^\circ \rangle \langle -60^\circ -45^\circ \rangle / \langle -60^\circ -45^\circ \rangle \langle 60^\circ 45^\circ \rangle]_4$
Lay-up 5	$[\langle 60^\circ 60^\circ \rangle \langle -60^\circ -60^\circ \rangle / \langle -60^\circ -60^\circ \rangle \langle 60^\circ 60^\circ \rangle]_4$
Lay-up 6	$[\langle 60^\circ 75^\circ \rangle \langle -60^\circ -75^\circ \rangle / \langle -60^\circ -75^\circ \rangle \langle 60^\circ 75^\circ \rangle]_4$
Lay-up 7	$[\langle 60^\circ 90^\circ \rangle \langle -60^\circ -90^\circ \rangle / \langle -60^\circ -90^\circ \rangle \langle 60^\circ 90^\circ \rangle]_4$

Table 4.3 Different lay-up designs for the laminate.

region of the plate toward the transverse edges. Furthermore, the displacement was redistributed in the least critical zone in the case of lay-up 4. Accordingly, the load redistribution can be a key factor to enhance the buckling behaviour in VAT laminates. A non-uniform pre-buckling stress state under constant uniaxial compression was observed, which considerably affected the buckling behaviour of the VAT laminate. In the buckling problem, as noted in Table 4.5, the variation of the fibre orientations ( $T_1$ ), mode shapes, and critical buckling loads led to significant changes. Precisely, a VAT plate with changes in the edge fibre orientation presented a different behaviour under a buckling load. Moreover, while  $T_1$  was increased from  $0^\circ$  to  $45^\circ$ , the first critical buckling load raised by 47.64%. The mode shapes and critical buckling loads were noted to be strongly dependent on the variation of the fibre orientations ( $T_1$ ). For example, when  $T_1$  was increased from  $0^\circ$  to  $45^\circ$ , the first critical buckling loads were increased by 47.64%.

Nevertheless, the results for  $T_1 = 0^\circ - 90^\circ$  corresponding to a steering angle of  $T_1 = 45^\circ$  included a remarkable rise in the first buckling load. With the change in  $T_1$ , the predicted buckling behaviour of the VAT plate in higher modes became more inaccurate. The sensitivity of the buckling load to the change in  $T_1$  for the first six critical loads is shown in Figure 4.10. These results confirm that the proposed CUF model can improve evaluate the geometric stiffness by predicting different critical buckling loads, as shown in Figure 4.11. It can be considered that the existing higher-order model can perform fine for complex B.C.s, geometries, and loading systems. Moreover, validate the performance of VAT laminates, several investigations were performed, such as the free-vibration analysis, as defined in the subsequent sections.

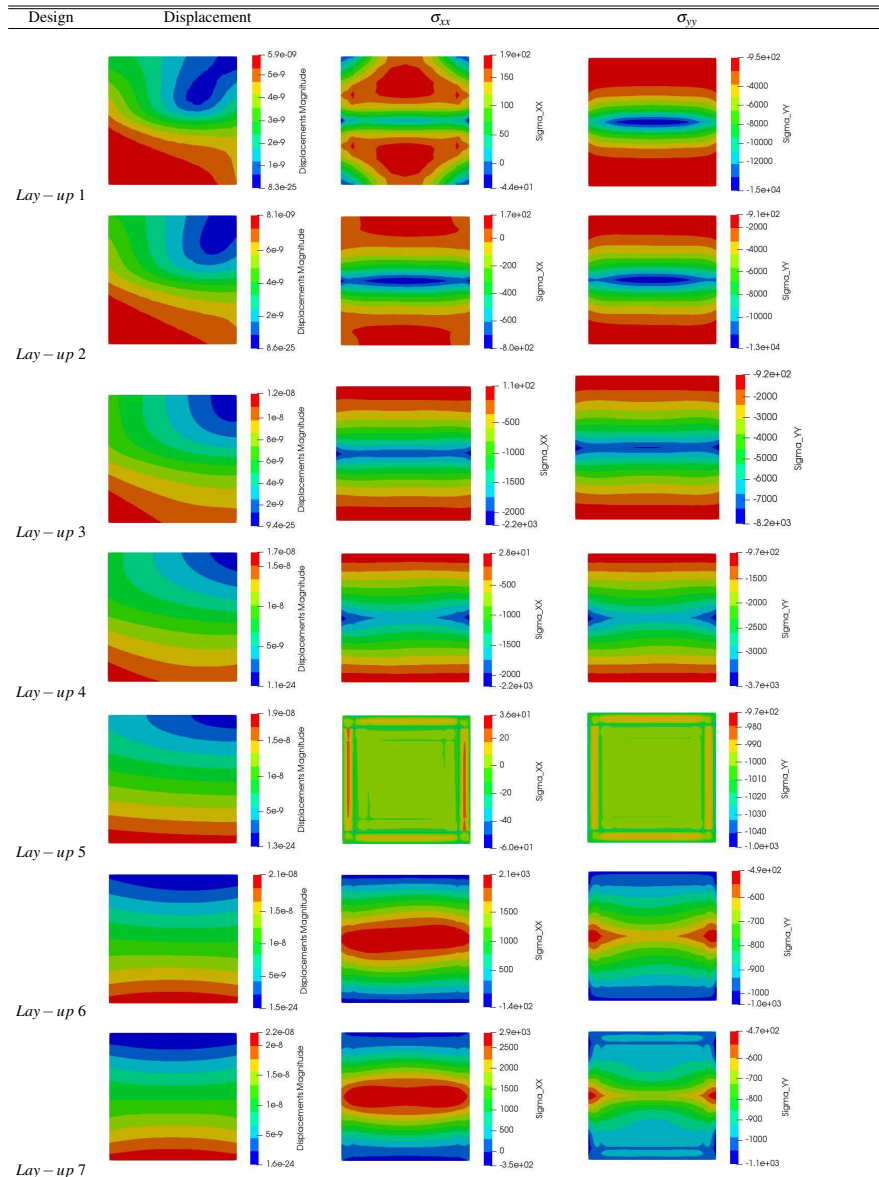


Table 4.4 Pre-buckling displacement and stress distribution for seven different designs of VAT fiber orientation angles under the SSSS B.C.

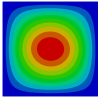
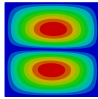
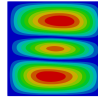
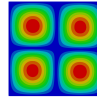
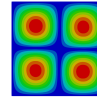
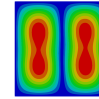
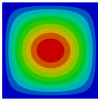
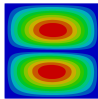
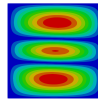
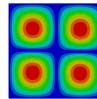
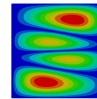
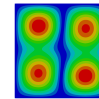
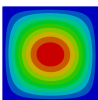
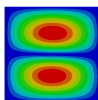
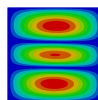
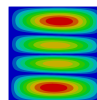
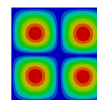
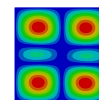
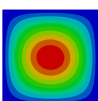
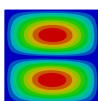
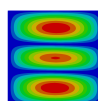
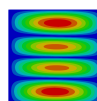
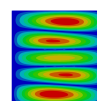
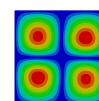
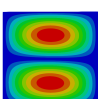
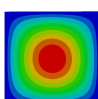
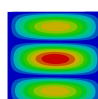
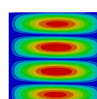
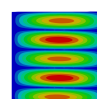
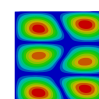
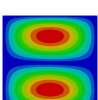
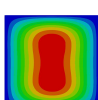
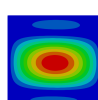
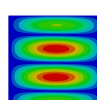
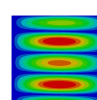
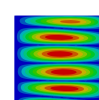
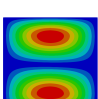
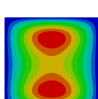
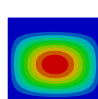
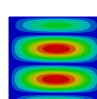
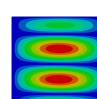
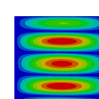
Design	Mode 1	Mode 2	Mode 3	Mode 4	Mode 5	Mode 6
Lay-up 1	 $F_{cr1} = 11.44 \text{ kN}$	 $F_{cr2} = 23.60 \text{ kN}$	 $F_{cr3} = 42.40 \text{ kN}$	 $F_{cr4} = 52.08 \text{ kN}$	 $F_{cr5} = 54.69 \text{ kN}$	 $F_{cr6} = 68.99 \text{ kN}$
Lay-up 2	 $F_{cr1} = 13.78 \text{ kN}$	 $F_{cr2} = 22.03 \text{ kN}$	 $F_{cr3} = 37.67 \text{ kN}$	 $F_{cr4} = 55.24 \text{ kN}$	 $F_{cr5} = 60.57 \text{ kN}$	 $F_{cr6} = 64.98 \text{ kN}$
Lay-up 3	 $F_{cr1} = 16.22 \text{ kN}$	 $F_{cr2} = 20.62 \text{ kN}$	 $F_{cr3} = 32.61 \text{ kN}$	 $F_{cr4} = 50.89 \text{ kN}$	 $F_{cr5} = 59.69 \text{ kN}$	 $F_{cr6} = 67.66 \text{ kN}$
Lay-up 4	 $F_{cr1} = 16.89 \text{ kN}$	 $F_{cr2} = 18.29 \text{ kN}$	 $F_{cr3} = 26.46 \text{ kN}$	 $F_{cr4} = 39.44 \text{ kN}$	 $F_{cr5} = 57.42 \text{ kN}$	 $F_{cr6} = 62.02 \text{ kN}$
Lay-up 5	 $F_{cr1} = 14.56 \text{ kN}$	 $F_{cr2} = 14.93 \text{ kN}$	 $F_{cr3} = 19.50 \text{ kN}$	 $F_{cr4} = 27.62 \text{ kN}$	 $F_{cr5} = 39.17 \text{ kN}$	 $F_{cr6} = 54.04 \text{ kN}$
Lay-up 6	 $F_{cr1} = 10.44 \text{ kN}$	 $F_{cr2} = 11.28 \text{ kN}$	 $F_{cr3} = 14.05 \text{ kN}$	 $F_{cr4} = 18.90 \text{ kN}$	 $F_{cr5} = 26.63 \text{ kN}$	 $F_{cr6} = 36.73 \text{ kN}$
Lay-up 7	 $F_{cr1} = 7.76 \text{ kN}$	 $F_{cr2} = 8.42 \text{ kN}$	 $F_{cr3} = 11.43 \text{ kN}$	 $F_{cr4} = 14.71 \text{ kN}$	 $F_{cr5} = 21.05 \text{ kN}$	 $F_{cr6} = 27.68 \text{ kN}$

Table 4.5 First six critical buckling mode shapes under the SSSS B.C. based on six different lay-up designs.

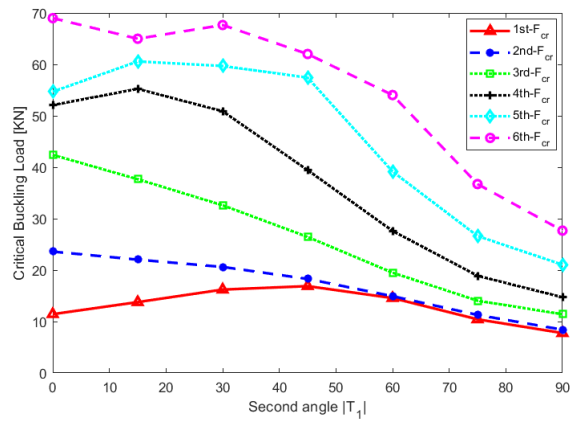


Fig. 4.10 First six critical buckling mode shapes under different  $T_1$ .

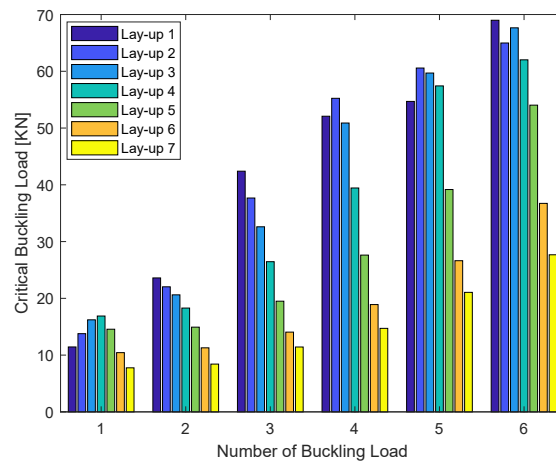


Fig. 4.11 First six critical buckling mode shapes under different  $T_1$  values vs. number of modes.



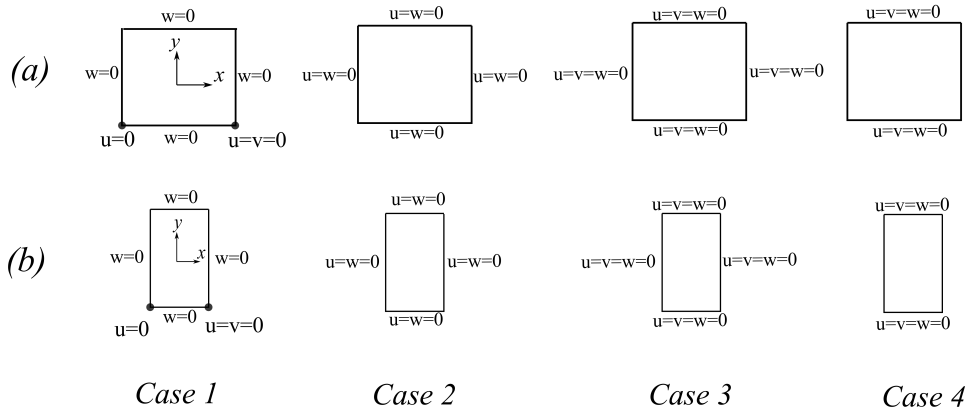


Fig. 4.12 Four-edge plates subjected to four different B.Cs, case 1 (SSSS), case 2 (SSSS-I), case 3 (CCCC) and case 4 (CFCF).

#### 4.1.4 Free Vibration Analysis

In this analysis, the VAT material specified in the earlier section was used to perform the free-vibration analysis regarding different models (Eq. 4.2). Various lay-up designs (based on Table 4.3) were considered to evaluate the natural frequency response in two different geometries: square and rectangle plates with  $a/t = 105.85$  and  $a/t = 52.92$  ( $a = 0.254$ ,  $b = 0.127$  m), as illustrate in Figures 4.12 (a) and 4.12 (b), respectively.

$$\underbrace{\begin{pmatrix} \text{square} \\ \text{rectangle} \end{pmatrix}}_{\text{Plate geometry}} \times \underbrace{\begin{pmatrix} \text{Case 1} \\ \text{Case 2} \\ \text{Case 3} \\ \text{Case 4} \end{pmatrix}}_{\text{B.C.}} \times \underbrace{\begin{pmatrix} \text{Lay-up 1} \\ \text{Lay-up 2} \\ \text{Lay-up 3} \\ \text{Lay-up 4} \\ \text{Lay-up 5} \\ \text{Lay-up 6} \\ \text{Lay-up 7} \end{pmatrix}}_{\text{Stacking sequence}} = \underbrace{(56)}_{\text{Models}} \quad (4.2)$$

The first six natural frequencies for the square and rectangle geometries for different B.Cs are reviewed in Tables 4.6 to 4.9. The consequences for the case 1 (SSSS), as reported in Table 4.6 and Figure 4.13 show that with an raise the fiber orientation angles ( $T_1$ ) from  $0^\circ$  to  $45^\circ$ , the frequency modes display a increase of 14.57%, whereas in lay-ups 5, 6, and 7 ( $60^\circ$  to  $90^\circ$ ) the frequency values reduce via 16.47%.

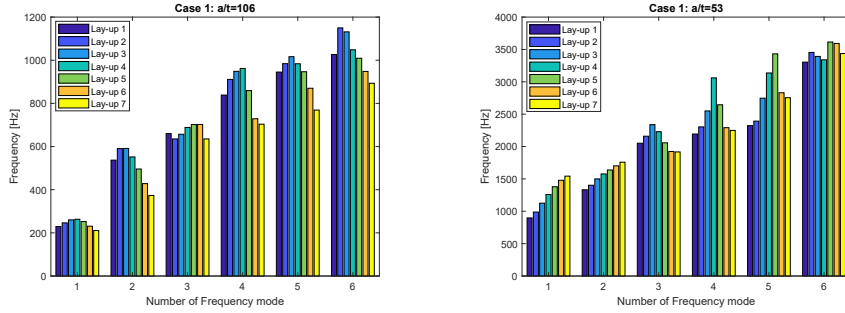


Fig. 4.13 Sensitivity of the first six frequencies under case 1 B.C. for different fiber orientations  $T_1$ .

In distinction, in the rectangular designs, with the rise in the  $T_1$  angle from  $0^\circ$  to  $90^\circ$ , the first frequencies grow by 71.91%. The free-vibration frequencies of B.C. cases 2 (SSSS-I) and 3 (CCCC) are prepared in Tables 4.7 and 4.8, sequentially, and the frequencies do not manifest significant changes (see Figures 4.14 and 4.15, respectively). Nevertheless, in case 4 (CFCF) of the boundary conditions, the results are shown in Table 4.9 show that in square plates, an increase in the fibre orientation angles ( $T_1$ ) leads to an increase of 130.96% in the natural frequency values. Moreover, the frequencies for the rectangle case display oscillations, as displayed in Figure 4.16. These findings describe that the frequency behaviours are strongly dependent on the geometry, boundary conditions, and stacking sequence designs.

a/h	Design	Mode 1	Mode 2	Mode 3	Mode 4	Mode 5	Mode 6
= 105.85	Lay-up 1	229.50	537.07	659.99	838.68	945.24	1026.53
	Lay-up 2	246.31	590.42	635.41	911.18	984.15	1149.90
	Lay-up 3	260.17	591.19	656.93	948.65	1016.47	1131.57
	Lay-up 4	262.96	551.92	688.61	961.98	983.72	1048.42
	Lay-up 5	252.34	495.98	701.96	859.34	946.74	1009.32
	Lay-up 6	230.86	428.17	702.29	728.86	870.24	948.18
	Lay-up 7	210.77	372.97	635.35	703.71	769.15	893.22
= 52.92	Lay-up 1	897.56	1332.14	2051.60	2193.36	2323.23	3304.48
	Lay-up 2	988.30	1402.41	2159.78	2303.63	2393.00	3454.18
	Lay-up 3	1125.46	1500.44	2338.30	2550.20	2747.62	3392.48
	Lay-up 4	1259.12	1576.96	2228.99	3060.88	3136.75	3339.63
	Lay-up 5	1379.00	1638.24	2057.49	2645.51	3431.71	3615.06
	Lay-up 6	1479.00	1702.01	1923.68	2291.65	2830.93	3593.33
	Lay-up 7	1543.10	1758.48	1916.83	2249.48	2754.41	3436.64

Table 4.6 First six natural frequencies for case 1- SSSS.

a/h	Design	Mode 1	Mode 2	Mode 3	Mode 4	Mode 5	Mode 6
= 105.85	Lay-up 1	485.38	898.62	1019.77	1389.39	1521.14	1824.45
	Lay-up 2	483.44	935.55	974.59	1401.63	1636.83	1697.43
	Lay-up 3	470.75	885.60	984.91	1392.64	1533.39	1747.67
	Lay-up 4	452.97	800.44	1011.30	1321.94	1396.73	1847.50
	Lay-up 5	436.04	716.54	1034.19	1150.35	1357.23	1748.45
	Lay-up 6	424.72	650.46	1004.93	1055.29	1326.70	1508.17
	Lay-up 7	420.64	611.19	914.40	1076.54	1307.15	1357.56
= 52.92	Lay-up 1	897.16	1330.80	2050.53	2190.15	2321.18	3298.19
	Lay-up 2	987.92	1401.45	2158.27	2301.56	2390.72	3450.16
	Lay-up 3	1125.45	1500.43	2338.29	2550.18	2747.59	3392.46
	Lay-up 4	1258.87	1576.27	2227.66	3058.72	3135.22	3337.48
	Lay-up 5	1378.90	1637.87	2056.67	2643.98	3429.08	3614.83
	Lay-up 6	1479.00	1702.01	1923.67	2291.64	2830.92	3593.32
	Lay-up 7	1543.09	1758.35	1916.47	2248.80	2753.17	3434.61

Table 4.7 First six natural frequencies for case 2- SSSS-I.

a/h	Design	Mode 1	Mode 2	Mode 3	Mode 4	Mode 5	Mode 6
= 105.85	Lay-up 1	485.52	899.09	1020.00	1390.14	1522.16	1824.80
	Lay-up 2	483.66	936.15	975.06	1402.73	1638.32	1698.27
	Lay-up 3	471.05	886.28	985.77	1394.25	1534.78	1749.73
	Lay-up 4	453.29	801.14	1012.23	1323.38	1398.49	1849.72
	Lay-up 5	436.28	717.03	1034.96	1151.26	1358.57	1750.10
	Lay-up 6	424.89	650.70	1005.31	1055.87	1327.43	1508.77
	Lay-up 7	420.77	611.32	914.56	1076.99	1307.54	1357.76
= 52.92	Lay-up 1	898.47	1333.59	2053.71	2195.50	2326.34	3307.40
	Lay-up 2	989.23	1403.79	2161.57	2306.00	2395.29	3456.95
	Lay-up 3	1126.72	1502.21	2341.32	2553.10	2751.29	3396.34
	Lay-up 4	1260.92	1579.44	2232.79	3066.07	3141.84	3346.17
	Lay-up 5	1380.96	1640.75	2060.86	2649.94	3437.33	3620.55
	Lay-up 6	1480.54	1703.27	1924.99	2293.35	2833.02	3595.84
	Lay-up 7	1544.27	1759.09	1917.67	2250.82	2755.95	3438.23

Table 4.8 First six natural frequencies for case 3- CCCC.

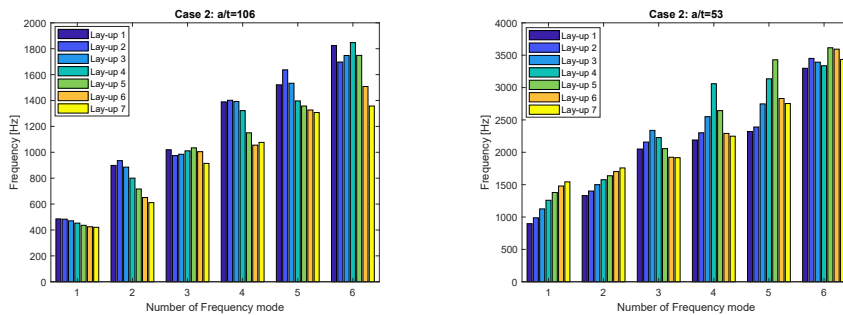


Fig. 4.14 Sensitivity of the first six frequencies under case 2 B.C. for different fiber orientations  $T_1$ .

a/h	Design	Mode 1	Mode 2	Mode 3	Mode 4	Mode 5	Mode 6
= 105.85	Lay-up 1	168.47	221.02	438.20	467.69	496.24	819.45
	Lay-up 2	191.95	251.97	508.91	510.87	574.94	938.46
	Lay-up 3	226.63	290.17	544.89	618.04	685.38	928.32
	Lay-up 4	271.46	332.93	560.23	753.28	822.39	895.22
	Lay-up 5	321.29	378.61	552.72	830.02	897.86	974.37
	Lay-up 6	364.45	418.01	527.06	738.07	1008.61	1061.33
	Lay-up 7	389.11	437.02	495.56	653.91	929.14	1064.60
= 52.92	Lay-up 1	715.46	825.44	1217.10	1748.81	1862.21	1990.40
	Lay-up 2	547.99	575.96	1075.40	1420.49	1440.48	1531.47
	Lay-up 3	579.07	597.58	1151.93	1440.75	1456.42	1519.91
	Lay-up 4	846.73	871.56	1375.78	1743.31	2205.91	2211.32
	Lay-up 5	1276.64	1331.63	1529.77	1842.07	2269.04	2825.54
	Lay-up 6	1477.97	1634.49	1683.48	1791.30	1993.34	2321.45
	Lay-up 7	1500.65	1497.18	1554.01	1812.39	2028.78	2381.92

Table 4.9 First six natural frequencies for case 4- CFCF.

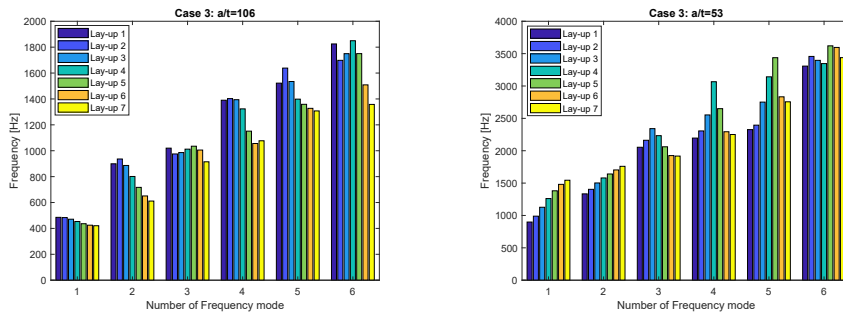


Fig. 4.15 Sensitivity of the first six frequencies under case 3 B.C. for different fiber orientations  $T_1$ .

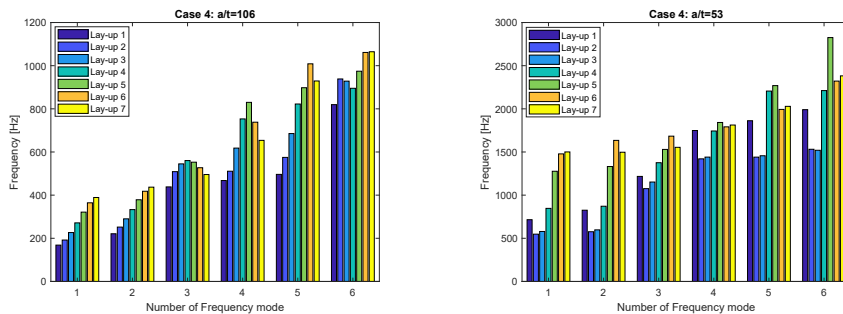


Fig. 4.16 Sensitivity of the first six frequency under case 4 B.C. for different fiber orientations  $T_1$ .

## 4.2 Conclusion

In this research, buckling, free-vibration, and static response analyses of VAT laminates were performed under the CUF procedure. The numerical 1D CUF beam theory was used to correctly define the fibre orientation smoothly and continuously. Numerical CUF models were performed for different lay-up designs to expose the critical fibre edge angles ( $T_1$ ) in the linear buckling analysis of a squared symmetric VAT plate. The results showed that higher critical buckling loads could lead to better local stiffness. Besides, by enhancing the degree of shape functions and the number of elements in the CUF framework, convergence and accurate results could be obtained. The CUF could well predict the buckling loads with a lower degree of freedom in contrast with the classical FEM model, along with lower computational costs. Furthermore, the free-vibration analysis was presented regarding various lay-up designs in various boundary conditions for square and rectangular geometries. The results revealed that while the fibre angles were varied from  $0^\circ$  to  $90^\circ$ , the natural frequencies increased in the rectangle models for three different cases of the boundary conditions. In the square geometries, the oscillation of the frequencies happened, depending upon the boundary conditions and fibre orientation angles. Moreover, the weighted index method could be used to eliminate the units of measurement and facilitate the clarification of the effect of different VAT lay-up designs in the different analyses. Consequently, the non-dimensional indexes can be used to select the effective lay-up design by improving the performance in further work.

# Chapter 5

## Optimization of VAT structures

### 5.1 Introduction

The FEM model provides a precise solution, but when designing with an optimization algorithm, it makes more effort to design VAT multi-layered composites. A vast variety of optimization methods in composite structures is provided by classical theories and the definition of laminate parameters, see [76–80]. One of the advantages of the classic approach is that because the laminate parameters are usually obtained by a set of fibre angles, they can provide optimal fibre angles for a multiple-ply laminate. Besides, some works focused on approximate optimal design, to overcome the time-consuming optimization methods that are known as surrogate models in a different program, see [81, 82]. A robust design optimization algorithm for VAT composite structures can be proposed when the properties of the constituting materials and the applied loads are uncertain, as shown by [83]. Through various design optimization algorithms, evolutionary strategies such as the Genetic Algorithm (GA) have been widely used and have been proposed to optimize composite structures. GA is a direct search optimization method that can be a useful model for composite problems by eliminating the need for any gradient information. It does not use sensitivity to find structural behaviour based on design variables. Nikbakht et al. [84], by a comprehensive review of a composite structure optimization, suggests that algorithm performance s can be more complex with random search problems, and that convergence velocity is less than local search with a specific starting point. In contrast, better results are obtained according to possible patterns, and the probability

of obtaining a global optimum is higher. These highlights allow the user to evaluate the efficiency and computational cost according to the need and is essentially suitable for optimization and reliability problems.

The novelty of the present work is the first development of a valid GA optimization method for variable angle composite beams according to the layerwise (LW) theory through CUF framework. The fibre orientation angle is considered as design variables and is examined through buckling and free vibration structural analysis and then the optimal results compared with those from classical composites and pieces of literature. All GA sample points were evaluated during the optimization process to show global optimization through the response surface. Besides, the GA outcomes on RS are compared with the RS results from Latin Hyper Cube Sampling (LHS) method, to show the ability of LHS to obtain the specific domain of optimum by a few computational efforts. Subsequently, it is highly recommended that in such an optimization problem of VAT, LHS method can be used as a step before optimization to reduce the search domain and computational costs.

Several extensive review papers have presented on each autonomous ability. Ghiasi et al.[85] reviewed the optimization methods in fibre curvilinear path. Then, Ribeiro et al, [86] presented the mechanical behaviour of variable stiffness laminated by focusing on buckling, failure and laminated with curvilinear path fibres. Finally, Gonzalez Lozano et al [87] engaged in designing the fibre path to manufacturing the optimal structure. For instance, the convergence rate and accuracy of the optimization algorithm are generally reduced as the number of design variables increases. Furthermore, the load path and stress trajectories are represented in Michell structures [88].

In several works of literature, to accelerate the design procedure by the reduced number of increased design variables, the optimization methods can apply in variable-stiffness panels to obtain accuracy and convergence rate [89], such desired stiffness and buckling capacity [90]. Olmedo et al.[10], in parallel, showing 80% improvement in buckling load which was calculated by Ritz method in compare with straight fibre composites with varying fibre angles linearly. Furthermore, Wu et al. [91] investigate pre-buckling and critical buckling load in the VAT with Rayleigh-Ritz and after that, they defined the optimization for maximum buckling load in a non-linear VAT. Optimization methods can predict the maximization in both local and global buckling with fixed mesh and finite element model [92].

In some instance, the buckling load is doubled in comparison with traditional composite in simply supported panels under axial compressive loads [93], also, two cases of stiffness variation in fibre orientation variation in the load direction adequate to enhance the transverse in-plane stresses distributed on the panel and second one perpendicular to the load, higher improvement by re-distribution of the in-plane load which applied. VAT plates required of discretization for each layer fibre orientation in FEM and a high number of elements should be obtained for the precise mode shapes [94]. Optimization on the best orientation of fibre are investigated in a different problem such as the minimum weight of composite laminate under constraints of stresses[95] by FEM, optimal orientation for elastic body considered for stress in-plane state to minimize the stiffness [96], [97].

## 5.2 Optimization of Variable Angle Tow

### 5.2.1 Direct search stochastic methods

In this study, GA is used to find the optimum results based on the following steps:

1. The GA algorithm begins with creating a random initial population,
2. Algorithm creates a sequence of new populations.

To solve the problem, the GA optimization in the MATLAB *R2017b* environment is associated with the 1D CUF VAT model in Fortran, see Figure. 5.1.

GA describes the results provided by the CUF framework for performing genetic operations. The GA repeated until a convergence criterion is met based on the convergence of the results based on minimizing the  $\frac{1}{F_{cr}}$  and  $\frac{1}{f_1}$  for first critical buckling and first natural vibration, respectively. At each step, the genetic algorithm randomly selected  $T_0$  and  $T_1$  (Fiber-orientation angles in VAT) from the current population and uses them as parents to produce children for the next generation to obtain the best and minimum objective function which is  $\frac{1}{F_{cr}}$  and  $\frac{1}{f_1}$  for optimization of first critical buckling and first natural vibration, respectively. The GA generic individual is a potential solution for the problem at hand. The GA is employed to generate the initial sample set in the design space. The population is large enough to obtain more accurate results. For setup design,  $T_0$  and  $T_1$  are two variables that



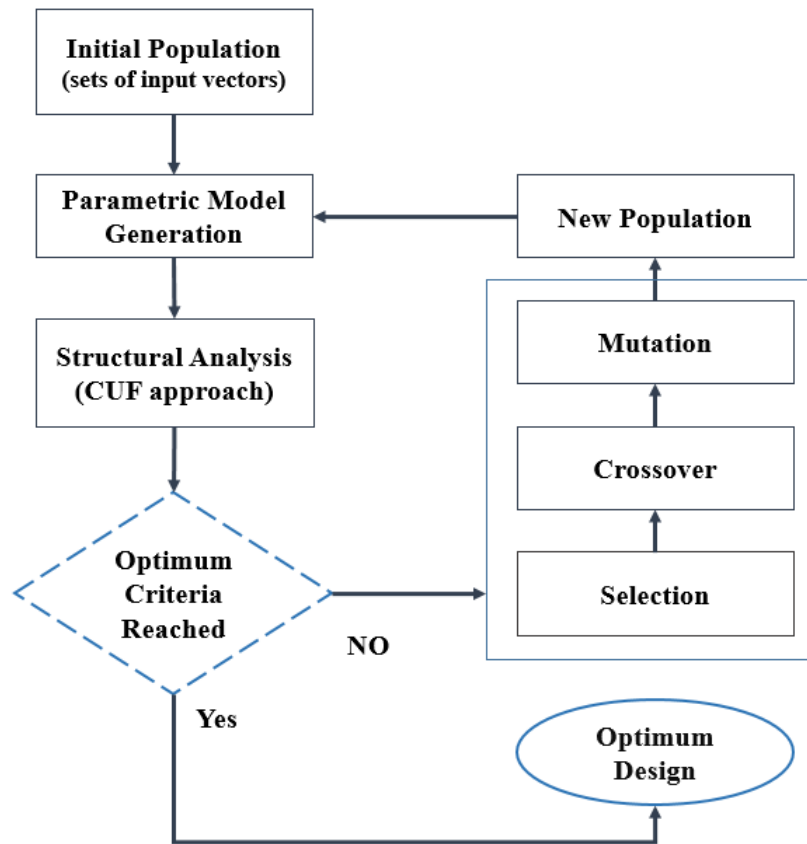
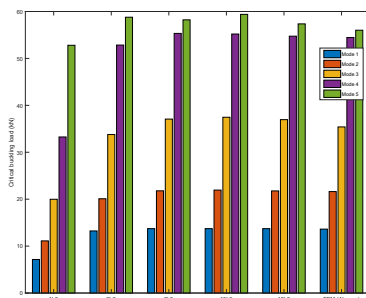


Fig. 5.1 Flowchart of Genetic algorithm procedure (MATLAB) in combination with CUF approach (FORTRAN).

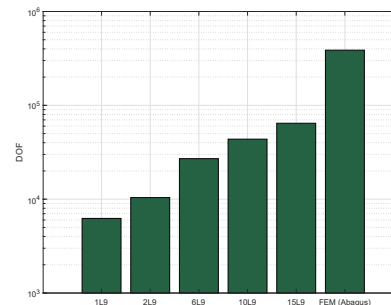
are set to  $0^\circ$  as the lower bound and  $90^\circ$  as the upper bound. The population type and size are double vector and 50, respectively. Also, the cross-over fraction is fixed on 0.8. Therefore, optimum values based on design variables are iteratively found through evolutionary algorithms. As a baseline, for buckling and free vibration analyses, quasi-isotropic (QI) laminates containing  $0^\circ$ ,  $\pm 45^\circ$  and  $90^\circ$  plies are used to define symmetric and balanced laminates. Furthermore, two constant stiffness (CS) laminates with  $[\pm 45]$ , and  $[0]_{16T}$  layup have been determined to compare with the VAT laminate reference design ( $VAT_1$ ) and the results of the current study.

### 5.2.2 Buckling Analysis

First, The  $VAT_1$  composite plate is designed in a 1D CUF framework with a different number of element satisfactory and valid with design criteria and requirement based on the Heo et al. [67] and [98]. VAT laminates were designed with  $[\langle 60^\circ | 15^\circ \rangle \langle -60^\circ | -15^\circ \rangle / \langle -60^\circ | -15^\circ \rangle \langle 60^\circ | 15^\circ \rangle]_s$  square and symmetrical laminates which in present study called  $VAT_1$ . As it can be seen by increasing the number of  $L9$  elements over the cross-section (Figure. 5.2a) and three-node beam element ( $B3$ ) through the beam length (Figure. 5.3a), the accuracy of the models improves. The buckling load which is highlighted in this study illustrated the monolithic convergence properties by the refinement of beam elements. Besides, the CUF approach showed that the degree of freedom (DOF) respect for FEM in ABAQUS [67] decreased significantly without considerable error, see Figure. 5.2b and Figure. 5.3b. To reduce the time saved during the optimization method, the first buckling load with the  $10B3$  element is chosen as a sufficiently accurate result for further evaluation.



(a) Cross-section refinement

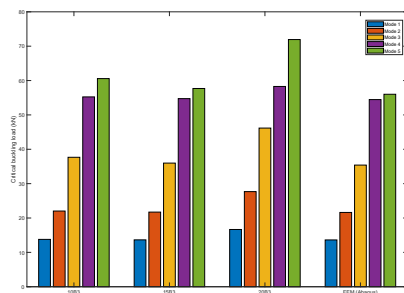


(b) DOF based on cross-section refinement

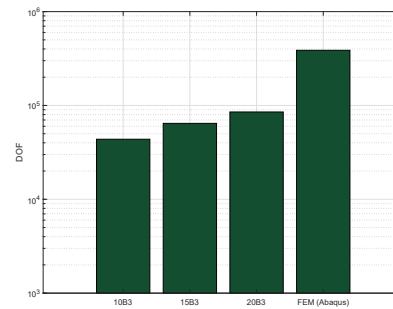
Fig. 5.2 1D CUF cross-section refinement with  $10B3$  effect on the buckling load in  $VAT_1$  in contrast with FEM and degree of freedom number.

Table 5.1 Reference laminate lay-up designs in contrast with optimum VAT plate.

Laminated scheme	Layup design
$QI$	$[45, 0, -45, 90]_{2S}$
$CS_1$	$[\pm 45]_{4S}$
$CS_2$	$[0]_{16T}$
$VAT_1$	$[\langle 60^\circ   15^\circ \rangle \langle -60^\circ   15^\circ \rangle / \langle -60^\circ   15^\circ \rangle \langle 60^\circ   15^\circ \rangle]_4$
$VAT_{OPT}$	$[\langle 9^\circ   51^\circ \rangle \langle -9^\circ   -51^\circ \rangle / \langle -9^\circ   -51^\circ \rangle \langle 9^\circ   51^\circ \rangle]_4$



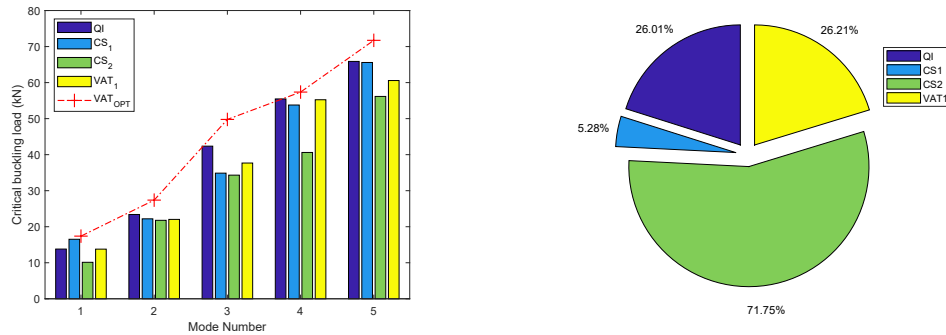
(a) Beam refinement



(b) DOF based on beam refinement

Fig. 5.3 1D CUF beam element refinement with 160L9 effect on the buckling load in  $VAT_1$  in contrast with FEM and degree of freedom number.

Through GA an optimal distribution of fibre angle of VAT ( $T_0$  and  $T_1$ ) obtained for the maximum buckling load subjected to simply supported boundary condition. The optimization procedure is based on the proposed linear equation of fibre orientation angle to design VAT plates for the maximum buckling load. A sufficiently large population and generation are employed to avoid local optimization decisions. The optimum results obtained for VAT laminates ( $VAT_{OPT}$ ) with a layup  $[\langle 9^\circ | 51^\circ \rangle \langle -9^\circ | -51^\circ \rangle / \langle -9^\circ | -51^\circ \rangle \langle 9^\circ | 51^\circ \rangle]_4$  which indicated the maximum buckling load among the optimization procedure respect to the initial buckling load based on  $VAT_1$  [67] and classical laminates, which mentioned in Table 5.1. The optimal design shows a small fibre angle ( $9^\circ$ ) in the centre of the laminates and extends to  $51^\circ$  at the edges. The VAT laminate with an optimum fibre orientation angle is illustrated for various layup designs in Figure. 5.4a.  $VAT_{OPT}$  improves its buckling load compared to classical composite laminates and  $VAT_1$ , which showed in Figure. 5.4b. The first modes of the buckling load as well as the amount of displacement range different



(a) Critical buckling load in different laminates (b) Pie chart of various laminates differences in percentage respect to  $VAT_{OPT}$

Fig. 5.4 Comparison between different layup design with the optimum result.

colours shown for different layouts, see Figure. 5.5. The first five buckling loads are shown in Figure. 5.6.

In addition, the distribution plots are used to show the relationship and convergence between the pair of variables and the results based on the GA sample points, see Figure. 5.7.

### Reduction of search domain by Latin Hypercubic

To reduce the timing burden in finding the optimum [99], the Latin Hypercube Sampling (LHS) method was used to generate some samples uniformly distributed in the searching domain [100]. After capturing the results from these samples, a high order polynomial was used as a curve-fitting model over both LHS samples and the GA population. By GA, the results for 798 samples are recorded during the optimization procedure. And in the LHS method, 40 different samples were generated in a randomly space-filling approach. The input variable parameters in both methods were ( $T_0$  and  $T_1$ ). By comparing the curve fitting obtained from GA and LHS methods in Figure. 5.8, it was concluded that the domain of global optimum, which is evident in GA results, is well characterized by the LHS method with a small number of samples (black dots indicate all sample points). LHS can capture the specific domain of the optimum by a small computational effort. Accordingly, the LHS method can reduce the computational cost of the optimization by reducing the searching domain. As it is suggested by Alinejad and et al. [81, 101] in the current

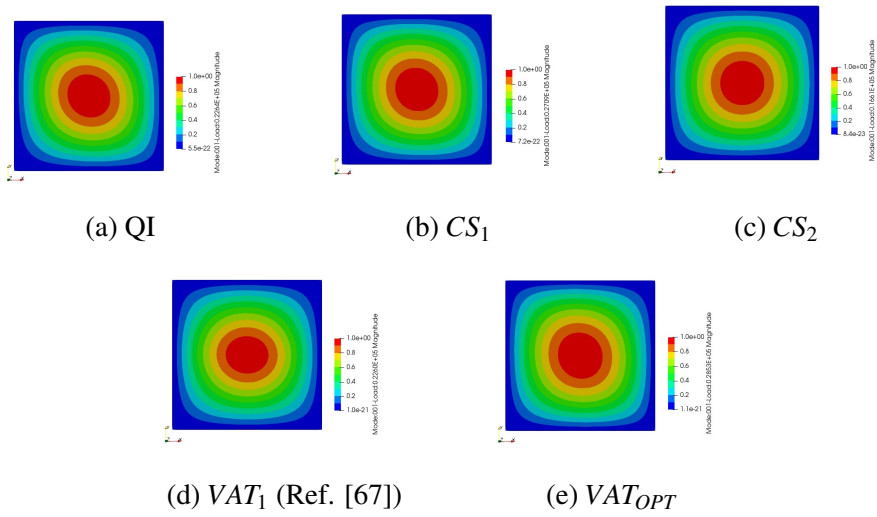


Fig. 5.5 The first buckling modes in different laminates.

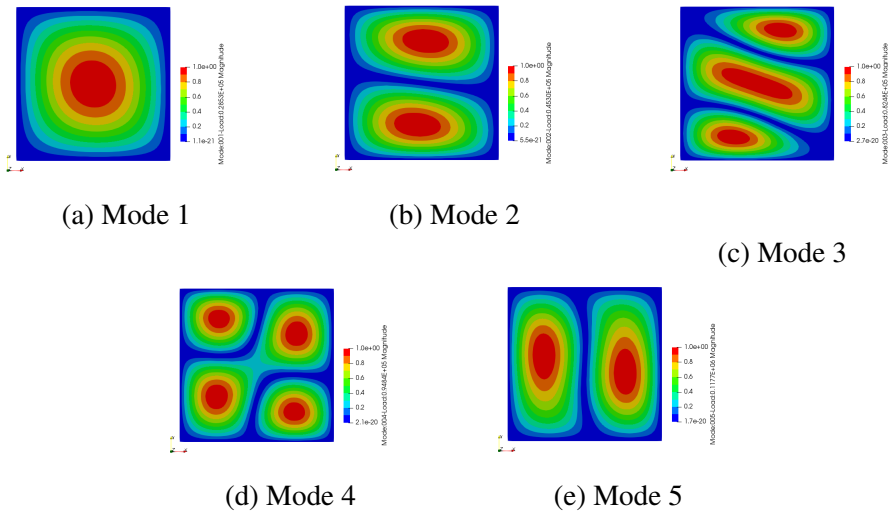


Fig. 5.6 The first five first buckling modes of optimum VAT laminates.

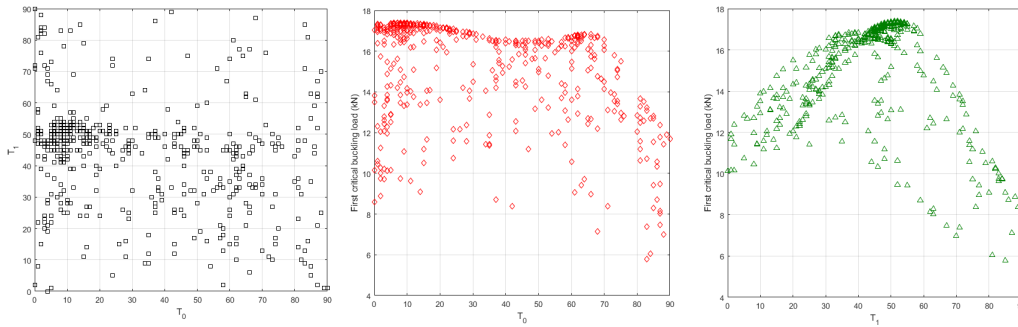
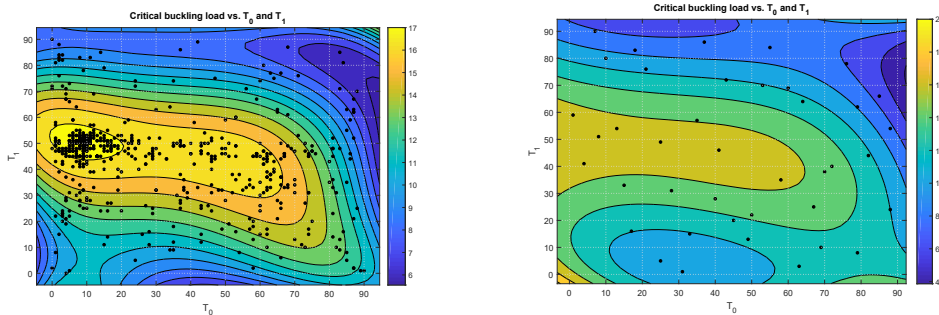


Fig. 5.7 Distribution of variables and first critical buckling load,  $T_0$ - $T_1$ , First buckling load- $T_0$  and First buckling load- $T_1$ .

study also, the LHS can be used an efficient method in the first step of optimization before using the GA or direct search methods in such problems. By this method, a large space of searching domain is eliminated from the rest of the process.

Consequently, it is highly suggested that in such optimization problems as in the current study, the Latin Hypercube Sampling method should be used first to reduce the searching domain before using the other optimization methods (such as GA, gradient base, direct search, etc) to reduce the computational costs.



(a) GA Contour plot of variables sample points ( $F_{cr}$  is represented by the colors)

(b) LHS countour plot

Fig. 5.8 Contour plots and response surfaces based on GA and LHS for  $T_0$  ,  $T_1$  which denotes variables and first critical buckling load as the response.

### **Interpreting and using ANN in current problem**

In any optimization problem, the main concerns are focused on the quality of validity/reliability and replicability. The attention can partially refer to the variable choice, reduction of risk of error and finally adequate detailed documentary methods. Therefore, appropriate knowledge for statistical issues and sensitivity is required. Based on the complexity of the VAT buckling problem, and for evaluation of the optimization problem, ANN is investigated as a post-processing technique to evaluate the optimum results. In this current study, we will consider the ANN as the supervised learning method. The aim of using ANN was first to show that the output of the GA optimization method was accurate as it was used for the first time in a combination of layerwise theory through the higher-order model of VAT structure. The second goal of using ANN was to show how many hidden layers of neurons can be suited for considering VAT problem in buckling analysis based on the type of structure, materials, and boundary condition. This is done by using different neural network models to find the best NN for this example.

For post-processing ANN, the output results of GA optimization saved in a file and to recap, and the ANN learning algorithm following:

- The start point is usually referred by the random value for the parameters of the network such as weights and thresholds (biases).
- An example of the sample set is selected from the input, then they will move within the network to achieve the prediction.
- The differences between prediction results within expected value which were labelled are investigated then.
- In the next step, the information of this propagate are used for updating the neural network parameters with the reduction of a gradient; so that total loss is reduced and a better model can be achieved.
- The iteration will continue based on the steps mentioned before until a good model is reached.

This study proposes a neural network-based prediction model for detection and prediction of the goals mentioned in the previous part. Performance measurement of Bayesian Regularization (BR) algorithm, Levenberg–Marquardt (LM) algorithm,

and Scaled Conjugate Gradient (SCG) algorithm has been analyzed, for more details and formulation, see [50].

The results in Figure 5.9 showed the performance of BR, LM and SCG algorithm. BR and LM indicated the convergence of  $R$ . Also, BR function illustrated the higher value of  $R$  parameter respect to LM in the start point (see Figure 5.9). The  $R$  value is an indication of the relationship between the outputs and targets and can vary between 0 and 1, which the best value is fit on 1, as it explained in the previous section. Moreover, the different number of the hidden layer are examined for a different mentioned algorithm to obtain an accurate number of hidden layer for current VAT buckling problem. The results showed by 30 hidden layer through BR algorithm, correct results can be obtained by the minimum error. Based on the 30 number of hidden layer in BR algorithm, three plots of training, testing and all of the results are shown in Figure 5.10. The dashed line in each plot represents the perfect result – outputs = targets. In current problem dashed line is completely covered by the solid line which represents the best fit linear regression line between outputs and targets, where  $R = 1$ , is an exact linear relationship between outputs and targets which can be obtained. In the next step, the error diagram, for training and test results are obtained and has shown in Figure 5.11. The blue bars represent the training data and the red bars are refers to the testing data. Current histogram can show the outliers, which are data points where the fit is significantly worse than the majority of data.

Finally, ANN can be proved the optimum results and showed the best fit model with 30 number of the hidden layer through the BR algorithm for VAT problem through the buckling load.

The layers are interconnected via nodes or neurons, with each layer using the output of the previous layer as input.



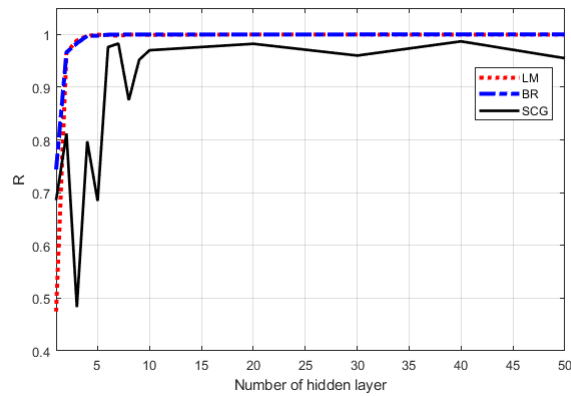


Fig. 5.9 Comparison between different fit ANN algorithm based on the number of hidden layer for VAT problem.

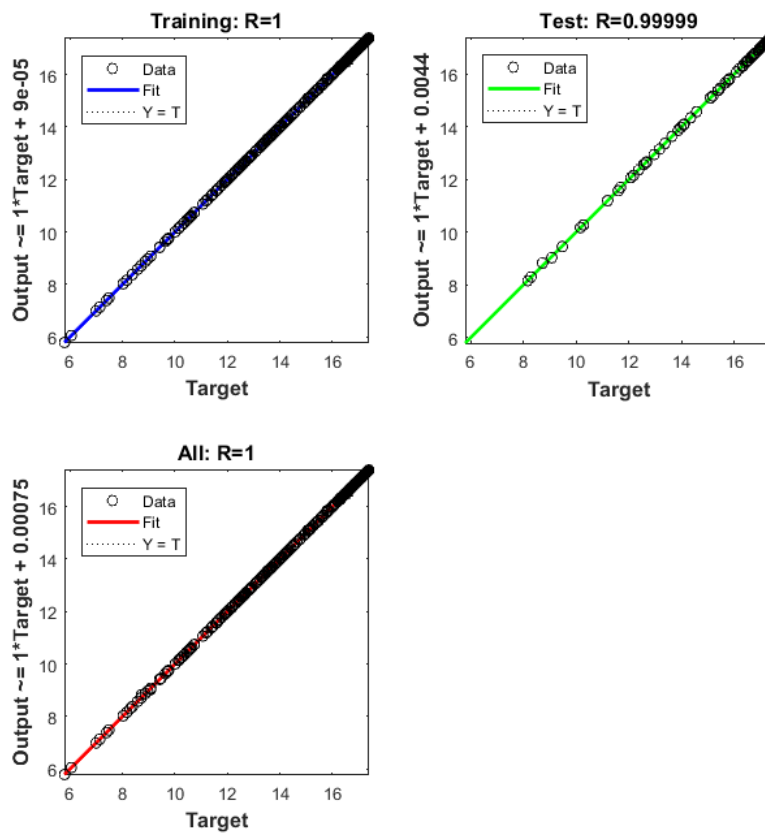


Fig. 5.10 Regression plot in the three subdivision: i) training, ii) testing and ii) all. The bubbles represent the perfect fit between the two values ( $R^2 = 1$ ), the coloured solid lines show the real correlation between the computed output and the initial target.

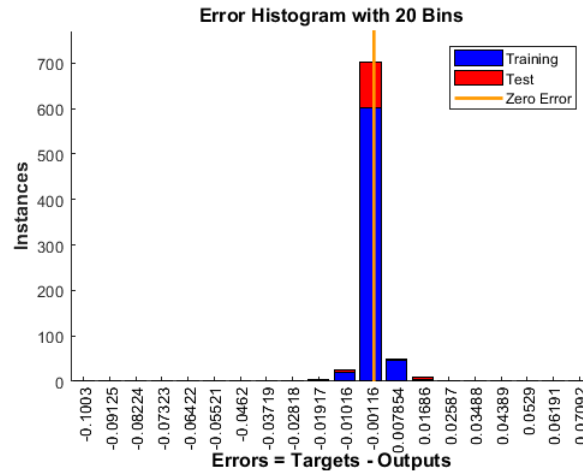


Fig. 5.11 Errors distribution concerning the training, and test sets.

### 5.2.3 Free Vibration

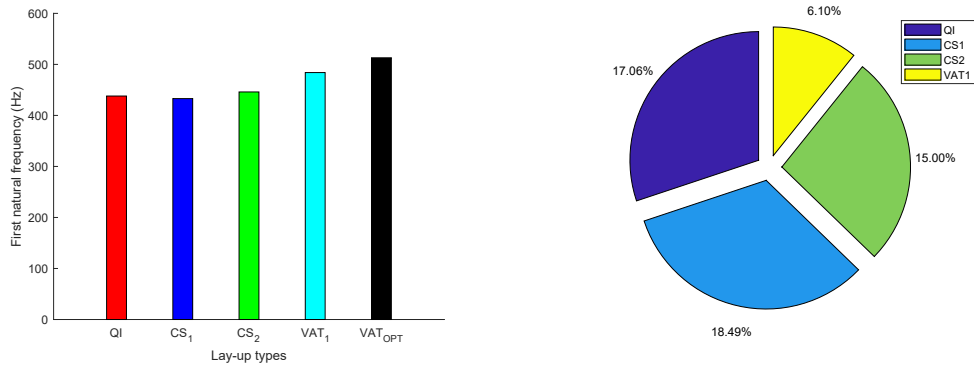
A fully clamped square plate of VAT laminated has been studied in this part based on [98]. For more validity, the present program has been used to study the optimization of VAT laminates. Also,  $QI$ ,  $CS_1$  and  $CS_2$  have been used to demonstrate the ability of optimization procedure and structural analysis of CUF in the LW model. In this study, the mesh with  $160L9$  on the cross-section and 10 has been used. GA is used to optimize fibre orientation based on the highest first natural frequency. Contrary to the optimal results, the first natural frequency of different laminates is reported in Table 5.2 and shown in Figure. 5.12a. First modal shape for different laminates is indicated in the Figure. 5.13. The optimal laminate has  $[\langle 90^\circ|0^\circ \rangle \langle -90^\circ|0^\circ \rangle / \langle -90^\circ|0^\circ \rangle \langle 90^\circ|0^\circ \rangle]_4$ . This means that the start of  $T_0$  has been reduced from  $90^\circ$  from the centre to  $0^\circ$  to the edges of the VAT square plate. The five natural frequencies of optimal laminates are shown in Figure. 5.14.

Bar plots in Fig. 5.15 shows the relationship between variable pairs and the first natural frequency. In Fig 5.15, plots show that both  $T_0$  and  $T_1$  are highly dependent on the first natural frequency.

Figure 5.16 presents the result of the optimization obtained through GA, which is achieved by the fourth-order polynomial function. The black dots show all the sample points in through all generation cycles. The colony of black dots are located

Table 5.2 Reference laminate lay-up designs in contrast with optimum VAT plate.

Laminated scheme	First natural frequency (Hz)
$QI$	438.385
$CS_1$	433.064
$CS_2$	446.235
$VAT_1$	438.659
$VAT_{OPT}$	513.159



(a) First natural frequency in different laminates (b) Pie chart for optimum VAT frequency improvement in contrast with different laminates

Fig. 5.12 Comparison between different layup design with the optimum result for dynamic analysis.

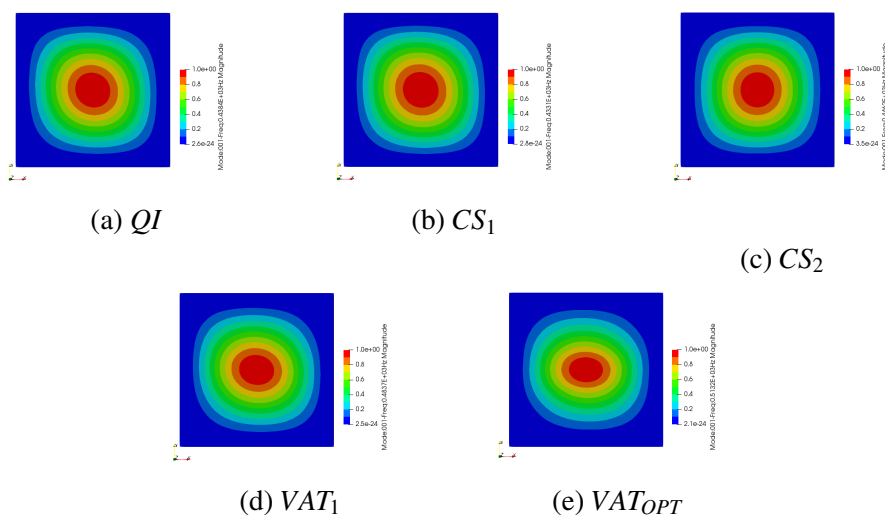


Fig. 5.13 The first natural frequency modes of laminates in different layup design.

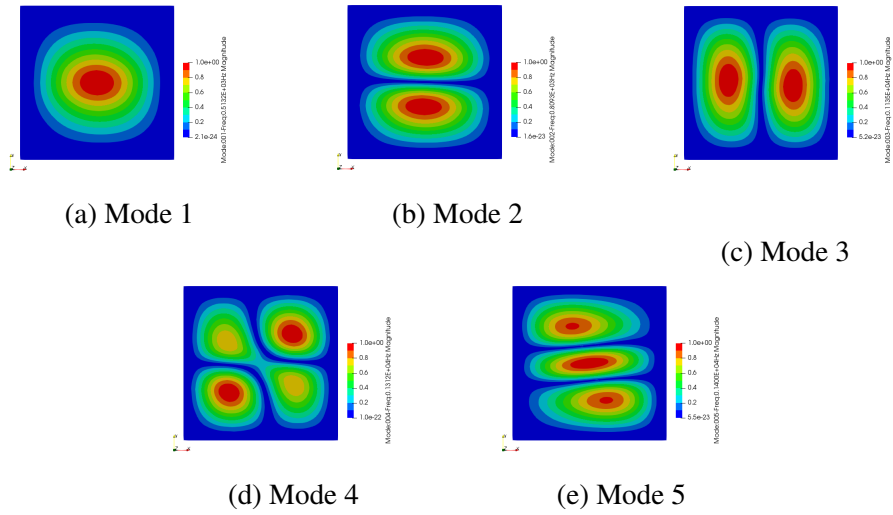


Fig. 5.14 The first five natural frequency modes.

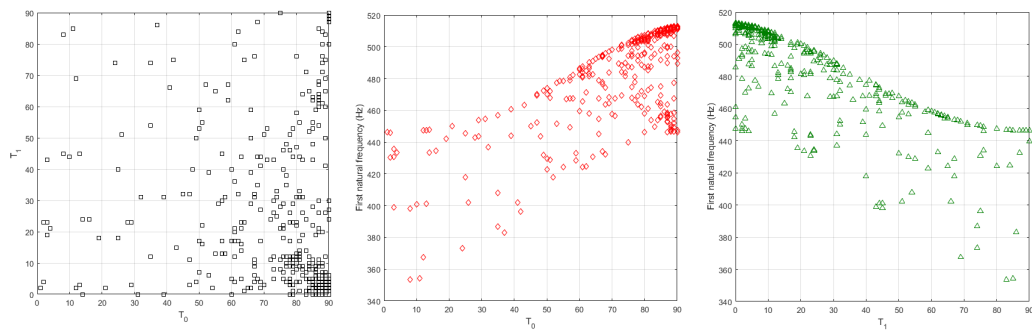
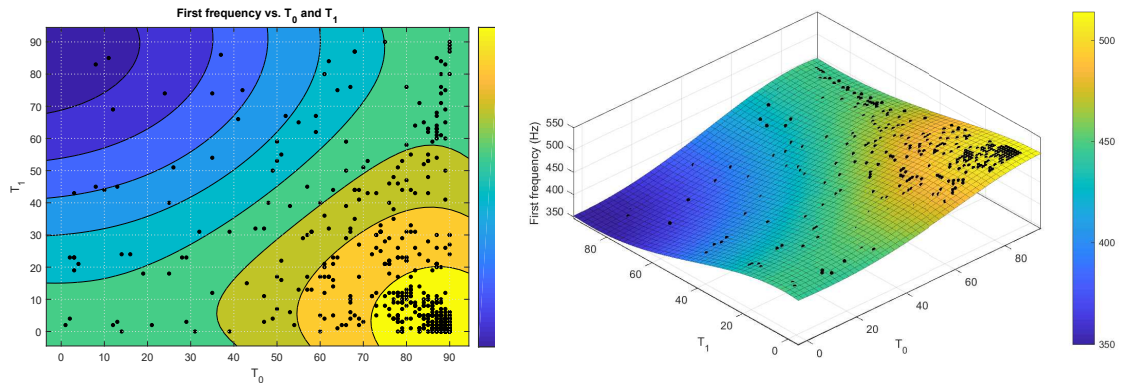


Fig. 5.15 Distribution of variables and first natural frequency,  $T_0$ - $T_1$ , First natural frequency- $T_0$  and First natural frequency- $T_1$ .



(a) Countour plot of variables where the  $f_1$  is represented by the colors

(b) Response surface

Fig. 5.16 Contour plot and response surface showing effects of variables (fiber orientation angles) during GA procedure in free vibration problem.

in the optimal area (yellow part), which display the convergence of the optimal results.

The base research of current chapter is presented in [98].

### 5.3 Conclusion

In the current research, the GA is recommended to optimize the buckling loads and free vibration problems of VAT composites by the LW theory through CUF approach. The current study presented in two main part: Firstly buckling analysis has done by CUF approach for different constant fibre laminates and VAT panels. In the next step, GA optimization has done and then the initial sample points of GA compared with the LHS method. In the second part, free vibration is investigated for different classical composites in contrast with VAT and optimum results which were obtained by GA. The observations can be summarized as follows:

1. In this study all CS and VAT laminates are based on LW theory to demonstrate the ability of the CUF approach to precise constructions layer by layer composites models. CUF shows the ability to achieve optimum results through the optimization method.

2. Due to the elimination of the calculation of laminate parameters or other additional calculation processes, LW can be introduced as an accurate model during the optimization procedure.
3. In the current study, GA has been used as a direct optimization method to predict the structural response in various analyzes by obtaining the  $T_0$  and  $T_1$  as design variables. Besides, GA showed good convergence results. Optimum results showed that the improvement of buckling load can be up to 71.75% in  $CS_2$  plates, 26.01% for QI, and 26.21% respect to  $VAT_1$  (reference design).
4. To reduce the time-consuming process of the GA algorithm, the LHS method can generate multiple samples uniformly distributed in the searching domain. Therefore, the optimization method can include the optimal results in small sample points by LHS, which can be considered for future studies.
5. In case of finding the optimal first natural frequency, GA in combination with CUF indicates optimal results, which shows an improvement of the first natural frequency up to 18.49% in  $CS_1$  plates, 17.06% for QI, 15.0% compared to  $CS_2$ .

In addition, the GA is provided to optimize the buckling load problem of VAT composites by the LW theory in CUF framework. Present VAT laminates built based on LW theory to show the ability of CUF approach to obtain accurate layer by layer composites model. The unified formulation showed the capability to achieve optimum results through the GA optimization procedure. LW model in combination with optimization can be introduced as an accurate model due to eliminating the calculation of the lamination parameters or other extra computation processes to obtain approximation results. The optimum results showed that improvement of the buckling load can be up to 27.67% respect to  $VAT_1$  in the reference design. The robustness outcomes confirm that the GA is a suitable method to use for the optimum concerning the VAT problem in LW model. The results show that a combination of CUF and GA can be provided as a suitable and reliable method to obtain a robust optimum for optimization of VAT problems in different structural analyses. In the end, ANN can be proved the optimum results and showed the best fit model with 30 number of the hidden layer through the BR algorithm for VAT problem through the buckling load.

# Chapter 6

## Isotropic Thin-Walled open-cross-section beams

### 6.1 Introduction

Thin-walled structures are widely used in engineering projects due to the advantages of load-bearing capacity, lightweight and low cost. They can use in different structures such as a bridge or tall buildings. In the current chapter, CUF is used for natural frequencies analyzing of thin-walled structures. The thin-walled structures are used with different cross-section, beam length and also different boundary conditions. The 1D CUF model can provide an improvement of numerical analysis efficiency and also decreasing the computational costs. In this study also Lagrange polynomial expansion is used for approximation of displacement field. The models which built-in 1D CUF then compared with those from three-dimensional models with/without warping effect. Moreover, the innovative method for solving current problems can be provided as an accurate model for complex thin-walled structures by reducing the cost of analysis.

The stability of in-walled structure always was an issue; therefore different methodology has been used to investigate the stability of them, such as different simple methods like classical theories and numerical solution in FEM. Vlasov [102] expand the bending theory, torsion and buckling of thin-walled structures with the open-walled and presented a systematic method for thin-walled structures analysis. While these theories did not evaluate the shear effect of structure. Bescoter [103]

studied on the effect of shear deformation through the torsion analysis of the thin-walled structure with closed-walls and with two generalized displacement function introduction. However, the method which presented by Benscoter was only for two certain shapes of cross-section and load, which was not usual. In the current study, CUF is used as an accurate framework for the calculation of bending frequencies plus reducing cost efficiency. Furthermore, the CUF approach shows the ability to use for analysing the behaviour of compact and a bridge-like section with generating the quasi three-dimensional stress field over the beam section [104]. The other examples which presented by Carrera et al. are [105–107]. The unified beam theory involving geometric nonlinearities is evaluated within CUF and a total Lagrangian approach, where the 1D structures employed an index notation and an overall extension of the variables that are primarily using arbitrary cross-sectional functions [108]. Carrera et al. [109] investigated the classical and refined beam and plate theories through the CUF framework for a novel refined beam element within advanced kinematics relying on the legendary polynomial expansion of the primary mechanical variables. Different types of structures were evaluated such as functionally graded sandwich beam, multilayer beams, thin/thick-walled box, as well as cylinders build in a sandwich structure, where the CUF used through free vibration analysis [110]. Given its natural advantages, CUF is expected to discover possible benefit in a growing quantity of engineering purposes.

## 6.2 Linear vibration

Researchers, engineers and designer are involved in determining the eigenvalues (natural frequencies) and eigenvectors (mode shapes) in open cross-section thin-walled beams. Therefore, the current study is focused on the free vibration of thin-walled beams with an open cross-section through CUF framework. For solving free vibration problems the modal parameters can be investigated. Linear vibration theory can be employed when we are faced with the small amplitude vibrations in long and slender beams; for instance in the bridge with long longitude, the wings of aircraft and the blades of helicopters. Generally, the linear vibration of the thin-walled beam within a cross-section which can be arbitrary can illustrate flexural-torsional coupling modes. Therefore, the torsion in this types of the beam with arbitrary cross-section showed the warping effects. Therefore, the cross-section is an



important factor in free vibration analysis [111]. As mentioned, in the current study, CUF is used for beam modelling and dynamic motion formulations. When the initial excitation happen in the system, free vibration can occurs. Free vibration means that there is not any external load in the system. For evaluating the free vibration analysis, we need to solve the problem of motion equation and condition of external load and eliminating the damping conditions. Therefore, the natural frequencies and modes of vibration can be obtain by calculating of eigenvalue problem. Finally, the eigenvalue formulation can be written as:

$$(K - \omega_i^2 M)\phi_i = 0 \quad (6.1)$$

Where  $K$  express the matrix of stiffness and  $M$  present the matrix of mass;  $\phi_i$  stand as eigenvector (shape of mode) and circular natural frequency showed by  $\omega$ .

To solve the eigenvalue problem, the eigenvector iteration methods are most well-known main solutions and the subspace spaces construction, which consist of subsets, for more details, see the article by the author of the forthcoming thesis [112]. Consequently, an example of the reference solution methods brings in [112], can be used after calculating the mass matrix of  $M$  and the stiffness matrix of  $K$ . The choice of useful solution method is based on the size of the matrices (the type of structure, DOF and research requirements modes). In the aforementioned example, the solution involves converting the problem into a sequence of static problems in the form ( $K * U = F$ ). Because most solution methods are based on power algorithms [111].

### 6.3 Free Vibration

In the current thesis, the 1D CUF framework is used to be compared and evaluated in different examples. LE solution results in CUF is compared with Chen's method [113]. Moreover, different classical theories like EBBT, TBT and 3D Solid models in Abaqus is compared with the CUF and Chen's methods. In Abaqus, the models are built in the quadratic form of elements. Different models are examined in various boundary condition and different open cross-section thin-walled beams for natural frequency analysis.

### 6.3.1 CUF and Chen's methods Evaluation

For the first time in current research, the CUF is used in contrast with Chen's method for investigating the thin-walled structures, that the results are published in [112]. In Chen's method, the finite element is used to consider the vibration behaviour in open cross-section thin-walled beams [113]. For solving these examples, Chen used the Euler beam kinematic, d'Alembert's principle, and the virtual work principle. In their study, mass and stiffness matrix are calculated separately using nodal force vector and element inertial nodal force vector concerning the element nodal parameters and their second-time derivations. In their study, five different numerical examples were chosen to be compared with literature [114–116].

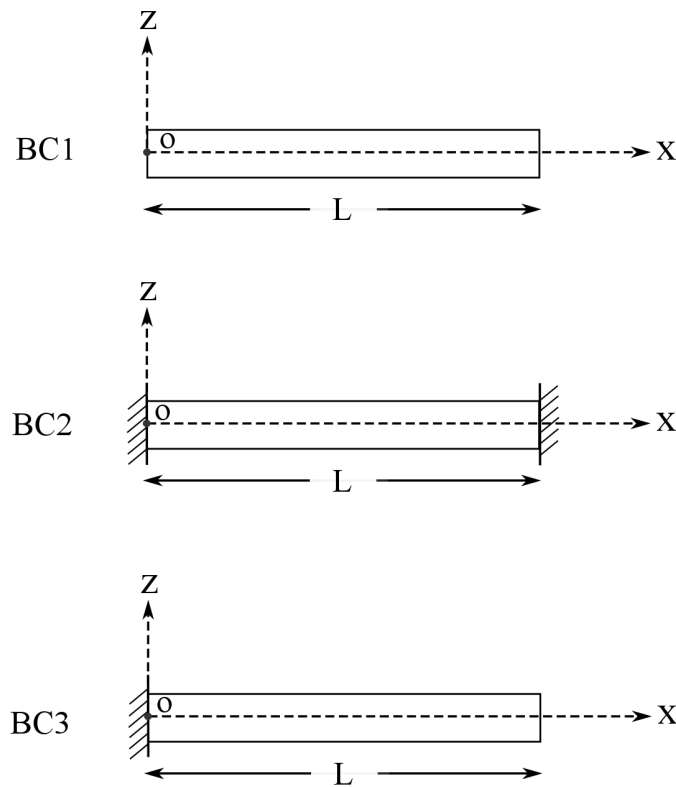
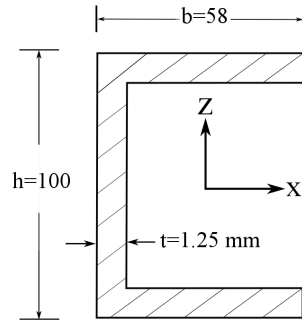
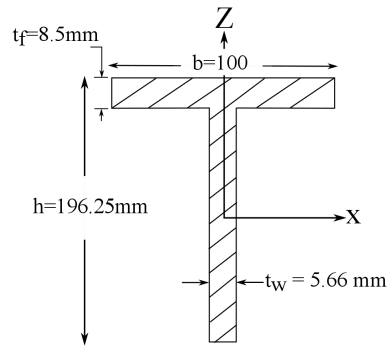


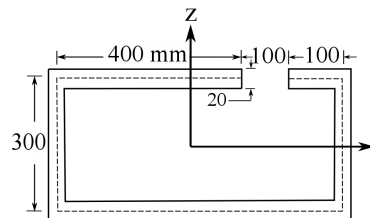
Fig. 6.1 Boundary conditions: free-free (BC1), doubly clamped beam (BC2) and Cantilever beam (BC3).



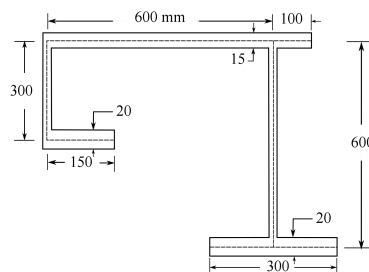
(a) Beam 1: Channel cross-section; mono-symmetric



(b) Beam 2: Tee cross-section; monosymmetric



(c) Beam 3: Arbitrary cross-section; non-symmetric



(d) Beam 4: Arbitrary cross-section; non-symmetric

Fig. 6.2 Beams with arbitrary cross section.

Model of beam	L (cm)	A (cm <sup>2</sup> )	E (GPa)	G (GPa)	$\rho$ (kg/m <sup>3</sup> )	$\nu$
Beam 1	128	2.669	216.4	80.10	7850	0.3
Beam 2	200	19.252	210	80.77	7800	0.3
Beam 3	1000	340	210	80.70	8002	0.3
Beam 4	1000	285	210	80.70	8002	0.3

Table 6.1 The geometry of beam and properties of material.

### 6.3.2 Mono-symmetric C-shaped cross-section beam

The first CUF model is built for Beam 1 which the cross-section of the beam is showed in Figure. 6.2, the detailed information is brought in Table 6.1 and finally, the boundary condition is illustrated in Figure 6.1. This example was selected for the comparative results in [117], that considered some changes by providing the exact member theory. In this example, Banerjee et al. [117] employed the exact dynamic stiffness matrix in use of typical beam member from established theory and tried to combined it in a novel and easy way to develop the algorithm of Wittrick-Williams. This algorithm used for convergence analysis of any desired natural frequencies. In the current study, the LE model of CUF is compared with the 3D solid model in Abaqus and the reference [117] which considered the with/without warping effect, refer to Table 6.2. Based on the Figure. 6.5b and 13B3 in Figure. 6.5c, a 1D CUF is used with 14L9 element which showed the well-convergence between 1D CUF and 3D solid FEM in Abaqus which called as Reference in all comparative tables which presented in this chapter plus the literature with warping effect. Then, in Figure. 6.3 the first five modal shapes of frequencies are shown based on Abaqus model and in Figure. 6.4 based on CUF. It is noted for Abaqus modelling both linear and quadratic elements were examined and finally the quadratic element is selected as the suitable order of geometric issues.

Table 6.2 First frequencies (Hz) for Beam 1 BC1.

Beam Element	DOF	Natural Frequency (Hz)					*a (%)
		Mode 1	Mode 2	Mode 3	Mode 4	Mode 5	
Abaqus (Quaderic element)	66801	21.88	139.13	151.71	153.53	154.50	Reference
CUF (14L9-13B3)	6480	21.94	139.80	152.34	154.14	155.15	0.27
Banerjee1996 (Warping included) [117]	-	22.04	152.08	412.23	-	-	0.73
Banerjee1996 (Warping ignored) [117]	-	19.90	30.69	46.28	-	-	-9.04

\*a Percentage difference from 3D solid Abaqus model (Reference)

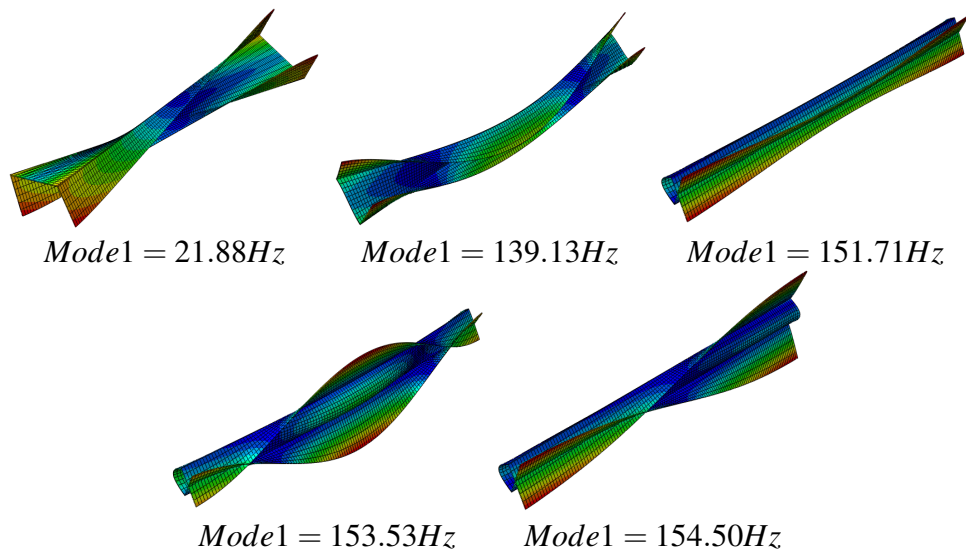


Fig. 6.3 Mode shapes of frequency in 3D FEM in Abaqus, Beam 1, BC1.

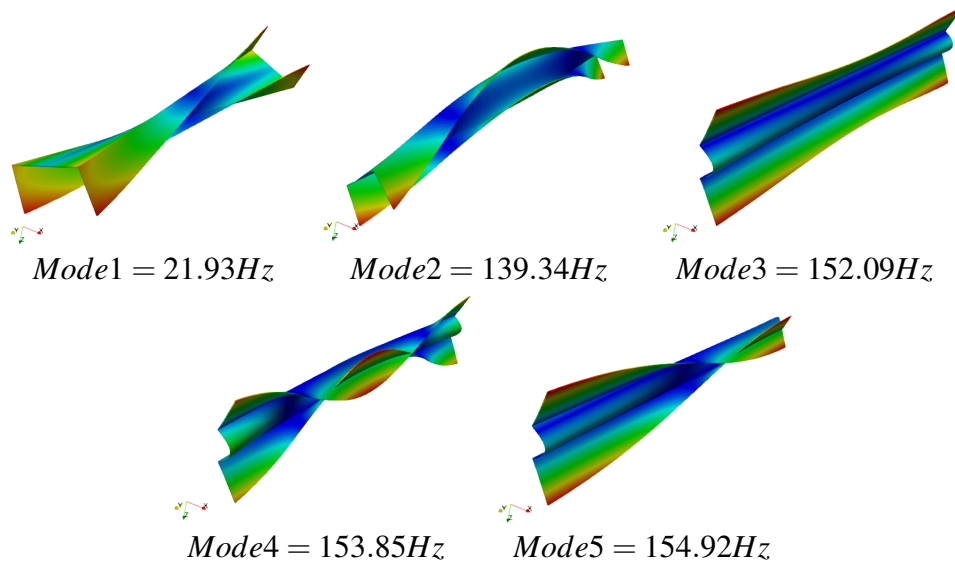


Fig. 6.4 Mode shapes of frequency in CUF, Beam 1, BC1.

Present beam also used for frequency consideration in current model based on the literature in Table Table 6.3; where different results from Hung Hu Chen (B3Dw), BC2CM, BC2x and Euler-Bernoulli and Timoshenko classical beam theories compared with 3D FEM in Abaqus. In this study, the cross-section of a beam built based on Figure. 6.5 and two different LE models with 5, 14L9, are used. Additionally, the beam element can be varied by B2, B3 or B4 elements through the beam axis in the CUF model. Moreover, 5, 13, 14, 100 B2, B3 and B4 are employed along the  $y - axis$  which are reported in Table. 6.4 and the CUF results are compared with those obtained in Abaqus by the parameter of \*a (%) which presented previously in Table. 6.3. In Table 6.4, convergence analysis has done for the beam elements from 5B2 to 100B4 and corresponding presented in Figure 6.6. By increasing the number of beam element, the structure can show less stiffness and therefore, lower frequency value can be obtained. Moreover, by evaluating the beam element, it is clear that the B4 element can show the most highly accurate results in contrast with 3D FEM model in Abaqus. Besides, increasing the number of cross-section element also has an impact on the results of natural frequencies, notice to Table 6.4.

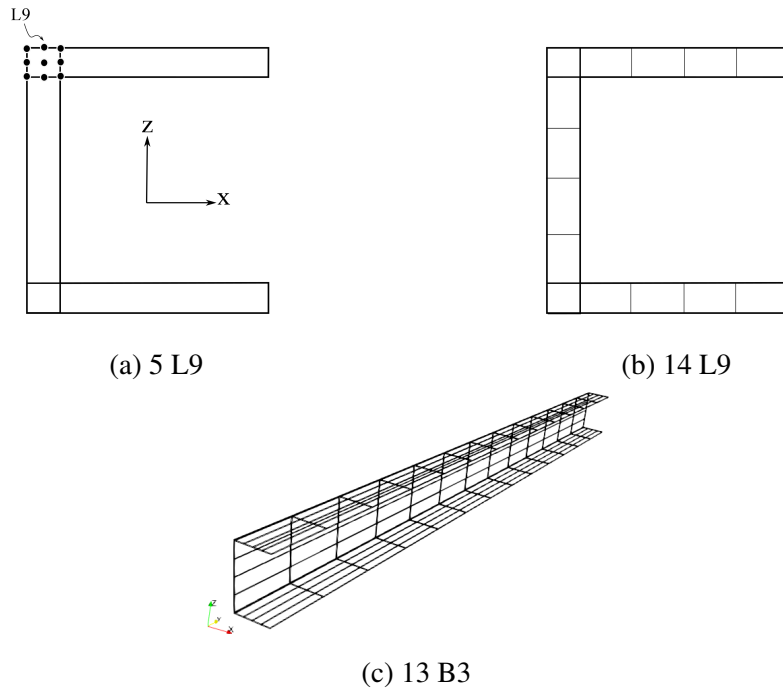


Fig. 6.5 1D CUF model with various discretization in beam 1 (a) over the cross sections and (b) along the beam.

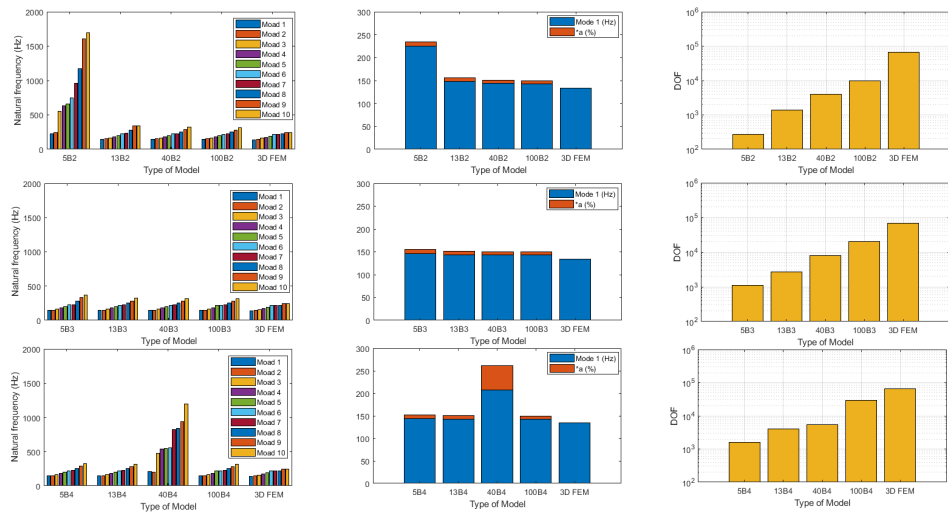


Fig. 6.6 Mesh study and convergence analysis of CUF model respect to 3D solid FEM in Abaqus.

Table 6.3 References for Beam 1 BC2 with quadratic elements.

Model	DOFs	Natural Frequency (Hz)										%a %
		Mode 1	Mode 2	Mode 3	Mode 4	Mode 5	Mode 6	Mode 7	Mode 8	Mode 9	Mode 10	
3D FEM (Abaqus)	66801	133.83	146.28	159.43	174.39	194.21	214.70	218.25	221.42	244.83	245.96	Reference
Hung Hu Chen (B3Dw) [111]	-	149.33	213.52	409.69	586.47	617.73	799.96	1143.36	1316.77	1653.35	1875.94	11.62
BC2CM [115]	-	149.40	x	410.57	x	624.53	803.84	x	1328.07	x	x	11.62
BC2x [113]	-	149.31	213.82	409.64	587.31	617.66	799.87	1145.00	1316.67	1653.17	1878.64	11.56
Euler-Bernoulli	243	213.85	465.65	587.51	1146.17	1262.30	1883.50	2050.94	2414.26	2795.76	3867.55	59.79
Timoshenko	243	210.97	438.14	570.67	1119.26	1092.39	1756.25	2017.51	2050.94	2545.31	3058.24	57.64

\*a Percentage difference from 3D solid Abaqus model (Reference)

Table 6.4 Natural frequencies of the C-shape cross-section beam with doubly clamped boundary condition through CUF framework, Beam 1-BC2.

Model	DOFs	Natural Frequency (Hz)										%a %
		Mode 1	Mode 2	Mode 3	Mode 4	Mode 5	Mode 6	Mode 7	Mode 8	Mode 9	Mode 10	
CUF 5×5B2	270	224.73	247.72	557.34	628.39	659.56	747.32	959.24	1174.60	1602.15	1690.85	67.92
CUF 5×13B2	1386	148.32	151.25	164.73	180.65	203.53	227.67	234.69	277.04	336.73	337.34	10.82
CUF 5×40B2	4059	143.86	150.71	164.37	179.18	199.05	221.49	223.62	252.27	285.56	323.44	7.49
CUF 5×100B2	9999	143.04	150.60	164.32	179.00	198.57	220.41	222.56	250.17	281.79	317.12	6.88
CUF 5×5B3	1089	146.37	151.02	164.47	179.82	202.41	224.83	227.90	280.81	330.63	372.62	9.37
CUF 5×13B3	2673	143.88	150.71	164.35	179.06	198.67	221.36	222.92	250.78	283.24	320.29	7.50
CUF 5×40B3	8019	142.99	150.60	164.31	178.98	198.50	220.33	222.40	249.84	281.18	316.09	6.84
CUF 5×100B3	19899	142.78	150.57	164.30	178.95	220.07	220.07	222.30	249.72	281.02	315.87	6.71
CUF 5×5B4	1584	144.43	150.78	164.37	179.07	198.70	222.08	223.68	252.74	289.53	326.77	7.92
CUF 5×13B4	3960	143.24	150.63	164.33	179.02	198.56	220.64	222.52	249.96	281.35	316.34	7.03
CUF 5×40B4	5445	206.86	201.73	474.30	537.34	547.09	552.79	823.51	836.60	940.35	1199.96	54.54
CUF 5×100B4	29799	142.72	150.56	164.30	178.94	220.00	220.00	222.27	249.68	280.97	315.80	6.64
CUF 14×13B3	7047	135.49	146.96	160.07	175.12	195.10	217.01	219.52	226.36	247.84	250.51	1.24
CUF 14×20B3	10701	135.10	146.90	160.05	175.08	195.00	216.42	219.23	226.21	247.14	250.45	0.94
CUF 14×13B4	10440	134.97	146.89	160.05	175.08	194.98	216.23	219.17	226.16	247.01	250.44	0.85
CUF 14×20B4	15921	134.78	146.86	160.04	175.05	194.94	215.95	219.09	226.08	246.91	250.40	0.68

\*a Percentage difference from 3D solid Abaqus model (Reference)

The first five modal shapes in 3D Abaqus are presented in Figure.6.7 and respectively in Figure.6.8 for first 10 frequencies. Furthermore, the 20th and 30th modal shaped have been reported that show how the high-frequency effect on the thin-walled open cross-section beams. By comparing the first five modal shapes between current method and 3D solid FEM, it can be seen that in some CUF modes such as mode 2 to mode 5, there are orthogonal modes respect to reference in Abaqus. By examining the mesh study in this model, the 14L9 was selected as the appropriate number of cross sectional element with B3 and B4 beam elements to show



results in comparison with classical theories, Hung Hu Chen modes and 3D FEM in Abaqus. The following example is given for the same Beam 1 geometry in BC3. A comparison of the reference results is reported in Table 6.5. EBBT and TBT show a significant difference with the 3D FEM and Hung Hu Chen model and other two references, as well as with the current CUF framework in Table 6.6.

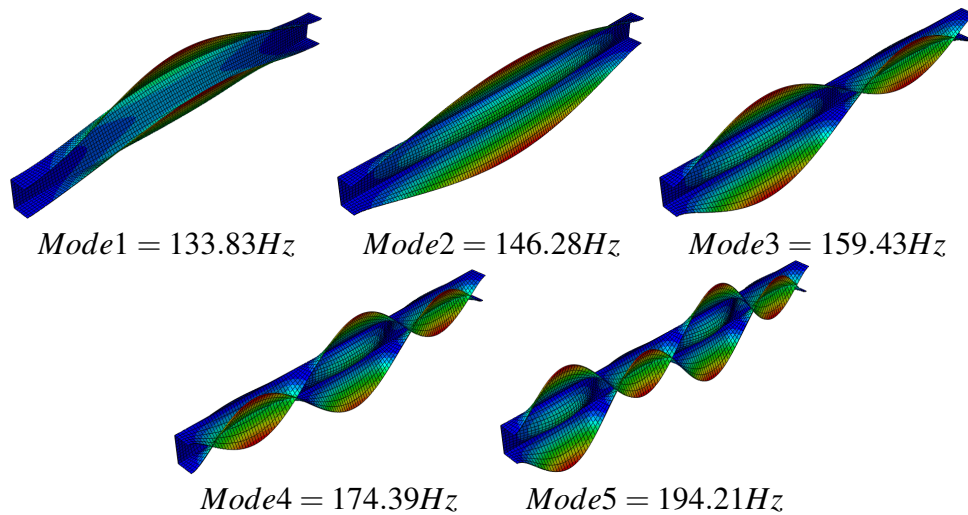


Fig. 6.7 Modal shapes in Beam 1 and BC2– quadratic element within Abaqus

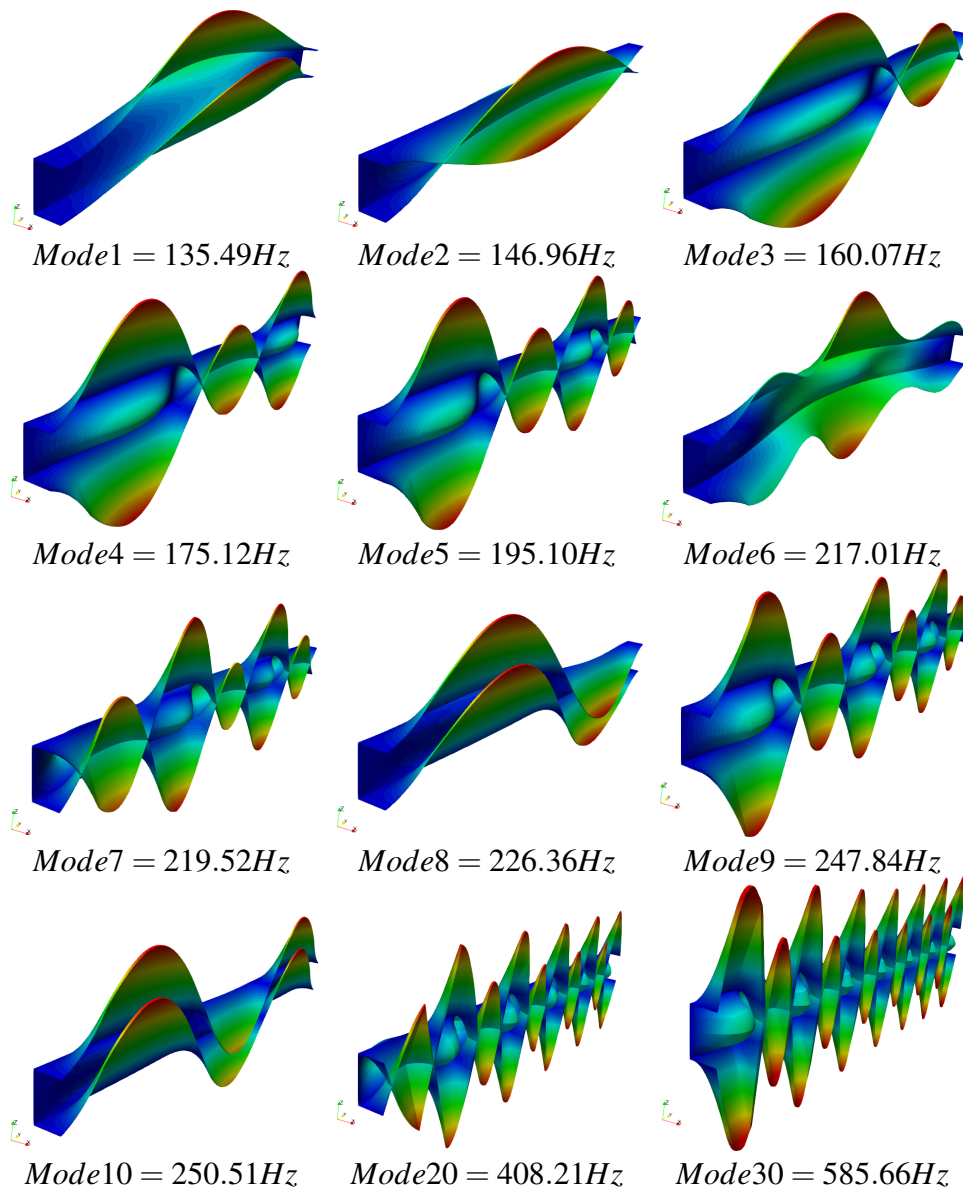


Fig. 6.8 Modal shapes in Beam 1 and BC2–quadratic element within CUF framework.

Table 6.5 Mesh study for Beam 1 BC3 with quadratic elements by different references.

Model	DOFs	Natural Frequency (Hz)										*a %
		Mode 1	Mode 2	Mode 3	Mode 4	Mode 5	Mode 6	Mode 7	Mode 8	Mode 9	Mode 10	
3D FEM (Abaqus)	66801	25.10	33.48	96.00	134.91	148.80	153.50	164.61	181.96	202.81	214.52	Reference
Hung Hu Chen (B3Dw) [111]	-	25.36	33.58	98.15	148.43	209.83	410.02	584.77	598.01	798.74	1025.77	0.71
BC2CM [115]	-	25.36	x	98.55	148.65	x	411.57	x	615.39	x	x	0.71
BC2x [113]	-	25.36	33.63	98.14	148.43	210.13	409.97	585.6	597.95	798.66	1025.78	0.71
Euler-Bernoulli	243	33.63	73.46	210.16	453.98	585.80	1025.47	1140.87	1243.91	1872.46	2366.22	33.98
Timoshenko	243	33.59	73.01	208.30	436.20	573.86	1025.47	1099.85	1143.18	1770.95	2067.04	33.82

\*a Percentage difference from 3D solid Abaqus model (Reference)

Table 6.6 Natural frequencies of the C-shape cross-section cantilever beam through CUF framework, Beam 1-BC3.

Model	DOFs	Natural Frequency (Hz)										*a %
		Mode 1	Mode 2	Mode 3	Mode 4	Mode 5	Mode 6	Mode 7	Mode 8	Mode 9	Mode 10	
CUF 14×13B3	7047	25.22	33.63	96.43	136.05	149.42	154.16	165.28	182.73	203.77	216.07	0.15
CUF 14×20B3	10701	25.18	33.57	96.28	135.85	149.39	154.13	165.26	182.68	203.63	215.77	0.0
CUF 14×13B4	10440	25.17	33.56	96.22	135.79	149.38	154.12	165.25	182.67	203.61	215.68	-0.03
CUF 14×20B4	15921	25.15	33.53	96.15	135.69	149.36	154.11	165.24	182.65	203.57	215.53	-0.11

\*a Percentage difference from 3D solid Abaqus model (Reference)

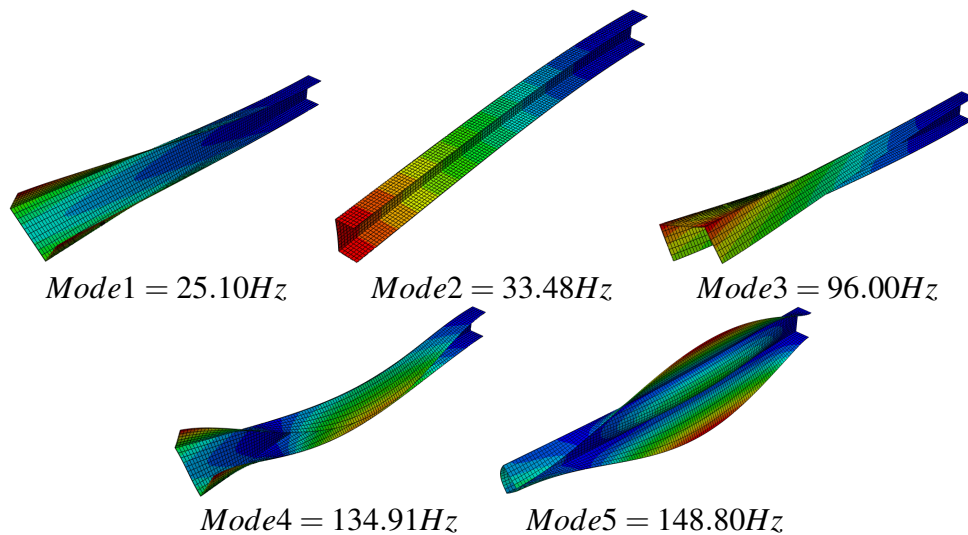


Fig. 6.9 Modal shapes in Beam 1 and BC3– quadratic element within Abaqus.

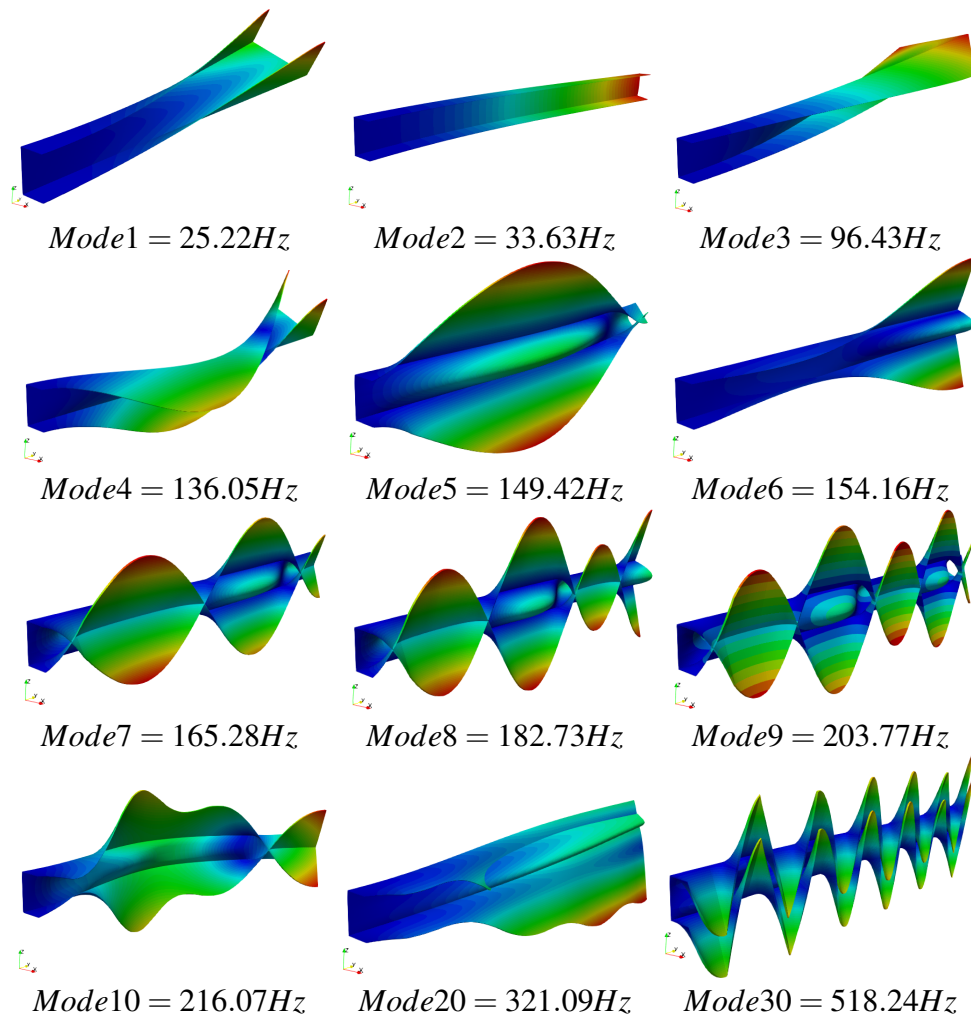


Fig. 6.10 Modal shapes in Beam 1 and BC3–quadratic element within CUF framework.

### 6.3.3 Tee-shaped mono-symmetric cross-section beam

The next example applies to the Tee-shaped mono symmetric cross-section beam, which is indicated in Figure. 6.11. First, 3D FEM in Abaqus is compared with those from references in Table 6.7 and CUF in Table 6.8 for doubly clamped boundary condition (B2). The first five natural frequencies are evaluated in Abaqus and the modal shapes are illustrated in Figure. 6.12. In the next step, the current beam was modelled in CUF framework for the firsts and higher modes in Figure. 6.13. Later, the same beam is evaluated for the BC3 Table 6.9 and 6.10, and the modal shapes are shown in Abaqus, see Figure. 6.14) and CUF as shown in Figure. 6.15 to determine how the boundary conditions are effected on the frequency modes.

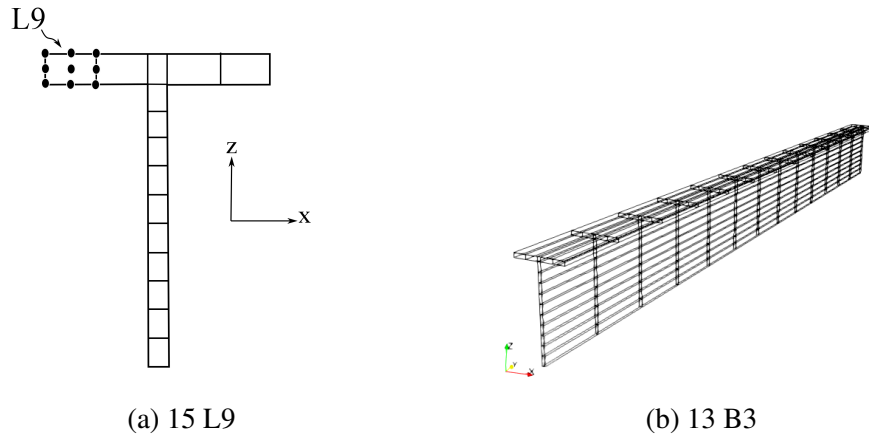


Fig. 6.11 1D CUF model discretization in beam 2 (a) over the cross sections and (b) through the beam.

Table 6.7 Reference study for Beam 2 BC2 with LEs on the cross section (L9).

Model	DOFs	Natural Frequency (Hz)										*a %
		Mode 1	Mode 2	Mode 3	Mode 4	Mode 5	Mode 6	Mode 7	Mode 8	Mode 9	Mode 10	
3D FEM (Abaqus)	129459	38.36	77.04	111.28	122.07	153.03	194.05	238.84	259.88	288.89	309.33	Reference
Hung Hu Chen (B3Dw) [111]	-	38.96	80.55	115.82	128.44	170.30	220.29	273.77	290.04	323.07	332.22	1.56
BC2CM [113]	-	38.97	80.58	115.82	128.46	170.36	214.65	273.92	290.04	323.08	332.48	1.59
Euler-Bernoulli	243	88.99	244.98	298.96	479.44	785.60	791.24	1180.78	1293.05	1503.49	1649.58	131.98
Timoshenko	243	88.46	241.82	272.97	469.06	698.46	765.80	1128.68	1260.87	1293.05	1554.94	130.60

\*a Percentage difference from 3D solid Abaqus model (Reference)

Table 6.8 Mesh study for Beam 2 BC2 with LEs on the cross section (L9).

Model	DOFs	Natural Frequency (Hz)										*a %
		Mode 1	Mode 2	Mode 3	Mode 4	Mode 5	Mode 6	Mode 7	Mode 8	Mode 9	Mode 10	
CUF 15 × 13B3	7533	38.60	77.46	111.78	122.79	153.77	195.23	241.02	260.83	293.18	310.99	0.62
CUF 15 × 20B3	11439	38.56	77.39	111.59	122.45	153.51	194.61	239.59	260.13	290.04	309.94	0.52
CUF 15 × 13B4	11160	38.55	77.37	111.54	122.35	153.45	194.48	239.30	259.90	289.42	309.61	0.49
CUF 15 × 20B4	17019	38.52	77.32	111.43	122.18	153.34	194.32	239.08	259.57	298.08	309.11	0.41

\*a Percentage difference from 3D solid Abaqus model (Reference)

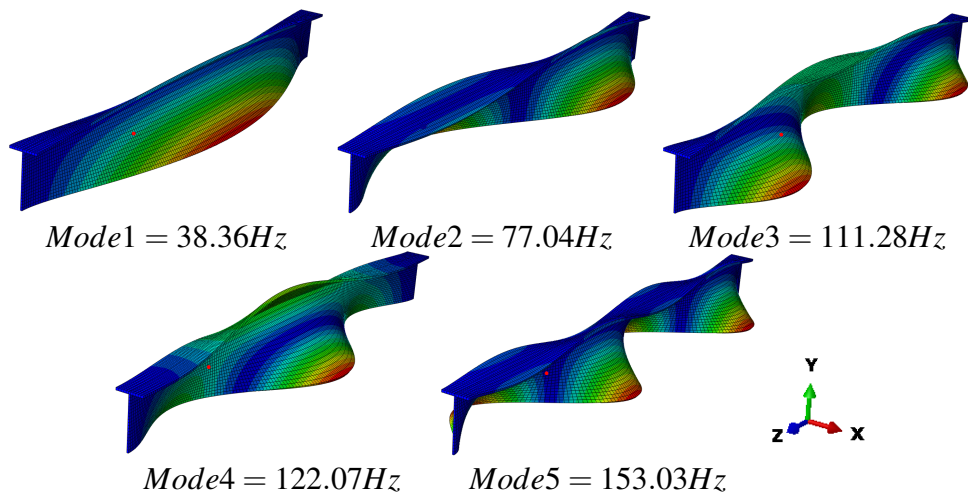


Fig. 6.12 Modal shapes in Beam 2 and BC2–quadratic element within Abaqus

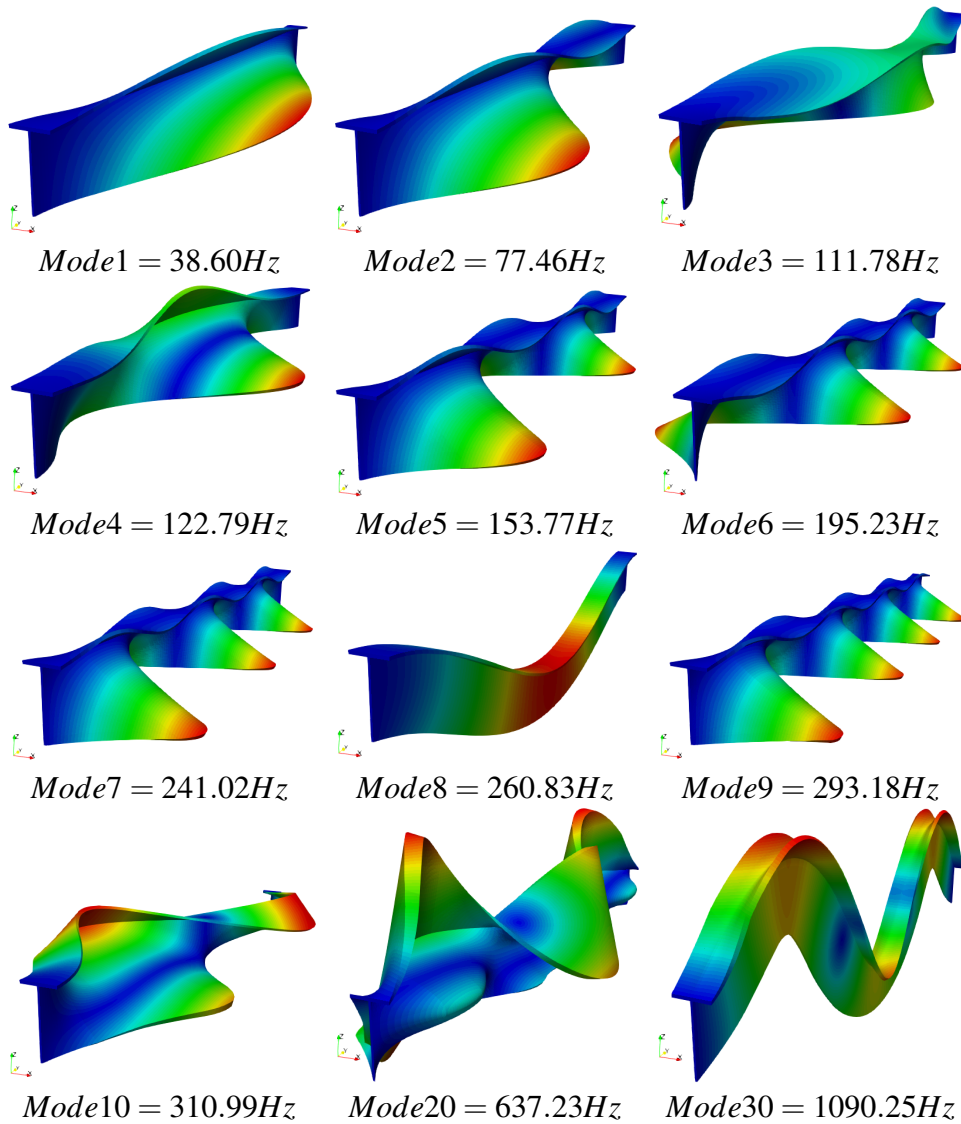


Fig. 6.13 Modal shapes in Beam 2 and BC2– quadratic element within CUF framework.

Table 6.9 References study for Beam 2 BC3 with quadratic elements.

Model	DOFs	Natural Frequency (Hz)										*a %
		Mode 1	Mode 2	Mode 3	Mode 4	Mode 5	Mode 6	Mode 7	Mode 8	Mode 9	Mode 10	
3D FEM (Abaqus)	129459	12.51	27.42	45.37	54.54	88.12	123.98	130.49	166.27	205.49	249.77	Reference
Hung Hu Chen (B3Dw) [111]	-	12.48	27.61	45.75	55.89	92.66	128.91	141.8	188.27	236.87	282.85	-0.23
BC2CM [113]	-	12.48	27.62	45.75	55.90	92.68	128.84	141.83	188.31	236.95	282.85	-0.23
Euler-Bernoulli	243	13.98	45.69	87.56	244.72	282.49	478.45	646.52	774.45	789.16	1176.95	11.75
Timoshenko	243	13.98	45.42	87.22	242.48	271.69	470.53	646.52	713.06	768.82	1133.95	11.75

\*a Percentage difference from 3D solid Abaqus model (Reference)

Table 6.10 Mesh study for Beam 2 BC3 with quadratic elements.

Model	DOFs	Natural Frequency (Hz)										*a %
		Mode 1	Mode 2	Mode 3	Mode 4	Mode 5	Mode 6	Mode 7	Mode 8	Mode 9	Mode 10	
CUF 15×13B3	7033	12.54	27.54	45.40	54.79	88.42	124.35	130.89	166.94	206.60	251.94	0.23
CUF 15×20B3	114391	12.52	27.52	45.33	54.75	88.37	124.20	130.75	166.66	205.94	250.41	0.07
CUF 15×13B4	11160	12.52	27.51	45.30	54.73	88.36	124.15	130.71	166.60	205.80	250.09	0.07
CUF 15×20B4	17019	12.51	27.50	45.27	54.71	88.33	124.07	130.65	166.54	205.71	249.95	0

\*a Percentage difference from 3D solid Abaqus Model (Reference)

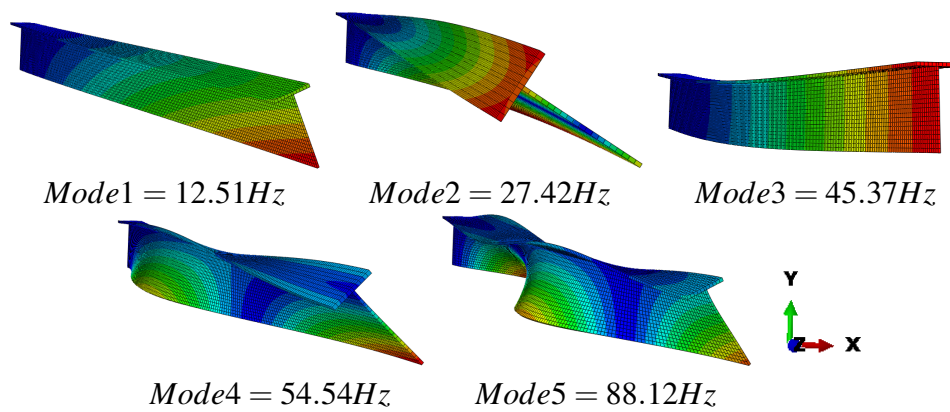


Fig. 6.14 Modal shapes in Beam 2 and BC3– quadratic element within Abaqus.

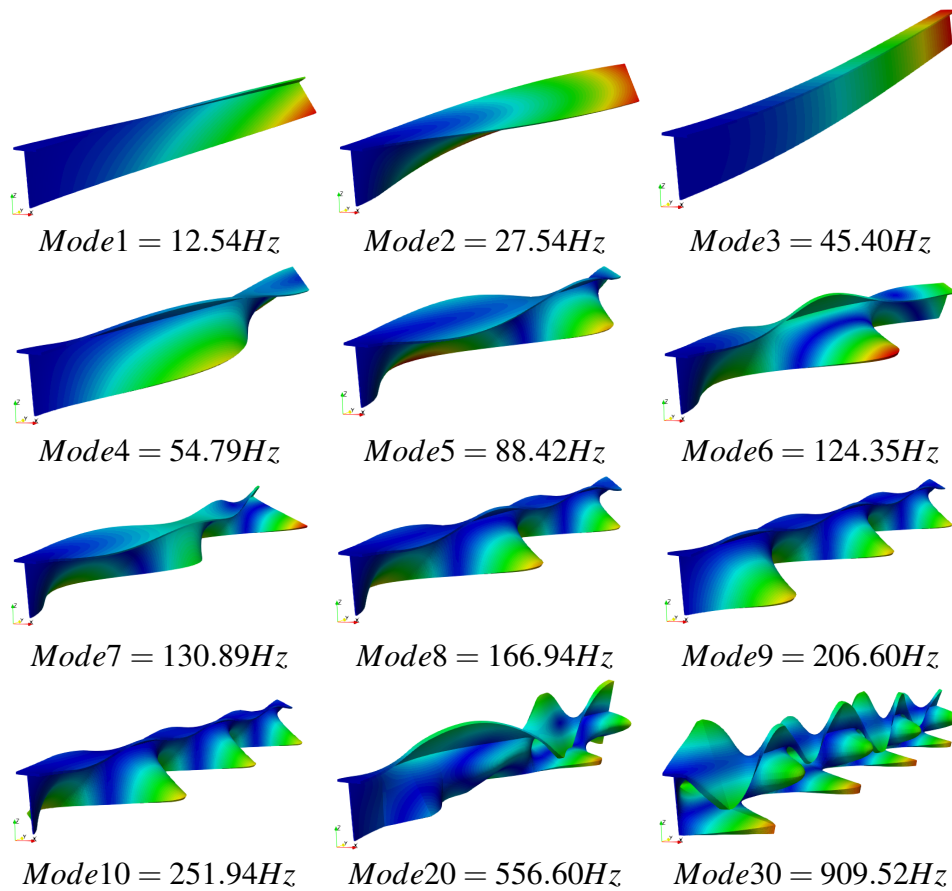


Fig. 6.15 Modal shapes in Beam 2 and BC3– quadratic element within CUF framework (15L9-13B3).

### 6.3.4 Arbitrary non-symmetric cross-section beams

In the current section, the arbitrary non-symmetric cross-section beams are displayed based on Figure. 6.15. First, current beam examined for BC2 and the results are compared for Reference models and CUF in Table 6.11 and 6.12, sequentially. Moreover, the modal shapes in Abaqus and CUF framework are presented in Figure. 6.17 and 6.18, accordingly. Then, The same beam evaluated in BC3 and the effects are reported in Table 6.13 and 6.14 and the modal shapes are shown in Figure 6.19 and 6.20 for the FEM model in Abaqus and CUF, respectively.

The next model for arbitrary non-symmetric cross-section beams solved in Figure 6.21. Consequently, the results are displayed in various frame and theories (Abaqus, references and CUF) as they are shown in Table 6.15 and 6.16 for BC2 and Table



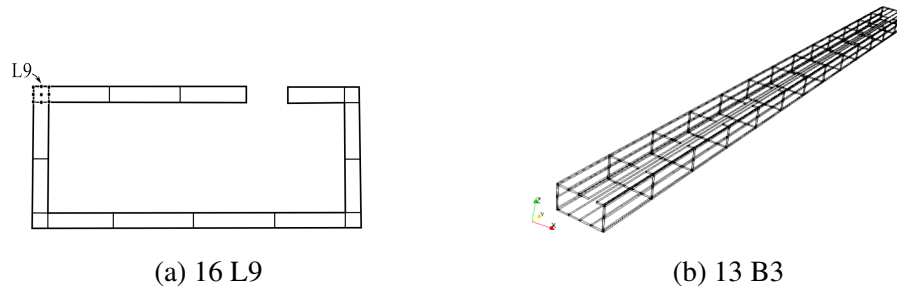


Fig. 6.16 1D CUF model discretization in beam 3 (a) over the cross sections and (b) through the beam.

6.17 and 6.18 for BC3. The modal shapes in FEM and CUF, also detailed in Figure. 6.22 and Figure. 6.23 for BC2 and 6.24 and 6.25 for BC3, apiece.

Table 6.11 Reference study for Beam 3 BC2 with quadratic element.

Model	DOFs	Natural Frequency (Hz)										*a %
		Mode 1	Mode 2	Mode 3	Mode 4	Mode 5	Mode 6	Mode 7	Mode 8	Mode 9	Mode 10	
3D ABAQUS Quadratic	163179	18.33	25.19	37.22	43.23	54.57	54.76	66.06	71.63	73.03	77.14	Reference
Hung Hu Chen (B3Dw) [111]	-	19.21	29.18	52.63	75.54	79.94	102.69	155.57	168.94	202.08	251.01	0.3
BC2CM [113]	-	19.21	29.18	52.63	75.54	79.94	102.7	155.58	168.94	202.08	251.11	0.3
Euler-Bernoulli	243	23.84	41.31	65.56	112.94	128.05	210.75	218.67	256.14	313.42	355.74	30.06
Timoshenko	243	23.59	40.02	64.05	105.73	123.16	199.05	197.02	256.14	290.07	307.90	28.69

\*a Percentage difference from 3D solid Abaqus model (Reference)

Table 6.12 Convergence analysis in Beam 3 BC2 with quadratic element.

Model	DOFs	Natural Frequency (Hz)										*a %
		Mode 1	Mode 2	Mode 3	Mode 4	Mode 5	Mode 6	Mode 7	Mode 8	Mode 9	Mode 10	
CUF 16×13B3	8019	18.49	25.39	37.51	43.61	55.29	55.18	66.62	72.87	74.10	78.30	0.87
CUF 16×20B3	12177	18.43	25.33	37.44	43.54	55.05	55.11	66.48	72.72	74.04	78.27	0.54
CUF 16×13B4	11880	18.41	25.31	37.42	43.52	55.06	55.01	66.43	72.67	74.02	78.27	0.43
CUF 16×20B4	18117	18.38	25.27	37.39	43.49	54.97	54.95	66.36	72.62	73.99	78.25	0.27

\*a Percentage difference from 3D solid Abaqus model (Reference)

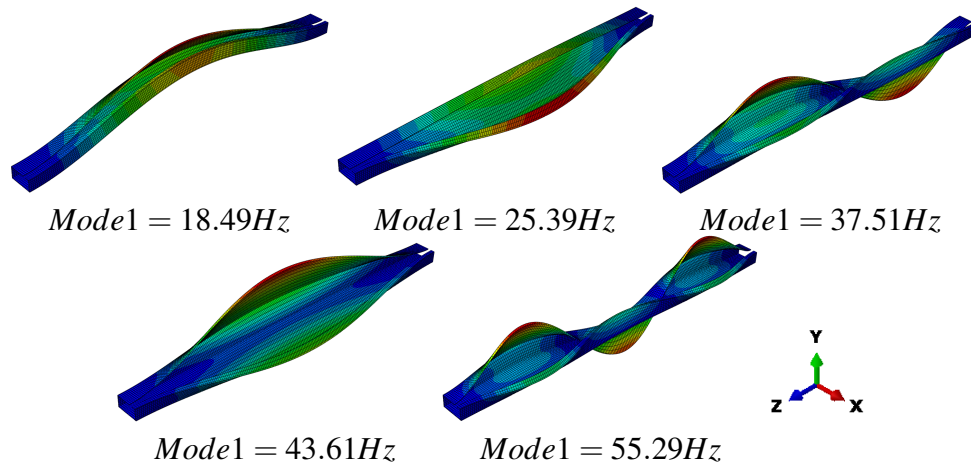


Fig. 6.17 Modal shapes in Beam 3 and BC2– quadratic element within Abaqus.

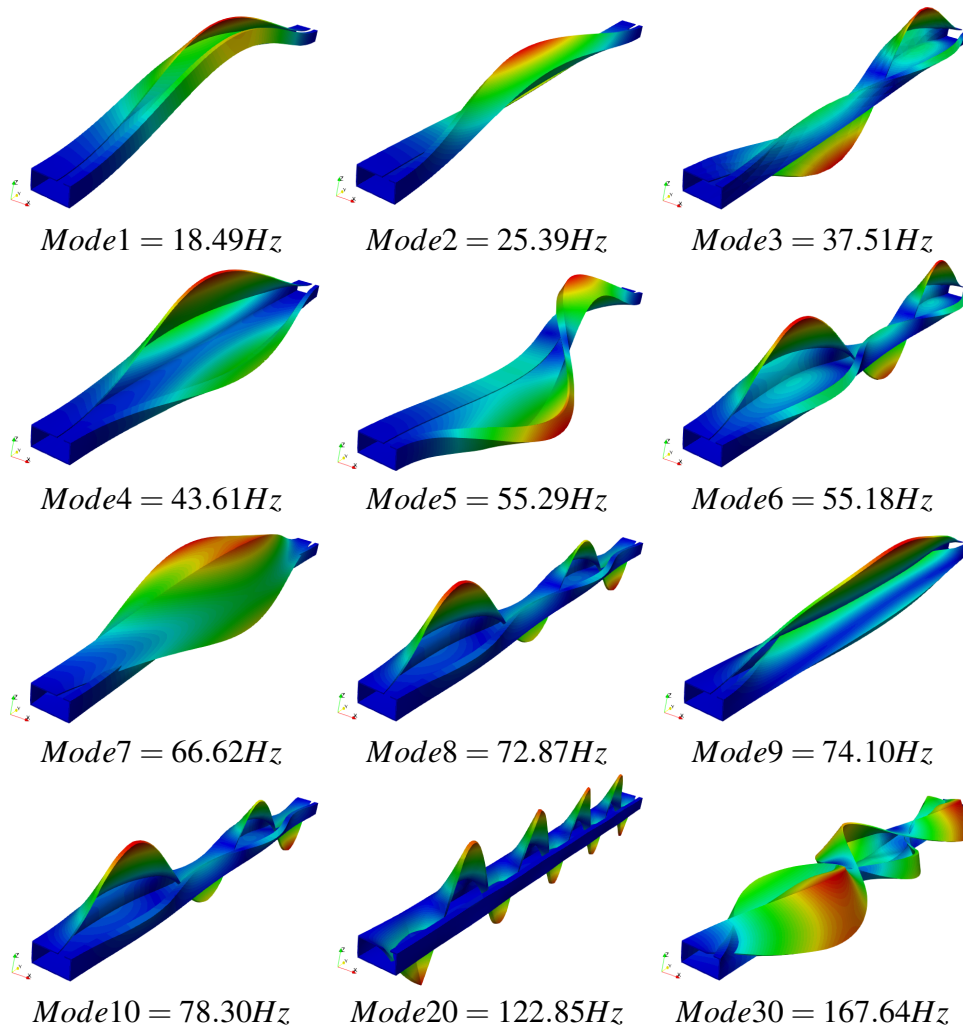


Fig. 6.18 Modal shapes in Beam 3 and BC2– quadratic element within CUF framework.

Table 6.13 Reference study for Beam 3 BC3 with LEs on the cross section (L9).

Model	DOFs	Natural Frequency (Hz)										*a %
		Mode 1	Mode 2	Mode 3	Mode 4	Mode 5	Mode 6	Mode 7	Mode 8	Mode 9	Mode 10	
3D FEM (Abaqus)	901284	3.26	4.79	12.35	18.40	25.45	37.57	38.09	43.84	55.40	56.05	Reference
Hung Hu Chen (B3Dw) [111]	-	3.27	4.81	12.63	19.17	28.84	52.71	73.68	79.77	102.56	128.07	0.3
BC2CM [113]	-	3.27	4.81	12.63	19.17	28.84	52.71	73.68	79.77	102.56	128.1	0.3
Euler-Bernoulli	243	3.75	6.50	23.44	40.48	65.41	112.10	127.58	128.07	209.76	216.34	15.03
Timoshenko	243	3.74	6.48	23.28	39.64	64.34	107.01	123.85	128.07	200.41	199.89	14.72

\*a Percentage difference from 3D solid Abaqus model (Reference)

Table 6.14 Mesh study for Beam 3 BC3 with LEs on the cross section (L9).

Model	DOFs	Natural Frequency (Hz)										*a %
		Mode 1	Mode 2	Mode 3	Mode 4	Mode 5	Mode 6	Mode 7	Mode 8	Mode 9	Mode 10	
CUF 16×13B3	8019	3.28	4.81	12.41	18.50	25.58	37.92	38.35	44.23	55.78	56.56	0.61
CUF 16×20B3	12177	3.27	4.81	12.39	18.47	25.55	37.91	38.31	44.19	55.69	56.48	0.30
CUF 16×13B4	11880	3.27	4.80	12.38	18.46	25.54	37.91	38.30	44.18	55.66	56.45	0.30
CUF 16×20B4	18117	3.27	4.80	12.37	18.44	25.52	37.90	38.28	44.16	55.62	56.42	0.30

\*a Percentage difference from 3D solid Abaqus model (Reference)

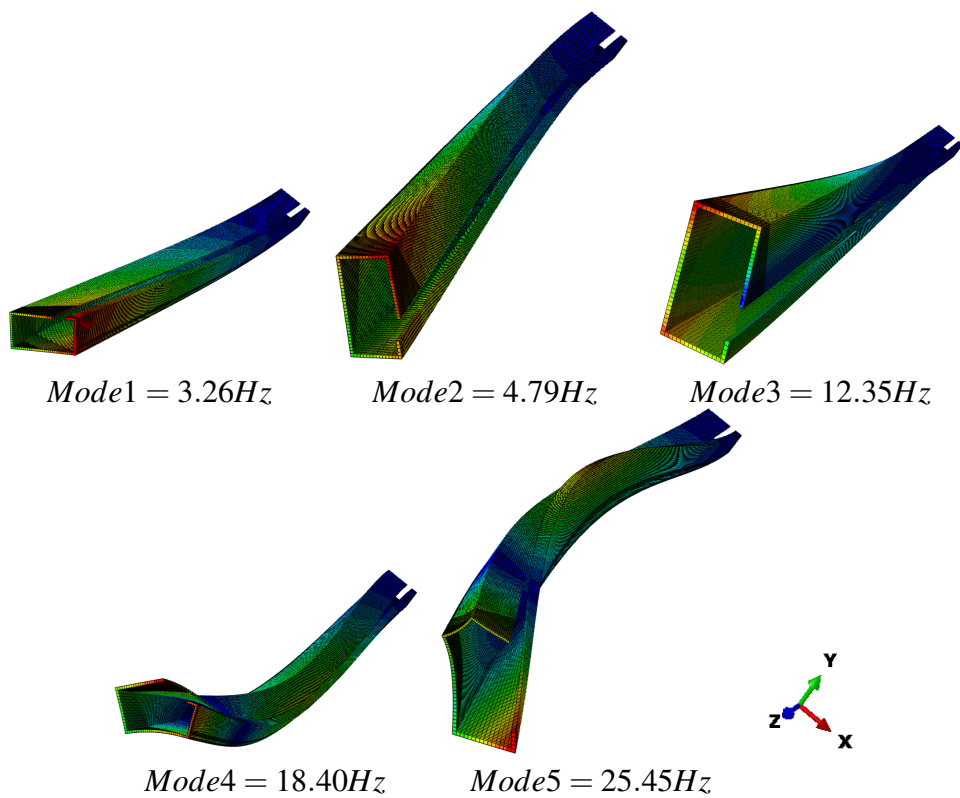


Fig. 6.19 Modal shapes in Beam 3 and BC3–quadratic element within Abaqus

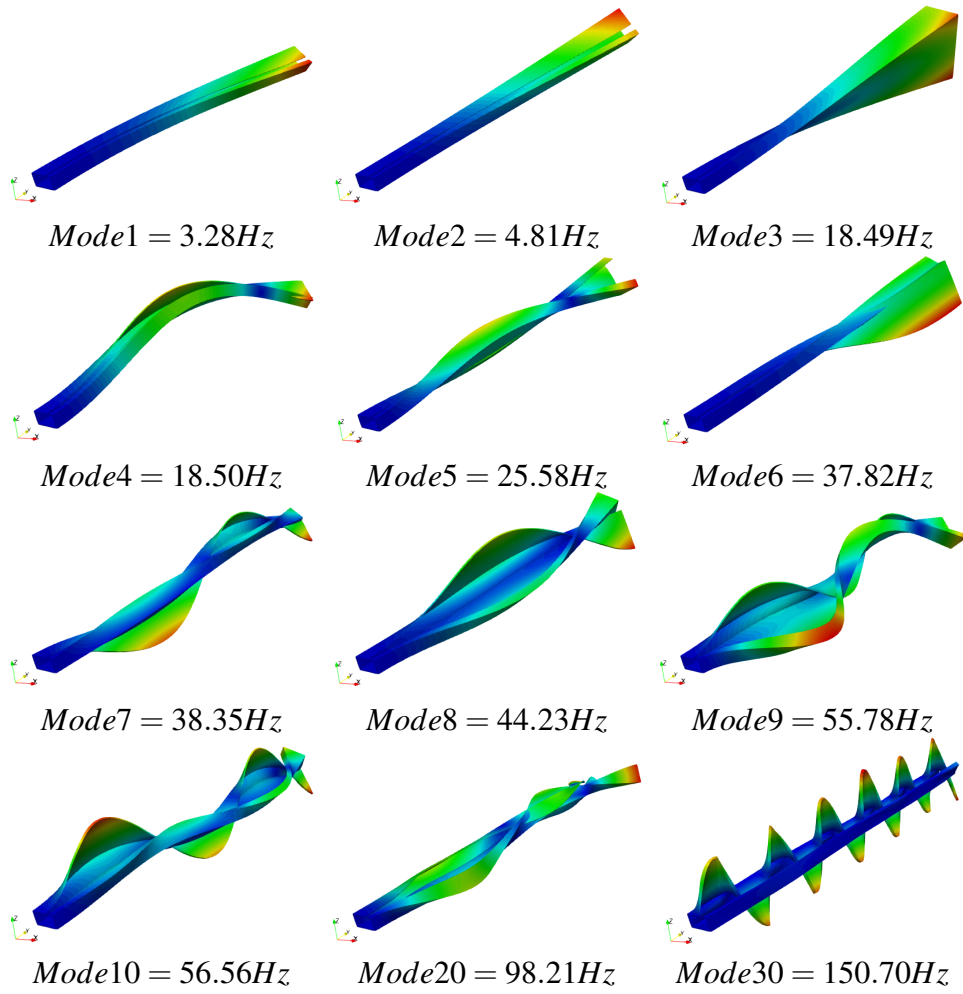


Fig. 6.20 Modal shapes in Beam 3 and BC3– quadratic element within CUF framework..

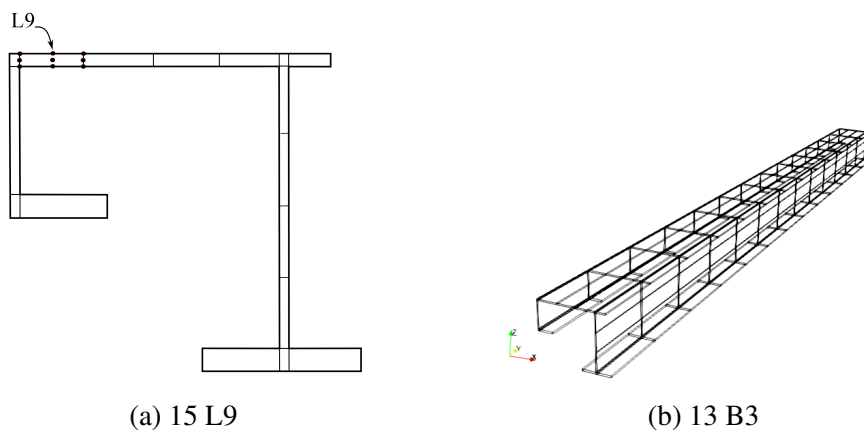


Fig. 6.21 1D CUF model discretization in beam 4 (a) over the cross sections and (b) through the beam.

Table 6.15 Reference study for Beam 4 BC2 with quadratic elements.

Model	DOFs	Natural Frequency (Hz)										*a %
		Mode 1	Mode 2	Mode 3	Mode 4	Mode 5	Mode 6	Mode 7	Mode 8	Mode 9	Mode 10	
3D FEM (Abaqus)	78444	17.00	39.46	45.69	66.86	70.56	74.88	87.45	87.66	95.30	97.63	Reference
Hung Hu Chen (B3Dw) [111]	-	17.86	36.53	48.90	83.58	95.41	100.03	157.03	194.07	223.21	233.44	5.05
BC2CM [113]	-	17.86	36.53	48.90	83.58	95.41	100.03	157.05	194.08	223.21	233.53	5.05
Euler-Bernoulli	243	34.53	52.57	94.65	142.95	183.98	256.14	274.62	300.84	442.36	443.86	103.11
Timoshenko	243	33.77	49.99	90.27	129.19	170.43	235.42	256.14	269.90	360.28	385.24	98.64

\*a Percentage difference from 3D solid Abaqus model (Reference)

Table 6.16 Convergence study in Beam 4 BC2– quadratic elements in CUF framework.

Model	DOFs	Natural Frequency (Hz)										*a %
		Mode 1	Mode 2	Mode 3	Mode 4	Mode 5	Mode 6	Mode 7	Mode 8	Mode 9	Mode 10	
CUF 15×13B3	7533	16.09	25.16	29.50	38.80	43.31	25.16	29.50	59.05	68.56	72.99	-5.35
CUF 15×20B3	11439	16.04	25.10	29.45	38.77	43.24	47.57	56.60	58.88	68.44	72.74	-5.64
CUF 15×13B4	11160	16.03	25.08	29.43	38.73	43.22	47.55	56.57	58.83	68.41	72.66	-5.70
CUF 15×20B4	17019	16.00	25.05	29.40	38.67	43.18	47.52	56.51	58.74	68.35	72.55	-5.88

\*a Percentage difference from 3D solid Abaqus model (Reference)

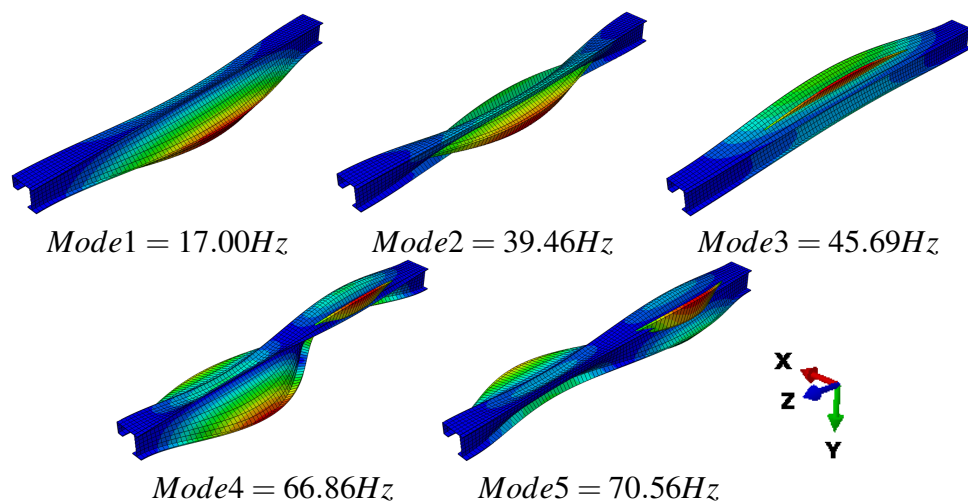


Fig. 6.22 Modal shapes in Beam 4 and BC2– quadratic element within 3D solid in Abaqus.

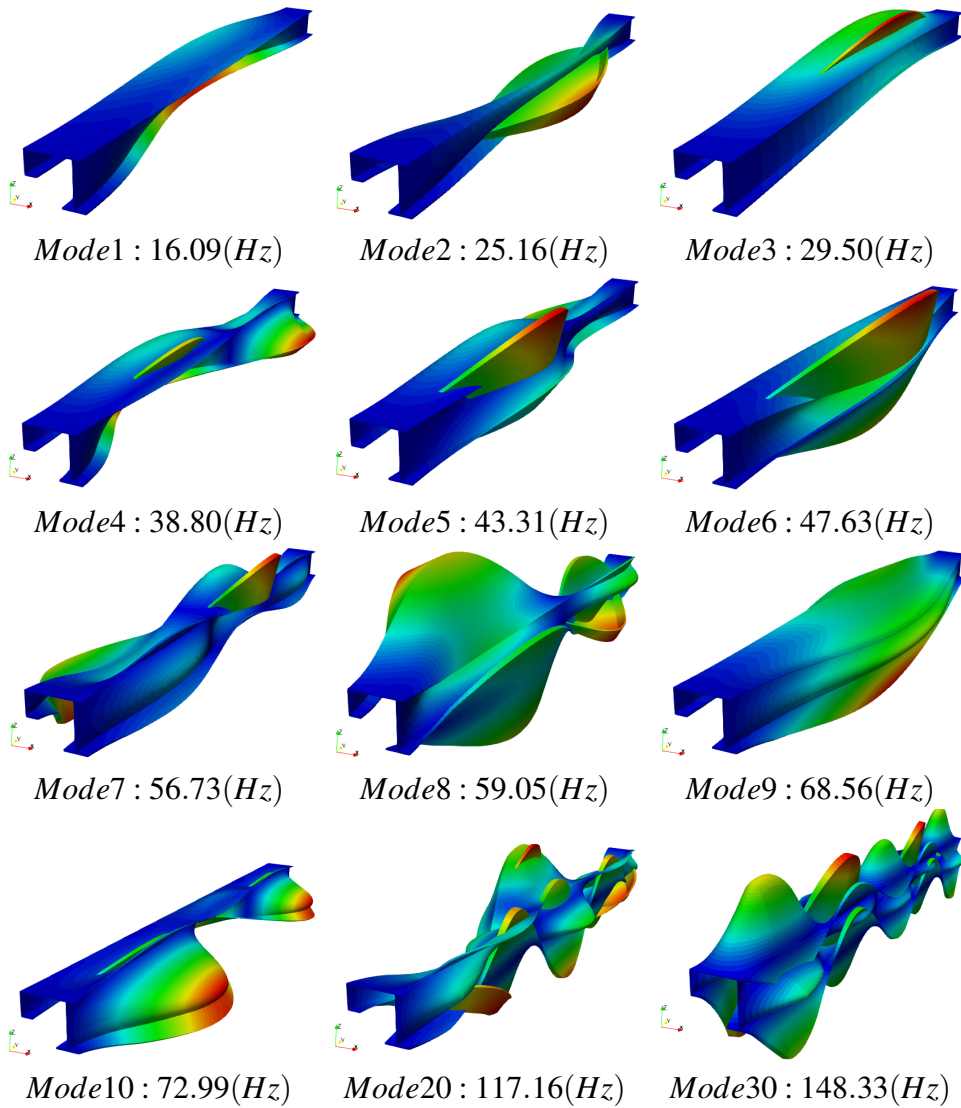


Fig. 6.23 Modal shapes in Beam 4 and BC2– quadratic element within CUF framework.

Table 6.17 Reference solutions in Beam 4 BC3 with quadratic element.

Model	DOFs	Natural Frequency (Hz)										*a %
		Mode 1	Mode 2	Mode 3	Mode 4	Mode 5	Mode 6	Mode 7	Mode 8	Mode 9	Mode 10	
3D FEM (Abaqus)	78444	3.13	5.70	12.23	15.98	16.16	25.24	29.21	38.46	38.67	42.51	Reference
Hung Hu Chen (B3Dw) [111]	-	3.16	5.77	13.45	17.88	35.85	49.01	81.01	95.34	99.47	128.07	0.95
BC2CM [113]	-	3.16	5.77	13.45	17.88	35.85	49.02	81.01	95.34	99.47	128.1	0.95
Euler-Bernoulli	243	5.43	8.28	33.89	51.35	94.17	128.07	141.24	182.58	270.06	297.98	73.48
Timoshenko	243	5.42	8.24	33.39	49.68	91.07	128.07	131.5	172.27	240.42	273.37	73.16

\*a Percentage difference from 3D solid Abaqus model (Reference)

Table 6.18 Convergence analysis in Beam 4 BC3– quadratic element in CUF model.

Model	DOFs	Natural Frequency (Hz)										*a %
		Mode 1	Mode 2	Mode 3	Mode 4	Mode 5	Mode 6	Mode 7	Mode 8	Mode 9	Mode 10	
CUF 15× 13B3	7533	3.16	5.72	12.34	16.17	16.33	25.65	29.84	39.18	40.71	44.47	0.95
CUF 15× 20B3	11439	3.15	5.71	12.32	16.31	16.15	25.62	29.81	39.12	40.71	44.43	0.63
CUF 15× 13B4	11160	3.15	5.71	12.32	16.15	16.30	25.61	29.80	39.10	40.71	44.41	0.63
CUF 15× 20B4	17019	3.15	5.71	12.31	16.14	16.29	25.60	29.78	39.06	40.70	44.40	0.63

\*a Percentage difference from 3D solid Abaqus model (Reference)

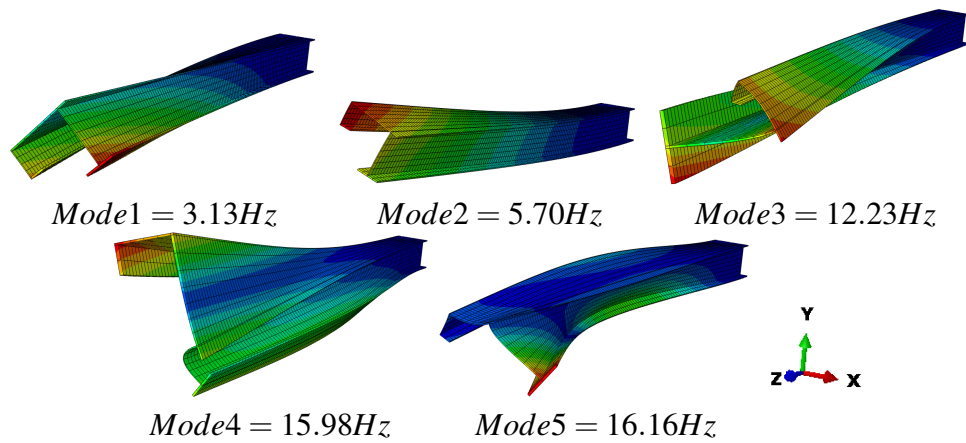


Fig. 6.24 Modal shapes in Beam 4 with BC3– 3D solid FEM in Abaqus with quadratic element.



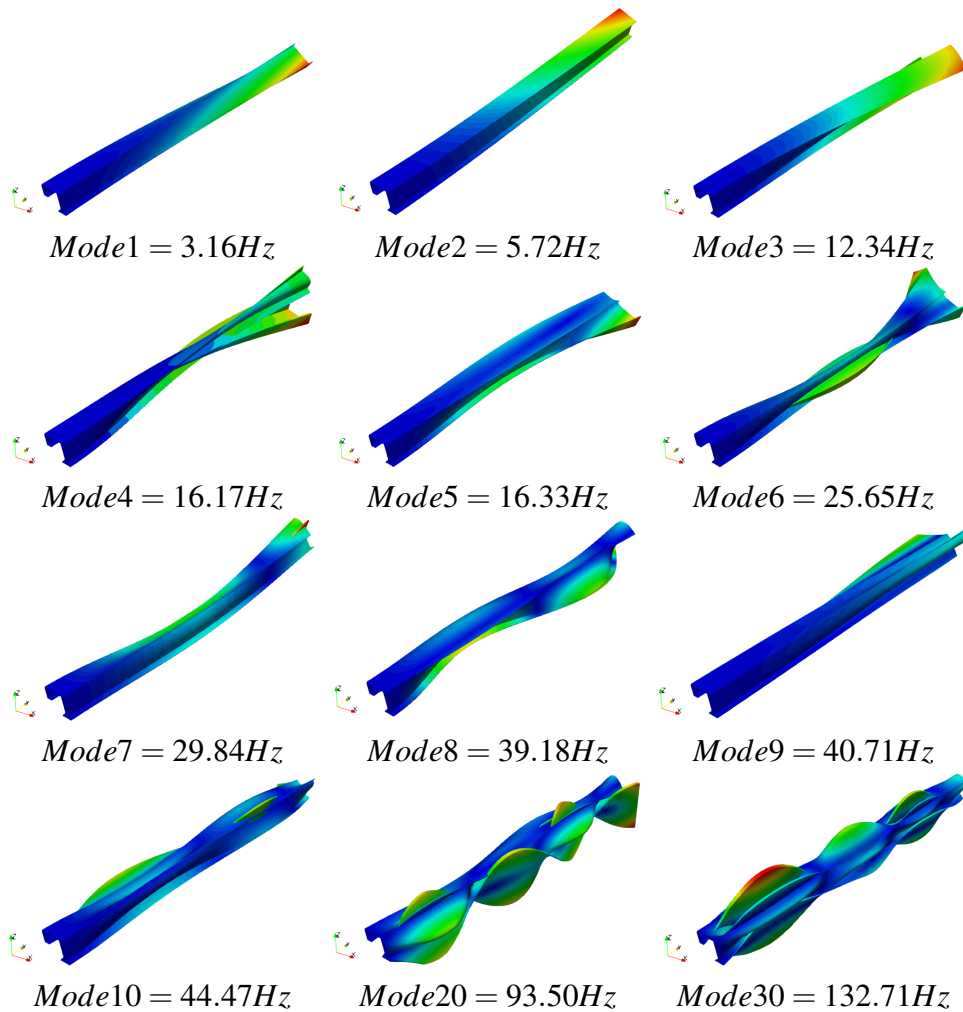


Fig. 6.25 Modal shapes in Beam 4 and BC3– quadratic element within CUF framework.

### 6.3.5 Doubly clamped T-shaped thin walled beam

As it mentioned in the Chapter 2, EBBT and TBT are the classical beam theories that are faced with the problem of detecting the non-classical effects like warping, out and in-plane effects, or coupling of torsion and bending and also local geometrical or mechanical boundary conditions. Especially in slender beams or thin-walled beam structures, these effects can rise [122]. Present study evaluate the classical beam theories (EBBT and TBT) in contrast with the shell models in Abaqus. Table. 6. 19 illustrated the antural frequencies based on EBBT, TBT, and Higher-order Taylor expansion and LE for a horizontal flange with T-shaped cross-section.

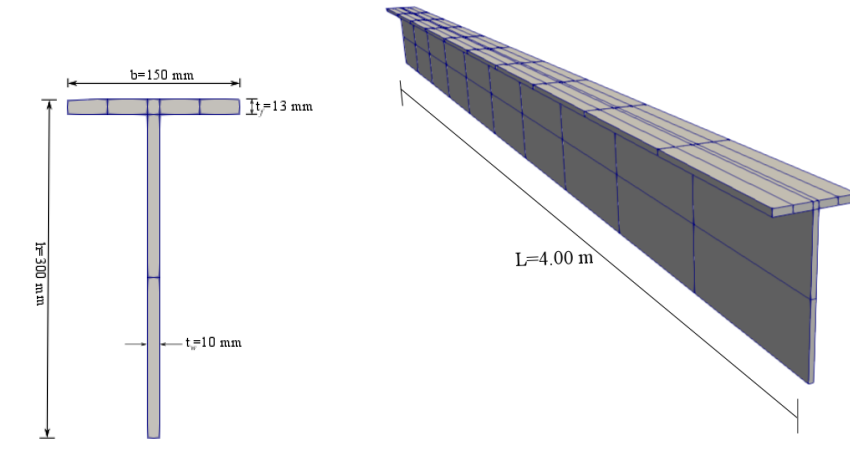


Fig. 6.26 T-shaped cross-section thin-walled beam.

Table 6.19 Doubly clamped T-shaped beam– Convergence analysis.

	Beam Element	Mode 1	Mode 2	Mode 3	Mode 4	Mode 5
Reference	Abaqus	18.61	39.25	45.80	61.78	85.63
CUF	EBBT	31.79	87.57	111.85	171.47	282.99
	TBT	31.70	86.99	107.86	169.54	278.19
	TE2	31.74	86.09	108.19	163.49	213.95
	TE4	29.43	71.85	71.38	105.85	114.81
	TE8	21.29	45.31	47.69	69.97	91.66
	TE12	19.56	41.42	46.43	64.32	83.00
	TE16	18.77	37.72	44.71	64.28	78.34
	LE	18.74	39.40	45.90	61.32	81.66

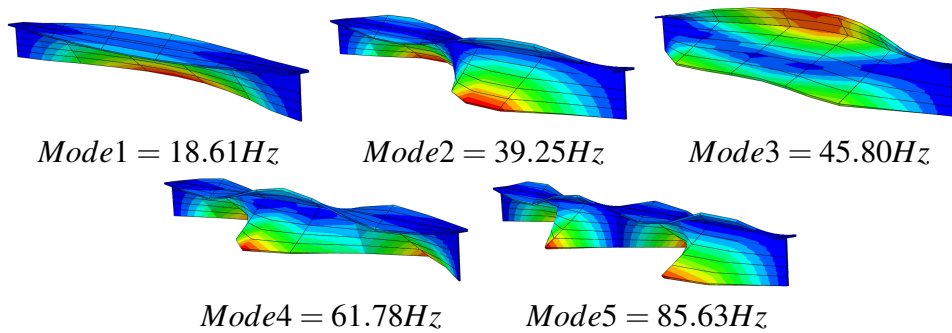


Fig. 6.27 Modal shapes in Doubly-clamped T-shaped beam– Abaqus.

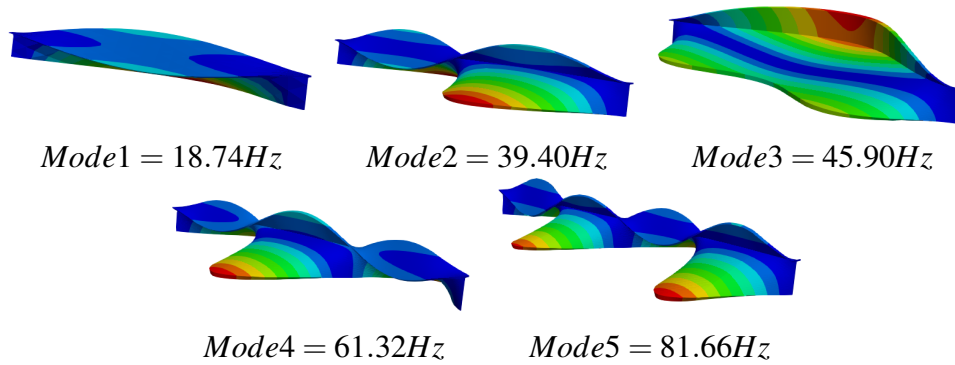


Fig. 6.28 Modal shapes in Doubly-clamped T-shaped beam– CUF framework.

### 6.3.6 Cantilever T-shaped beam

In this section, the eigenvector are presented in Figure 6.29 for 3D solid model in Abaqus for the beam with BC3.

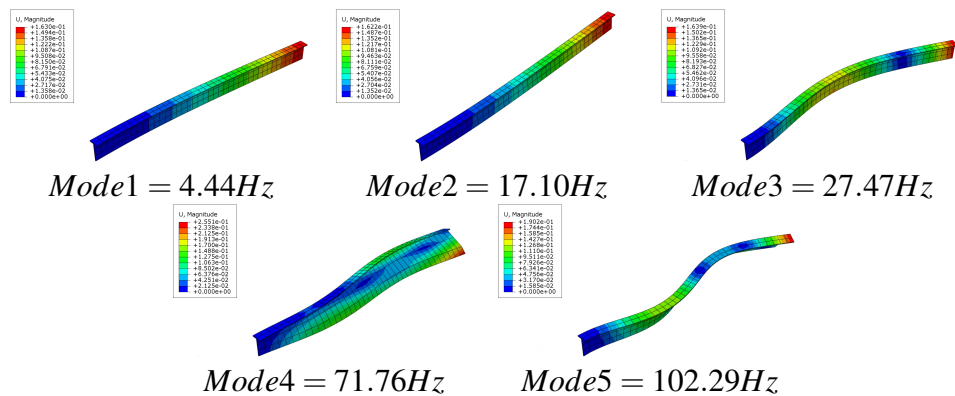


Fig. 6.29 Modal shapes in T-shaped cross-section- 3D solid Abaqus.

### 6.3.7 Cantilever C-shaped- open walled beam

Present problem bring in Figure 6.30 and the results based on 1D CUF for BC3 are shown in Table 6.20 respect to the analytical results in [111]. See also the modal shapes in Figure 6.31.

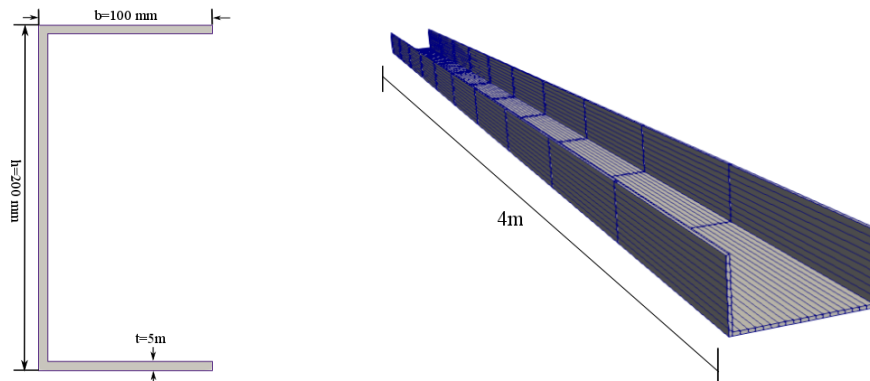


Fig. 6.30 C-shaped thin-walled beam.

Table 6.20 Analytical solution for eigenvalues respect to CUF framework in C-shaped cantilever cross-section- RTO: Rotational Terms Omitted, RTI: Rotational Terms Included.

Model Type	Mode 1	Mode 2	Mode 3	Mode 4	Mode 5
Analytical result (RTO) [111]	$F_1 = 5.69$	$F_2 = 7.47$	$F_3 = 18.75$	$F_4 = 31.50$	$F_5 = 35.68$
Analytical result (RTI) [111]	$F_1 = 5.69$	$F_2 = 7.47$	$F_3 = 18.72$	$F_4 = 31.48$	$F_5 = 35.65$
CUF	$F_1 = 5.71$	$F_2 = 7.78$	$F_3 = 18.73$	$F_4 = 33.14$	$F_5 = 35.46$

### 6.3.8 Doubly clamped T-shaped cross-section

In current section, the cross-section mentioned by Figure.6.31 is presented with BC2, see the results in Table 6.21. Natural frequency modal shapes also are shown in Figure. 6.32.

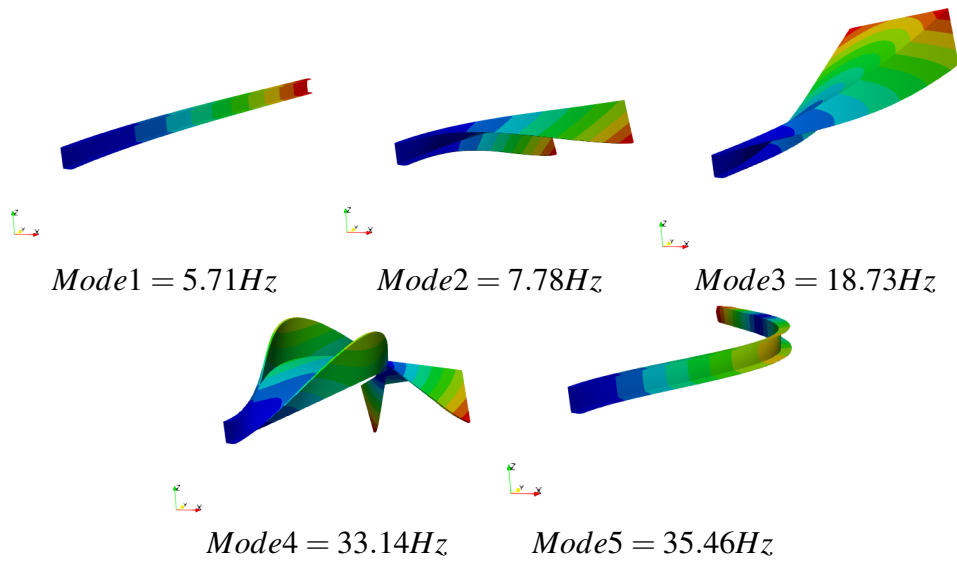


Fig. 6.31 Modal shapes in U-shaped cantilever– CUF framework.

Table 6.21 Analytical natural frequencies respect to CUF procedure in C-shaped doubly-clamped cross-section.

Model type	Mode 1	Mode 2	Mode 3	Mode 4	Mode 5
Analytical result [111]	$F_1 = 31.92$	$F_2 = 36.23$	$F_3 = 80.75$	$F_4 = 99.87$	$F_5 = 115.10$
CUF	$F_1 = 30.13$	$F_2 = 36.01$	$F_3 = 78.69$	$F_4 = 96.11$	$F_5 = 108.01$

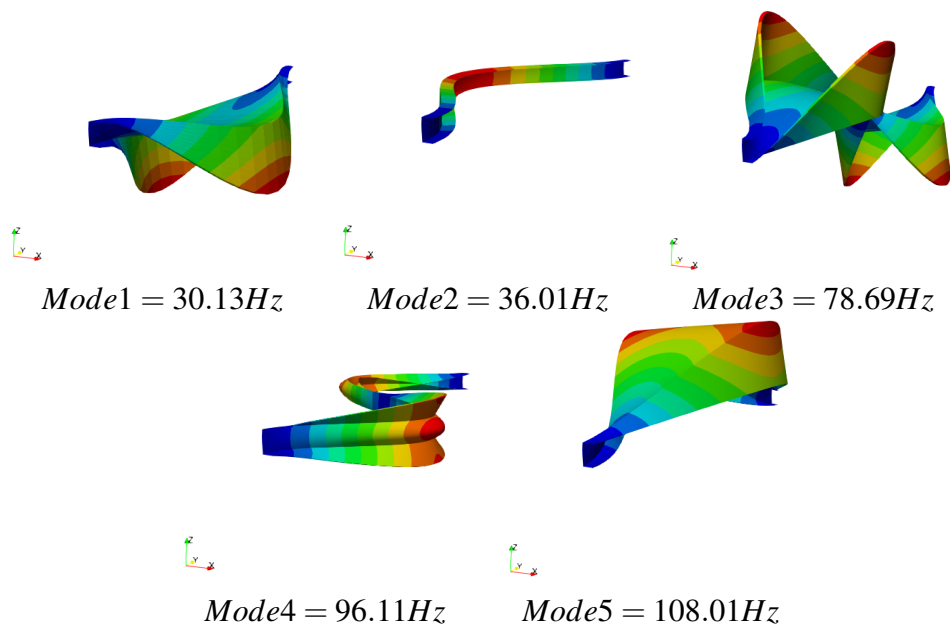


Fig. 6.32 Modal shapes in C-shaped Doubly-clamped cross-section– CUF framework.

The outcome of this chapter is presented in [112].

## 6.4 Conclusion

In the current research, the 1D CUF introduced to evaluate the natural frequencies in the thin-walled beam structures with different geometries of cross-section, various lengths of the beam and also different boundary conditions. In CUF, the long dimension of beams is considered to be model as a 1D model for improving the efficiency of analysis.

1. For the approximation of displacement field, Lagrange expansion are used over the cross-section and the results showed high reliability.
2. In the beams with thin-walled geometries, the discretization of the structure has done by the finite number of 1D beam elements and the results showed a good agreement with the solutions in the kinds of literature.
3. In a different model, the validation and capabilities of the CUF model were investigated and the listed results proved a good solution correlation with the analytical and 3D solid model, with/without warping effects.

Additionally, it has been argued that the innovative procedure performed in this chapter can be employed as a precise tool for structural analysis for complicated cross-section thin-walled beams to overcome computational costs. Additionally, the innovative and precise CUF procedure shows the potential value for evaluation of structural analysis for complex cross-section with the advantage of overcoming to the high computational costs.

# References

- [1] André S de Lima, Alfredo R de Faria, and José JR Faria. Critical review of displacement-based laminate theories and modeling techniques.
- [2] PD Mangalgi. Composite materials for aerospace applications. *Bulletin of Materials Science*, 22(3):657–664, 1999.
- [3] S Budhe, MD Banea, and S de Barros. Bonded repair of composite structures in aerospace application: a review on environmental issues. *Applied Adhesion Science*, 6(1):3, 2018.
- [4] Z. Gürdal, B.F. Tatting, and C.K. Wu. Variable stiffness composite panels: Effects of stiffness variation on the in-plane and buckling response. *Composites Part A: Applied Science and Manufacturing*, 39(5):911 – 922, 2008.
- [5] M.W. Hyer and H.H. Lee. The use of curvilinear fiber format to improve buckling resistance of composite plates with central circular holes. *Composite Structures*, 18(3):239–261, 1991.
- [6] ZAFER GURDAL; REYNALDO OLMEDO. In-plane response of laminates with spatially varying fiber orientations - variable stiffness concept. *AIAA Journal*, 31(4):751–758, 1993.
- [7] A.W. Leissa and A.F. Martin. Vibration and buckling of rectangular composite plates with variable fiber spacing. *Composite Structure*, 14(4):339–357, 1990.
- [8] Riccardo Vescovini and Lorenzo Dozio. A variable-kinematic model for variable stiffness plates: Vibration and buckling analysis. *Composite Structures*, 142:15 – 26, 2016.
- [9] Luciano Demasi, Yonas Ashenafi, Rauno Cavallaro, and Enrico Santarpia. Generalized unified formulation shell element for functionally graded variable-stiffness composite laminates and aeroelastic applications. *Composite Structures*, 131:501–515, 2015.
- [10] R. Olmedo and Z. Gurdal. Buckling response of laminates with spatially varying fiber orientations. *Structural Dynamics and Materials Conference, Structures*, 1993.



- [11] B Tatting and Z Gürdal. Analysis and design of tow-steered variable stiffness composite laminates. In *American Helicopter Society Hampton Roads Chapter, Structure Specialists' Meeting, Williamsburg, VA*, 2001.
- [12] C. Waldhart. Analysis of tow-placed, variable-stiffness laminates. *Master of Science dissertation*, Virginia Tech, 1996.
- [13] Xiaodong Chen and Guojun Nie. Prebuckling and buckling analysis of moderately thick variable angle tow composite plates considering the extension-shear coupling. *Composite Structures*, 242:112093, 2020.
- [14] Broderick H. Coburn, Zhangming Wu, and Paul M. Weaver. Buckling analysis of stiffened variable angle tow panels. *Composite Structures*, 111:259 – 270, 2014.
- [15] Broderick H. Coburn and Paul M. Weaver. Buckling analysis, design and optimisation of variable-stiffness sandwich panels. *International Journal of Solids and Structures*, 96:217 – 228, 2016.
- [16] M. Hachemi, S. M. Hamza-Cherif, and A. Houmat. Free vibration analysis of variable stiffness composite laminate plate with circular cutout. *Australian Journal of Mechanical Engineering*, 18(1):63–79, 2020.
- [17] Z. Kheladi, Sidi Mohammed Hamza-Cherif, and M. E. A. Ghernaout. Free vibration analysis of variable stiffness laminated composite beams. *Mechanics of Advanced Materials and Structures*, 0(0):1–28, 2020.
- [18] Giuseppe Sciascia, Vincenzo Oliveri, Alberto Milazzo, and Paul M. Weaver. Ritz solution for transient analysis of variable-stiffness shell structures. *AIAA Journal*, 58(4):1796–1810, 2020.
- [19] E. Carrera, M. Cinefra, M. Petrolo, and E. Zappino. *Finite Element Analysis of Structures Through Unified Formulation*. John Wiley & Sons, 2014.
- [20] Giunta G. Carrera, E. and M. Petrolo. *Beam Structures: Classical and Advanced Theories*. Wiley, Hoboken, 2011.
- [21] E. Carrera. Evaluation of layerwise mixed theories for laminated plates analysis. *AIAA Journal*, 36(5):830–839, 1998.
- [22] E Carrera. Layer-wise mixed models for accurate vibrations analysis of multilayered plates. 1998.
- [23] E. Carrera, A. Pagani, and S. Valvano. Shell elements with through-the-thickness variable kinematics for the analysis of laminated composite and sandwich structures. *Composites Part B: Engineering*, 111:294 – 314, 2017.
- [24] Erasmo Carrera and Stefano Valvano. Analysis of laminated composite structures with embedded piezoelectric sheets by variable kinematic shell elements. *Journal of Intelligent Material Systems and Structures*, 28(20):2959–2987, 2017.

- [25] Alfonso Pagani, Stefano Valvano, and Erasmo Carrera. Analysis of laminated composites and sandwich structures by variable-kinematic mitc9 plate elements. *Journal of Sandwich Structures & Materials*, 20(1):4–41, 2018.
- [26] Yang Yan, Alfonso Pagani, and Erasmo Carrera. Exact solutions for free vibration analysis of laminated, box and sandwich beams by refined layerwise theory. *Composite Structures*, 175:28 – 45, 2017.
- [27] Masoud Tahani. Analysis of laminated composite beams using layerwise displacement theories. *Composite Structures*, 79(4):535 – 547, 2007.
- [28] Ayoob Entezari, Mohammad Ali Kouchakzadeh, Erasmo Carrera, and Matteo Filippi. A refined finite element method for stress analysis of rotors and rotating disks with variable thickness. *Acta Mechanica*, 228(2):575–594, 2017.
- [29] E. Carrera, A. Entezari, M. Filippi, and M. A. Kouchakzadeh. 3d thermoelastic analysis of rotating disks having arbitrary profile based on a variable kinematic 1d finite element method. *Journal of Thermal Stresses*, 39(12):1572–1587, 2016.
- [30] Serge Abrate and Marco Di Sciuva. Equivalent single layer theories for composite and sandwich structures: A review. *Composite Structures*, 179:482–494, 2017.
- [31] Eric Reissner. The effect of transverse shear deformation on the bending of elastic plates. *J. appl. Mech.*, pages A69–A77, 1945.
- [32] RD0044 Mindlin. Influence of rotatory inertia and shear on flexural motions of isotropic, elastic plates. *J. appl. Mech.*, 18:31–38, 1951.
- [33] Julio F Davalos, Youngchan Kima, and Ever J Barberob. Analysis of laminated beams with a layer-wise constant shear theory. *Composite Structures*, 28:241–253, 1994.
- [34] Dahsin Liu and Xiaoyu Li. An overall view of laminate theories based on displacement hypothesis. *Journal of composite materials*, 30(14):1539–1561, 1996.
- [35] Chun-Ying Lee and Dahsin Liu. An interlaminar stress continuity theory for laminated composite analysis. *Computers & structures*, 42(1):69–78, 1992.
- [36] Erasmo Carrera. Historical review of zig-zag theories for multilayered plates and shells. *Appl. Mech. Rev.*, 56(3):287–308, 2003.
- [37] SG Lekhnitskii. Strength calculation of composite beams. *Vestnik inzhen i tekhnikov*, 9:137–148, 1935.
- [38] SA Ambartsumian. On the theory of bending of anisotropic plates and shallow shells. *Journal of Applied Mathematics and Mechanics*, 24(2):500–514, 1960.

- [39] A Pagani, M Petrolo, G Colonna, and E Carrera. Dynamic response of aerospace structures by means of refined beam theories. *Aerospace Science and Technology*, 46:360–373, 2015.
- [40] KJ Bathe. Finite element procedures, 1996, ch. 6.
- [41] E Carrera, A Pagani, PH Cabral, A Prado, and G Silva. Component-wise models for the accurate dynamic and buckling analysis of composite wing structures. In *ASME 2016 International Mechanical Engineering Congress and Exposition*. American Society of Mechanical Engineers Digital Collection, 2017.
- [42] Dirk P Kroese, Tim Brereton, Thomas Taimre, and Zdravko I Botev. Why the monte carlo method is so important today. *Wiley Interdisciplinary Reviews: Computational Statistics*, 6(6):386–392, 2014.
- [43] G Giunta. *Deterministic and stochastic hierarchical analysis of failure and vibration of composite plates and shells*. PhD thesis, Phd thesis, Politecnico Di Torino, 2008.
- [44] Anders Olsson, Göran Sandberg, and Ola Dahlblom. On latin hypercube sampling for structural reliability analysis. *Structural safety*, 25(1):47–68, 2003.
- [45] Stephanie Glen. Latin hypercube sampling: Simple definition.
- [46] George EP Box and Kenneth B Wilson. On the experimental attainment of optimum conditions. *Journal of the royal statistical society: Series b (Methodological)*, 13(1):1–38, 1951.
- [47] D.J. Lekou. 10 - probabilistic design of wind turbine blades. In Povl Brøndsted and Rogier P.L. Nijssen, editors, *Advances in Wind Turbine Blade Design and Materials*, Woodhead Publishing Series in Energy, pages 325 – 359. Woodhead Publishing, 2013.
- [48] Christelle Salameh. *Vibrations ambiantes, contenu spectral et dommages sismiques: nouvelle approche adaptée à l'échelle urbaine. Application à Beyrouth*. PhD thesis, Grenoble Alpes, 2016.
- [49] H. Akaike. A new look at the statistical model identification. *IEEE Transactions on Automatic Control*, 19(6):716–723, 1974.
- [50] Monika Arora, Farhan Ashraf, Vipul Saxena, Garima Mahendru, Monica Kaushik, and Pritish Shubham. A neural network-based comparative analysis of br, lm, and scg algorithms for the detection of particulate matter. In *Advances in Interdisciplinary Engineering*, pages 619–634. Springer, 2019.
- [51] David B Fogel, Lawrence J Fogel, and VW Porto. Evolving neural networks. *Biological cybernetics*, 63(6):487–493, 1990.

- [52] Noboru Murata, Shuji Yoshizawa, and Shun-ichi Amari. Network information criterion-determining the number of hidden units for an artificial neural network model. *IEEE transactions on neural networks*, 5(6):865–872, 1994.
- [53] Gaurang Panchal, Amit Ganatra, YP Kosta, and Devyani Panchal. Searching most efficient neural network architecture using akaike’s information criterion (aic). *International Journal of Computer Applications*, 1(5):41–44, 2010.
- [54] Robert M. Jones. *Mechanics Of Composite Materials*. CRC Press, 2018.
- [55] Dianzi Liu, Vassili V. Toropov, David C. Barton, and Osvaldo M. Querin. Weight and mechanical performance optimization of blended composite wing panels using lamination parameters. *Structural and Multidisciplinary Optimization*, 52(3):549–562, Sep 2015.
- [56] Mohammad Rouhi, Hossein Ghayoor, Jeffrey Fortin-Simpson, Tom T. Zaccchia, Suong V. Hoa, and Mehdi Hojjati. Design, manufacturing, and testing of a variable stiffness composite cylinder. *Composite Structures*, 184:146 – 152, 2018.
- [57] Mazen A. Albazzan, Ramy Harik, Brian F. Tatting, and Zafer Gürdal. Efficient design optimization of nonconventional laminated composites using lamination parameters: A state of the art. *Composite Structures*, 209:362 – 374, 2019.
- [58] N. Zehnder and P. Ermanni. Optimizing the shape and placement of patches of reinforcement fibers. *Composite Structures*, 77(1):1 – 9, 2007.
- [59] N. Zehnder and P. Ermanni. A methodology for the global optimization of laminated composite structures. *Composite Structures*, 72(3):311 – 320, 2006.
- [60] Jung-Seok Kim, Chun-Gon Kim, and Chang-Sun Hong. Optimum design of composite structures with ply drop using genetic algorithm and expert system shell. *Composite Structures*, 46(2):171 – 187, 1999.
- [61] Shahriar Setoodeh, Zafer Gürdal, and Layne T. Watson. Design of variable-stiffness composite layers using cellular automata. *Computer Methods in Applied Mechanics and Engineering*, 195(9):836 – 851, 2006.
- [62] C.S. Lopes, Z. Gürdal, and P.P. Camanho. Variable-stiffness composite panels: Buckling and first-ply failure improvements over straight-fibre laminates. *Computers & Structures*, 86(9):897 – 907, 2008. Composites.
- [63] P. Jana and K. Bhaskar. Stability analysis of simply-supported rectangular plates under non-uniform uniaxial compression using rigorous and approximate plane stress solutions. *Thin-Walled Structures*, 44(5):507 – 516, 2006.
- [64] Gholamreza Soleimani; Kolahchi Reza; Baseri, Vahid; Jafari. Analytical solution for buckling of embedded laminated plates based on higher order shear deformation plate theory. *Steel and Composite Structures*, 21(4):883–919, 2016.

- [65] Mohamed Ait Amar Meziane, Hadj Henni Abdelaziz, and Abdelouahed Tounsi. An efficient and simple refined theory for buckling and free vibration of exponentially graded sandwich plates under various boundary conditions. *Journal of Sandwich Structures & Materials*, 16(3):293–318, 2014.
- [66] Yuhua Tang and Xinwei Wang. Buckling of symmetrically laminated rectangular plates under parabolic edge compressions. *International Journal of Mechanical Sciences*, 53(2):91 – 97, 2011.
- [67] Peng Hao, Xiaojie Yuan, Hongliang Liu, Bo Wang, Chen Liu, Dixiong Yang, and Shuangxi Zhan. Isogeometric buckling analysis of composite variable-stiffness panels. *Composite Structures*, 165:192 – 208, 2017.
- [68] S.M. Ibrahim, E. Carrera, M. Petrolo, and E. Zappino. Buckling of composite thin walled beams by refined theory. *Composite Structures*, 94(2):563 – 570, 2012.
- [69] E. Carrera, A. Pagani, and J. R. Banerjee. Linearized buckling analysis of isotropic and composite beam-columns by carrera unified formulation and dynamic stiffness method. *Mechanics of Advanced Materials and Structures*, 23(9):1092–1103, 2016.
- [70] E. Carrera, A. Pagani, , and M. Petrolo. Component-wise method applied to vibration of wing structures. *Journal of Applied Mechanics*, 80(4):Paper 041012, 2013.
- [71] E. Carrera, M. Maiarú, and M. Petrolo. Component-wise analysis of laminated anisotropic composites. *International Journal of Solids and Structures*, 49(13):1839 – 1851, 2012.
- [72] E. Carrera, A. Pagani, and M. Petrolo. Refined 1D finite elements for the analysis of secondary, primary, and complete civil engineering structures. *Journal of Structural Engineering*, 141:04014123/1–14, 2015.
- [73] A. Viglietti, E. Zappino, and E. Carrera. Free vibration analysis of variable angle-tow composite wing structures. *Aerospace Science and Technology*, 92:114 – 125, 2019.
- [74] A. Viglietti, E. Zappino, and E. Carrera. Analysis of variable angle tow composites structures using variable kinematic models. *Composites Part B: Engineering*, 171:272 – 283, 2019.
- [75] Carrera E. Pagani A. Zappino E. Fallahi N., Viglietti A. Effect of fiber orientation path on the buckling, free vibration, and static analyses of variable angle tow panels. *FACTA UNIVERSITATIS, Series: Mechanical Engineering*, pages 1–26, 2020.
- [76] Stephen W Tsai, John C Halpin, Nicolas J Pagano, et al. Composite materials workshop. 1968.

- [77] Hisao Fukunaga and Garret N Vanderplaats. Stiffness optimization of orthotropic laminated composites using lamination parameters. *AIAA journal*, 29(4):641–646, 1991.
- [78] B Liu, RT Haftka, and P Trompette. Maximization of buckling loads of composite panels using flexural lamination parameters. *Structural and Multidisciplinary Optimization*, 26(1-2):28–36, 2004.
- [79] Mark W. Bloomfield, J. Enrique Herencia, and Paul M. Weaver. Enhanced two-level optimization of anisotropic laminated composite plates with strength and buckling constraints. *Thin-Walled Structures*, 47(11):1161 – 1167, 2009.
- [80] Shahriar Setoodeh, Mostafa M Abdalla, Samuel T IJsselmuiden, and Zafer Gürdal. Design of variable-stiffness composite panels for maximum buckling load. *Composite structures*, 87(1):109–117, 2009.
- [81] Farhad Alinejad and Daniele Botto. Innovative adaptive penalty in surrogate-assisted robust optimization of blade attachments. *Acta Mechanica*, 230(8):2735–2750, Aug 2019.
- [82] Alexander I.J. Forrester and Andy J. Keane. Recent advances in surrogate-based optimization. *Progress in Aerospace Sciences*, 45(1):50 – 79, 2009.
- [83] Xiao-Yi Zhou, Xin Ruan, and P.D. Gosling. Robust design optimization of variable angle tow composite plates for maximum buckling load in the presence of uncertainties. *Composite Structures*, 223:110985, 2019.
- [84] S. Nikbakt, S. Kamarian, and M. Shakeri. A review on optimization of composite structures part i: Laminated composites. *Composite Structures*, 195:158 – 185, 2018.
- [85] Hossein Ghiasi, Kazem Fayazbakhsh, Damiano Pasini, and Larry Lessard. Optimum stacking sequence design of composite materials part ii: Variable stiffness design. *Composite Structures*, 93(1):1 – 13, 2010.
- [86] Pedro Ribeiro, Hamed Akhavan, Andrzej Teter, and Jerzy Warmański. A review on the mechanical behaviour of curvilinear fibre composite laminated panels. *Journal of Composite Materials*, 48(22):2761–2777, 2014.
- [87] G. Gonzalez Lozano, A. Tiwari, and C. Turner. A design algorithm to model fibre paths for manufacturing of structurally optimised composite laminates. *Composite Structures*, 204:882 – 895, 2018.
- [88] D.W. Kelly and M.W. Tosh. Interpreting load paths and stress trajectories in elasticity. *Engineering Computations*, 17(2):117–135, 2000.
- [89] M.W. Hyer and H.H. Lee. The use of curvilinear fiber format to improve buckling resistance of composite plates with central circular holes. *Composite Structures*, 18(3):239 – 261, 1991.

- [90] Peng Hao, Chen Liu, Xuanxiu Liu, Xiaojie Yuan, Bo Wang, Gang Li, Manhong Dong, and Liang Chen. Isogeometric analysis and design of variable-stiffness aircraft panels with multiple cutouts by level set method. *Composite Structures*, 206:888 – 902, 2018.
- [91] Zhangming Wu, Paul M. Weaver, Gangadharan Raju, and Byung Chul Kim. Buckling analysis and optimisation of variable angle tow composite plates. *Thin-Walled Structures*, 60:163 – 172, 2012.
- [92] Dan Wang, Mostafa M. Abdalla, and Weihong Zhang. Buckling optimization design of curved stiffeners for grid-stiffened composite structures. *Composite Structures*, 159:656 – 666, 2017.
- [93] M. M. Abdalla, Z. Gürdal, and G. F. Abdelal. Thermomechanical response of variable stiffness composite panels. *Journal of Thermal Stresses*, 32(1-2):187–208, 2008.
- [94] Z. Gürdal S. T. Ijsselmuiden, M. M. Abdalla. Optimization of variable-stiffness panels for maximum buckling load using lamination parameters. *AIAA Journal*, 48(1):134–143, 2010.
- [95] Levend Parnas, Süha Oral, and Ümit Ceyhan. Optimum design of composite structures with curved fiber courses. *Composites Science and Technology*, 63(7):1071 – 1082, 2003.
- [96] G. S. Landriani and M. Rovati. Optimal design for two-dimensional structures made of composite materials. *ASME. J. Eng. Mater. Technol.*, 113(1):88–92, 1991.
- [97] Composite wing structural design optimization with continuity constraints. *19th AIAA Applied Aerodynamics Conference*, 2001.
- [98]
- [99] D Botto and F Alinejad. Innovative design of attachment for turbine blade rotating at high speed. In *ASME Turbo Expo 2017: Turbomachinery Technical Conference and Exposition*. American Society of Mechanical Engineers Digital Collection, 2017.
- [100] Fan Ye, Hu Wang, and Guangyao Li. Variable stiffness composite material design by using support vector regression assisted efficient global optimization method. *Structural and Multidisciplinary Optimization*, 56(1):203–219, 2017.
- [101] Farhad Alinejad, D Botto, M Gola, and A Bessone. Reduction of the design space to optimize blade fir-tree attachments. In *ASME Turbo Expo 2018: Turbomachinery Technical Conference and Exposition*. American Society of Mechanical Engineers Digital Collection, 2018.
- [102] VZ Vlasov and Thin-Walled Elastic Beams. Thin-walled elastic beams. *Israel Program for Scientific Translations, Jerusalem, Israel*, 1961.

- [103] Stanley U Bescoter. *Secondary stresses in thin-walled beams with closed cross-sections*. PhD thesis, California Institute of Technology, 1950.
- [104] Erasmo Carrera, Marco Petrolo, and Enrico Zappino. Performance of cuf approach to analyze the structural behavior of slender bodies. *Journal of Structural Engineering*, 138(2):285–297, 2012.
- [105] M Petrolo, E Zappino, and E Carrera. Refined free vibration analysis of one-dimensional structures with compact and bridge-like cross-sections. *Thin-Walled Structures*, 56:49–61, 2012.
- [106] Munise Didem Demirbas, Umut Caliskan, Xiangyang Xu, and Matteo Filippi. Evaluation of the bending response of compact and thin-walled fg beams with cuf. *Mechanics of Advanced Materials and Structures*, pages 1–10, 2020.
- [107] Min Dan, Alfonso Pagani, and Erasmo Carrera. Free vibration analysis of simply supported beams with solid and thin-walled cross-sections using higher-order theories based on displacement variables. *Thin-Walled Structures*, 98:478–495, 2016.
- [108] A Pagani and E Carrera. Unified formulation of geometrically nonlinear refined beam theories. *Mechanics of Advanced Materials and Structures*, 25(1):15–31, 2018.
- [109] Erasmo Carrera, Alberto G de Miguel, and Alfonso Pagani. Hierarchical theories of structures based on legendre polynomial expansions with finite element applications. *International Journal of Mechanical Sciences*, 120:286–300, 2017.
- [110] Daoud S Mashat, E Carrera, Ashraf M Zenkour, Sadah A Al Khateeb, and M Filippi. Free vibration of fgm layered beams by various theories and finite elements. *Composites Part B: Engineering*, 59:269–278, 2014.
- [111] Wassim Jrad. *Dynamic behavior of thin-walled beams: Analytical, numerical and experimental approaches*. PhD thesis, Université de Lorraine, 2019.
- [112] Xiangyang Xu, Nasim Fallahi, and Hao Yang. Efficient cuf-based fem analysis of thin-wall structures with lagrange polynomial expansion. *Mechanics of Advanced Materials and Structures*, 0(0):1–22, 2020.
- [113] Hong Hu Chen and Kuo Mo Hsiao. Quadruply coupled linear free vibrations of thin-walled beams with a generic open section. *Engineering Structures*, 30(5):1319 – 1334, 2008.
- [114] A. Prokić. On triply coupled vibrations of thin-walled beams with arbitrary cross-section. *Journal of Sound and Vibration*, 279(3):723 – 737, 2005.
- [115] F Mohri, L Azrar, and M Potier-Ferry. Vibration analysis of buckled thin-walled beams with open sections. *Journal of Sound Vibration*, 275:434–446, 2004.



- 
- [116] Li Jun, Shen Rongying, Hua Hongxing, and Jin Xianding. Coupled bending and torsional vibration of axially loaded bernoulli–euler beams including warping effects. *Applied Acoustics*, 65(2):153 – 170, 2004.
- [117] J.R. Banerjee, S. Guo, and W.P. Howson. Exact dynamic stiffness matrix of a bending-torsion coupled beam including warping. *Computers & Structures*, 59(4):613 – 621, 1996.
- [118] Erasmo Carrera and Gaetano Giunta. Refined beam theories based on a unified formulation. *International Journal of Applied Mechanics*, 2(01):117–143, 2010.
- [119] E. Carrera. Theories and finite elements for multilayered plates and shells: a unified compact formulation with numerical assessment and benchmarking. *Archives Comput Methods*, 10(3):215–296, 2003.
- [120] Erasmo Carrera and Marco Petrolo. On the effectiveness of higher-order terms in refined beam theories. *Journal of Applied Mechanics*, 78(2):021013, 2011.
- [121] E. Carrera, G. Giunta, P. Nali, and M. Petrolo. Refined Beam Elements With Arbitrary Cross-Section Geometries. *Comput. Struct.*, 88(5–6):283–293, 2010.
- [122] Marco Petrolo, Erasmo Carrera, and Ali Saeghier Ali Saeed Alawami. Free vibration analysis of damaged beams via refined models. *Advances in aircraft and spacecraft science*, 3(1):095, 2016.
- [123] Hamed Akhavan and Pedro Ribeiro. Natural modes of vibration of variable stiffness composite laminates with curvilinear fibers. *Composite Structures*, (93):3040–3047, 2011.

# Appendix A

## Validation of Variable Angle Tow Composites

In this section the work is used to compare the present VAT model with literature results. The reference uses a finite element based on the Third-order Deformation Theory (TSDT). The studied case concerns a plate characterized by the following dimensions:  $a = b = 1$  m. Two thicknesses are considered: 0.01 and 0.1 as thin and thick thickness, respectively. The orthotropic material has the following properties:  $E1 = 173$  GPa,  $E2 = 7.2$  GPa,  $G12 = 3.76$  GPa,  $G13 = 3.76$  GPa,  $G23 = 3.76$  GPa,  $\nu=0.29$  and  $\rho=1540$  kg/m<sup>3</sup>. In this case, the fiber follows the path introduced in Chapter 4. The plate is a three layer laminate, and the lamination of each layer will be expressed as  $\langle T0|T1 \rangle$ . The model is described using the LE formulation which allows a layer-wise approach to be employed. 10 B3 elements are used over  $y$ -axis, and thirty 9-node Lagrange elements are used to describe the cross-section of the plate (10L9 elements for each layer). Two lamination are implemented and studied. The first one, called lamination a, is represented by the following  $T0$  and  $T1$ :  $\langle 0^\circ, 45^\circ \rangle$ ,  $\langle -45^\circ, -60^\circ \rangle$ ,  $\langle 0^\circ, 45^\circ \rangle$ . Lamination  $b$  is the second case and defined in a symmetric lay-ups  $\langle 90^\circ, 45^\circ \rangle$ ,  $\langle 60^\circ, 30^\circ \rangle$ ,  $\langle 90^\circ, 45^\circ \rangle$ .

and it follows the linear formulation of VAT which is mentioned in Chapter 4. The VAT plate is analyzed considering the four edges clamped. The reference presents the results using as units of measure  $rad/s$ . This work gives the frequencies expressed in  $Hz$ . For this reason, the reference results are divided by  $2\pi$ .

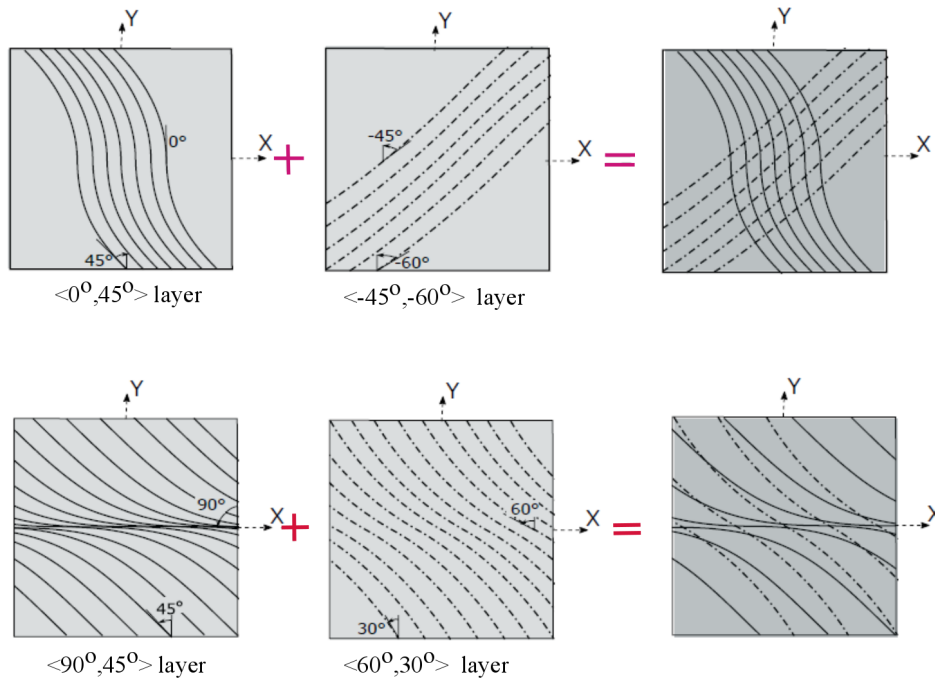


Fig. A.1 Lamination of first ply (Lamina a) and second lamination (Lamina b)

For validation of the results obtained through CUF approach, first nine frequencies are compared with those from reference as it reported in Table A.1. Two different thickness (thin and thick) are considered for two different lamination design. In current example, Lagrange model is used.

Two types of square plate: thin (0.01 m) and thick plate (0.1 m) are investigated in two different three layers of Variable angle tow composite material. The results show that the Z is not effective on the thin plates frequencies, therefore based on the DOF, the lowest number could be more suitable to investigation of this type of laminate, while in y and x axis is a obey to the Quadratic equation based on the Fig. A.12 and A.13. in the other hand in thick plate the behavior of the mode shapes are dependent to the y, x and z in a complex function of the surface.

h/a		Mode 1	Mode 2	Mode 3	Mode 4	Mode 5	Mode 6	Mode 7	Mode 8	Mode 9
[< 0,45 >, < -45, -60 >, < 0,45 >]										
0.01	Ref. [123]	92,26	130,82	195,19	237,86	274,99	282,67	340,09	389,10	431,02
	Ref. [2]	94,44	135,36	206,4	247,05	287,67	307,89	361,64	433,83	476,36
	VAT LE Model	94,44	135,36	206,4	247,05	287,67	307,89	361,64	433,83	476,36
0.1	Ref. [123]	614,11	909,55	1233,02	1338,63	1485,64	1798,60	1932,28	1965,59	2152,26
	Ref. [2]	609,79	903,63	1216,04	1328,41	1469,33	1774,84	1931,36	1930,15	2113,88
	VAT LE Model	609,79	903,63	1216,04	1328,41	1469,33	1774,84	1931,36	1930,15	2113,88
[< 90,45 >, < 60,30 >, < 90,45 >]										
0.01	Ref. [123]	113,18	145,25	212,66	269,06	292,47	316,49	362,78	392,79	465,04
	Ref. [2]	114,32	148,92	223,15	279,6	303,8	332,45	381,32	425,44	507,54
	VAT LE Model	114,32	148,92	223,15	279,6	303,8	332,45	381,32	425,44	507,54
0.1	Ref. [123]	682,20	917,49	1304,68	1313,59	1466,64	1714,97	1920,80	1991,02	2001,10
	Ref. [2]	672,68	909,02	1270,07	1301,02	1441,95	1690,38	1904,58	1943,18	1943,44
	VAT LE Model	672,68	909,02	1270,07	1301,02	1441,95	1690,38	1904,58	1943,18	1943,44

Table A.1 VAT plates under clamped boundary condition-free vibration analysis.

h/a	y,x	z	DOF	Mode 1	Mode 2	Mode 3	Mode 4	Mode 5	Mode 6	Mode 7	Mode 8	Mode 9	
[< 0,45 >, < -45, -60 >, < 0,45 >]													
0.01				92,26	130,82	195,19	237,86	274,99	282,67	340,09	389,10	431,02	
				94,44	135,36	206,4	247,05	287,67	307,89	361,64	433,83	476,36	
		10	3	9261	94,44	135,36	206,4	247,05	287,67	307,89	361,64	433,83	476,36
		10	6	17199	94,44	135,36	206,4	247,05	287,67	307,89	361,64	433,83	476,36
		10	9	25137	94,44	135,35	206,37	247,04	287,64	307,81	361,59	433,69	476,26
0.1				614,11	909,55	1233,02	1338,63	1485,64	1798,60	1932,28	1965,59	2152,26	
				609,79	903,63	1216,04	1328,41	1469,33	1774,84	1931,36	1930,15	2113,88	
		10	3	9261	609,79	903,63	1216,04	1328,41	1469,33	1774,84	1931,36	1930,15	2113,88
		10	6	17199	608,59	900,61	1213,25	1322,16	1465,07	1764,99	1925,79	1923,28	2106,45
		10	9	25137	608,50	900,39	1213,03	1321,71	1464,75	1764,25	1922,78	1925,32	2105,83
[< 90,45 >, < 60,30 >, < 90,45 >]													
0.01				113,18	145,25	212,66	269,06	292,47	316,49	362,78	392,79	465,04	
				114,32	148,92	223,15	279,6	303,8	332,45	381,32	425,44	507,54	
		10	3	9261	114,32	148,92	223,15	279,6	303,8	332,45	381,32	425,44	507,54
		10	6	17199	114,32	148,92	223,15	279,6	303,8	332,45	381,32	425,44	507,54
		10	9	25137	114,31	148,91	223,13	279,59	303,78	332,41	381,28	425,39	507,48
0.1				682,20	917,49	1304,68	1313,59	1466,64	1714,97	1920,80	1991,02	2001,10	
				672,68	909,02	1270,07	1301,02	1441,95	1690,38	1904,58	1943,18	1943,44	
		10	3	9261	672,68	909,02	1270,07	1301,02	1441,95	1690,38	1904,58	1943,18	1943,44
		10	6	17199	671,70	907,62	1267,13	1298,94	1438,64	1687,22	1900,40	1938,03	1950,84
		10	9	25137	671,61	907,50	1266,83	1298,67	1438,35	1686,93	1900,06	1937,48	1950,79

Table A.2 Convergence analysis for linear natural frequencies [Hz] for clamped VSCL plates.

h/a		Mode 1	Mode 2	Mode 3	Mode 4	Mode 5	Mode 6	Mode 7	Mode 8	Mode 9
[< 0,45 >, < -45, -60 >, < 0,45 >]										
0.01	Ref. [123]	92,26	130,82	195,19	237,86	274,99	282,67	340,09	389,10	431,02
	Ref. [2]	94,44	135,36	206,4	247,05	287,67	307,89	361,64	433,83	476,36
	VAT LE Model	94,44	135,36	206,4	247,05	287,67	307,89	361,64	433,83	476,36
0.1	Ref. [123]	614,11	909,55	1233,02	1338,63	1485,64	1798,60	1932,28	1965,59	2152,26
	Ref. [2]	609,79	903,63	1216,04	1328,41	1469,33	1774,84	1931,36	1930,15	2113,88
	VAT LE Model	609,79	903,63	1216,04	1328,41	1469,33	1774,84	1931,36	1930,15	2113,88
[< 90,45 >, < 60,30 >, < 90,45 >]										
0.01	Ref. [123]	113,18	145,25	212,66	269,06	292,47	316,49	362,78	392,79	465,04
	Ref. [2]	114,32	148,92	223,15	279,6	303,8	332,45	381,32	425,44	507,54
	VAT LE Model	114,32	148,92	223,15	279,6	303,8	332,45	381,32	425,44	507,54
0.1	Ref. [123]	682,20	917,49	1304,68	1313,59	1466,64	1714,97	1920,80	1991,02	2001,10
	Ref. [2]	672,68	909,02	1270,07	1301,02	1441,95	1690,38	1904,58	1943,18	1943,44
	VAT LE Model	672,68	909,02	1270,07	1301,02	1441,95	1690,38	1904,58	1943,18	1943,44

Table A.3 Linear natural frequencies [Hz] for clamped VSCL plates.

h/a		y,x	z	DOF	Mode 1	Mode 2	Mode 3	Mode 4	Mode 5	Mode 6	Mode 7	Mode 8	Mode 9
[< 0,45 >, < -45, -60 >, < 0,45 >]													
0.01	Ref. [123]				92,26	130,82	195,19	237,86	274,99	282,67	340,09	389,10	431,02
	Ref. [2]				94,44	135,36	206,4	247,05	287,67	307,89	361,64	433,83	476,36
	VAT LE Model	10	3	9261	94,44	135,36	206,4	247,05	287,67	307,89	361,64	433,83	476,36
	Refined VAT LE Model	10	6	17199	94,44	135,36	206,4	247,05	287,67	307,89	361,64	433,83	476,36
Refined VAT LE Model	10	9	25137	94,44	135,35	206,37	247,04	287,64	307,81	361,59	433,69	476,26	
0.1	Ref. [123]				614,11	909,55	1233,02	1338,63	1485,64	1798,60	1932,28	1965,59	2152,26
	Ref. [2]				609,79	903,63	1216,04	1328,41	1469,33	1774,84	1931,36	1930,15	2113,88
	VAT LE Model	10	3	9261	609,79	903,63	1216,04	1328,41	1469,33	1774,84	1931,36	1930,15	2113,88
	Refined VAT LE Model	10	6	17199	608,59	900,61	1213,25	1322,16	1465,07	1764,99	1925,79	1923,28	2106,45
Refined VAT LE Model	10	9	25137	608,50	900,39	1213,03	1321,71	1464,75	1764,25	1922,78	1925,32	2105,83	
[< 90,45 >, < 60,30 >, < 90,45 >]													
0.01	Ref. [123]				113,18	145,25	212,66	269,06	292,47	316,49	362,78	392,79	465,04
	Ref. [2]				114,32	148,92	223,15	279,6	303,8	332,45	381,32	425,44	507,54
	VAT LE Model	10	3	9261	114,32	148,92	223,15	279,6	303,8	332,45	381,32	425,44	507,54
	Refined VAT LE Model	10	6	17199	114,32	148,92	223,15	279,6	303,8	332,45	381,32	425,44	507,54
Refined VAT LE Model	10	9	25137	114,31	148,91	223,13	279,59	303,78	332,41	381,28	425,39	507,48	
0.1	Ref. [123]				682,20	917,49	1304,68	1313,59	1466,64	1714,97	1920,80	1991,02	2001,10
	Ref. [2]				672,68	909,02	1270,07	1301,02	1441,95	1690,38	1904,58	1943,18	1943,44
	VAT LE Model	10	3	9261	672,68	909,02	1270,07	1301,02	1441,95	1690,38	1904,58	1943,18	1943,44
	Refined VAT LE Model	10	6	17199	671,70	907,62	1267,13	1298,94	1438,64	1687,22	1900,40	1938,03	1950,84
Refined VAT LE Model	10	9	25137	671,61	907,50	1266,83	1298,67	1438,35	1686,93	1900,06	1937,48	1950,79	

Table A.4 Convergence analysis in VAT plates under clamped boundary condition-free vibration analysis.

h/a	y,x	z	DOF	Mode 1	Mode 2	Mode 3	Mode 4	Mode 5	Mode 6	Mode 7	Mode 8	Mode 9				
[< 0,45 >, < -45, -60 >, < 0,45 >]																
0.01				Ref. [123]	92.26	130.82	195.19	237.86	274.99	282.67	340.09	389.10	431.02			
				Ref. [2]	94.44	135.36	206.4	247.05	287.67	307.89	361.64	433.83	476.36			
				Refined VAT LE Model	15	3	20181	92.90	132.28	198.95	240.46	278.75	291.10	346.62	404.04	444.98
				Refined VAT LE Model	15	6	37479	92.90	132.26	198.92	240.45	278.72	291.01	346.55	403.87	444.86
0.1				Ref. [123]	614.11	909.55	1233.02	1338.63	1485.64	1798.60	1932.28	1965.59	2152.26			
				Ref. [2]	609.79	903.63	1216.04	1328.41	1469.33	1774.84	1931.36	1930.15	2113.88			
				Refined VAT LE Model	15	3	20181	608.75	901.35	1213.15	1322.76	1465.30	1767.14	1916.30	1925.01	2107.32
				Refined VAT LE Model	15	6	37479	607.50	898.25	1210.24	1316.39	1460.89	1757.04	1909.29	1919.29	2099.65
0.01				Ref. [123]	113.18	145.25	212.66	269.06	292.47	316.49	362.78	392.79	465.04			
				Ref. [2]	114.32	148.92	223.15	279.6	303.8	332.45	381.32	425.44	507.54			
				Refined VAT LE Model	15	3	20181	113.39	146.22	215.56	272.00	295.30	319.78	364.25	400.21	474.79
				Refined VAT LE Model	15	6	37479	113.39	146.21	215.54	271.98	295.28	319.75	364.22	400.17	474.74
0.1				Ref. [123]	682.20	917.49	1304.68	1313.59	1466.64	1714.97	1920.80	1991.02	2001.10			
				Ref. [2]	672.68	909.02	1270.07	1301.02	1441.95	1690.38	1904.58	1943.18	1943.44			
				Refined VAT LE Model	15	3	20181	672.30	907.44	1268.94	1296.92	1438.76	1684.82	1892.06	1938.62	1950.20
				Refined VAT LE Model	15	6	37479	671.28	905.97	1265.85	1294.71	1435.29	1681.47	1887.63	1933.24	1950.12
0.1				Ref. [123]	682.20	917.49	1304.68	1313.59	1466.64	1714.97	1920.80	1991.02	2001.10			
				Ref. [2]	672.68	909.02	1270.07	1301.02	1441.95	1690.38	1904.58	1943.18	1943.44			
				Refined VAT LE Model	15	3	20181	672.30	907.44	1268.94	1296.92	1438.76	1684.82	1892.06	1938.62	1950.20
				Refined VAT LE Model	15	6	37479	671.28	905.97	1265.85	1294.71	1435.29	1681.47	1887.63	1933.24	1950.12

Table A.5 Convergence analysis in VAT plates under clamped boundary condition-free vibration analysis..

h/a	y,x	z	DOF	Mode 1	Mode 2	Mode 3	Mode 4	Mode 5	Mode 6	Mode 7	Mode 8	Mode 9				
[< 0,45 >, < -45, -60 >, < 0,45 >]																
0.01				Ref. [123]	92,26	130,82	195,19	237,86	274,99	282,67	340,09	389,10	431,02			
				Ref. [2]	94,44	135,36	206,4	247,05	287,67	307,89	361,64	433,83	476,36			
				Refined VAT LE Model	20	3	35301	92.50	131.14	196.81	238.79	276.38	286.32	342.52	395.43	436.45
				Refined VAT LE Model	20	6	65559	92.49	131.40	196.78	238.77	276.35	286.24	342.46	395.28	436.34
0.1				Ref. [123]	614,11	909,55	1233,02	1338,63	1485,64	1798,60	1932,28	1965,59	2152,26			
				Ref. [2]	609,79	903,63	1216,04	1328,41	1469,33	1774,84	1931,36	1930,15	2113,88			
				Refined VAT LE Model	20	3	35301	608.41	900.75	1212.39	1321.46	1464.25	1765.34	1923.29	1913.33	2105.55
				Refined VAT LE Model	20	6	65559	607.14	897.61	1209.42	1315.02	1459.78	1755.15	1906.24	1917.40	2097.78
0.01				Ref. [123]	113,18	145,25	212,66	269,06	292,47	316,49	362,78	392,79	465,04			
				Ref. [2]	114,32	148,92	223,15	279,6	303,8	332,45	381,32	425,44	507,54			
				Refined VAT LE Model	20	3	35301	113.15	145.52	213.52	269.84	293.06	316.63	359.48	393.97	466.28
				Refined VAT LE Model	20	6	65559	113.15	145.51	213.50	269.82	293.04	316.60	359.44	393.93	466.23
0.1				Ref. [123]	682,20	917,49	1304,68	1313,59	1466,64	1714,97	1920,80	1991,02	2001,10			
				Ref. [2]	672,68	909,02	1270,07	1301,02	1441,95	1690,38	1904,58	1943,18	1943,44			
				Refined VAT LE Model	20	3	35301	672.18	907.12	1268.61	1296.11	1438.04	1683.68	1889.58	1950.31	1937.60
				Refined VAT LE Model	20	6	65559	671.14	905.61	1265.48	1293.84	1434.51	1680.26	1885.06	1932.13	1950.23
0.1				Ref. [123]	682,20	917,49	1304,68	1313,59	1466,64	1714,97	1920,80	1991,02	2001,10			
				Ref. [2]	672,68	909,02	1270,07	1301,02	1441,95	1690,38	1904,58	1943,18	1943,44			
				Refined VAT LE Model	20	3	35301	672.18	907.12	1268.61	1296.11	1438.04	1683.68	1889.58	1950.31	1937.60
				Refined VAT LE Model	20	6	65559	671.14	905.61	1265.48	1293.84	1434.51	1680.26	1885.06	1932.13	1950.23

Table A.6 Convergence analysis in VAT plates under clamped boundary condition-free vibration analysis..

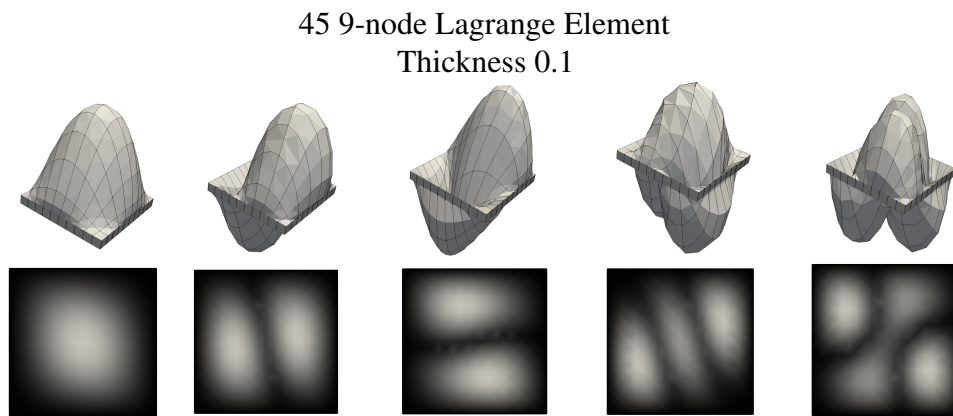


Fig. A.2 Frequency modes for laminate a with three layers under CCCC-thick plate.

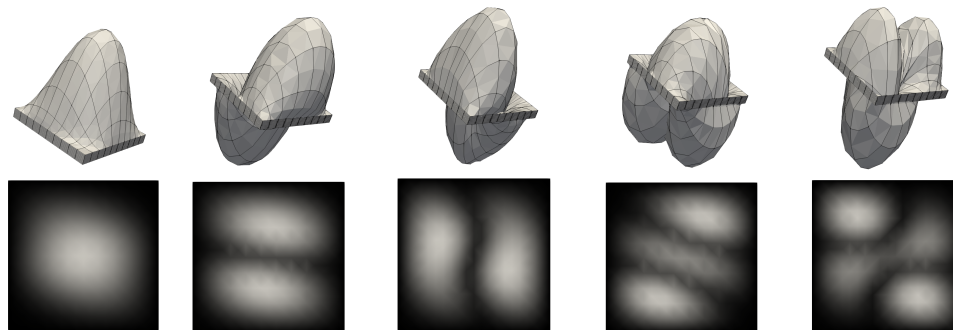


Fig. A.3 Frequency modes for laminate b with three layers under CCCC-thick plate.

20 9, 9 0.01 9-node Lagrange Element  
Thickness 0.01

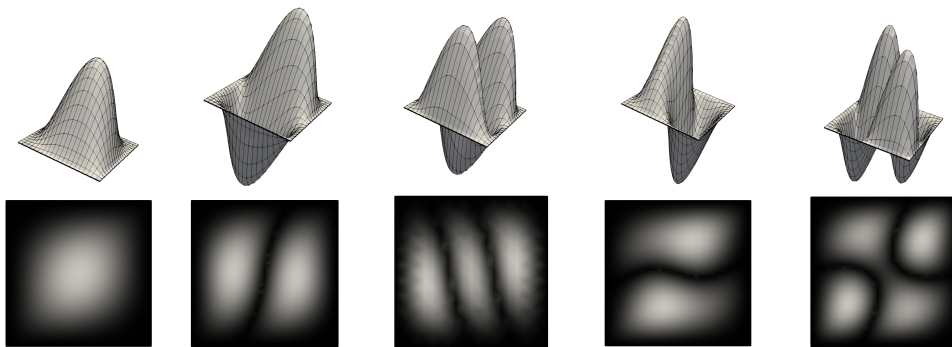


Fig. A.4 Frequency modes for laminate b with three layers under CCCC-thin plate.

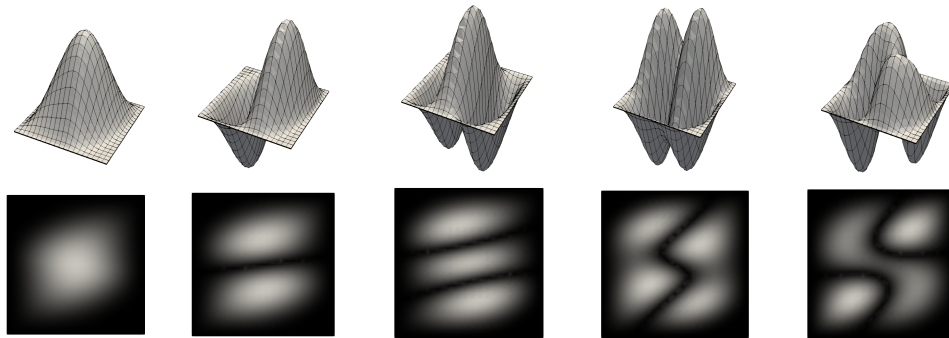


Fig. A.5 Frequency modes for laminate b with three layers under CCCC-thin plate.



h/a		y,x	z	DOF	Mode 1	Mode 2	Mode 3	Mode 4	Mode 5	Mode 6	Mode 7	Mode 8	Mode 9
[< 0,45 >, < -45, -60 >, < 0,45 >]													
0.01					92,26	130,82	195,19	237,86	274,99	282,67	340,09	389,10	431,02
					94,44	135,36	206,4	247,05	287,67	307,89	361,64	433,83	476,36
	Refined VAT LE Model	30	3	78141	92.29	130.93	195.58	237.95	275.16	283.58	340.36	390.48	431.87
	Refined VAT LE Model	30	6	145119	92.29	130.92	195.55	237.94	275.14	283.52	340.31	390.34	431.77
					92.29	130.92	195.55	237.94	275.13	283.51	340.30	390.33	431.77
0.1					614,11	909,55	1233,02	1338,63	1485,64	1798,60	1932,28	1965,59	2152,26
					609,79	903,63	1216,04	1328,41	1469,33	1774,84	1931,36	1930,15	2113,88
	Refined VAT LE Model	30	3	78141	608.22	900.40	1211.96	1320.76	1463.70	1764.40	1911.93	1922.49	2104.70
	Refined VAT LE Model	30	6	145119	606.93	897.22	1208.93	1314.25	1459.15	1754.11	1904.73	1916.50	2096.83
					606.82	897.01	1208.65	1313.80	1458.78	1753.35	1904.20	1915.92	2096.13
[< 90,45 >, < 60,30 >, < 90,45 >]													
0.01					113,18	145,25	212,66	269,06	292,47	316,49	362,78	392,79	465,04
					114,32	148,92	223,15	279,6	303,8	332,45	381,32	425,44	507,54
	Refined VAT LE Model	30	3	78141	113.04	145.14	212.41	268.71	291.91	314.98	356.95	390.76	462.13
	Refined VAT LE Model	30	6	145119	113.04	145.14	212.40	268.70	291.90	314.96	356.92	390.73	461.94
					113.04	145.14	212.39	268.70	291.90	314.96	356.92	390.73	461.93
0.1					682,20	917,49	1304,68	1313,59	1466,64	1714,97	1920,80	1991,02	2001,10
					672,68	909,02	1270,07	1301,02	1441,95	1690,38	1904,58	1943,18	1943,44
	Refined VAT LE Model	30	3	78141	672.12	906.93	1268.47	1295.70	1437.68	1683.13	1888.48	1937.15	1950.24
	Refined VAT LE Model	30	6	145119	671.07	905.40	1265.30	1293.38	1434.10	1679.64	1883.87	1931.61	1950.15
					670.95	905.24	1264.90	1293.12	1433.72	1679.24	1883.42	1930.90	1950.13

Table A.7 Convergence analysis in VAT plates under clamped boundary condition-free vibration analysis..

h/a	Goodness of fit	Mode 1	Mode 2	Mode 3	Mode 4	Mode 5	Mode 6	Mode 7	Mode 8	Mode 9
[< 0,45 >, < -45, -60 >, < 0,45 >]										
0.01	SSE	3.4331e-27	2.5042e-26	1.6964e-26	2.2618e-26	3.8774e-26	2.5849e-26	4.8468e-26	8.0779e-26	9.0473e-26
0.1	SSE	1.1632e-25	4.5236e-25	7.7548e-25	7.2378e-25	9.3058e-25	1.2925e-24	3.9808e-24	1.4476e-24	2.0680e-24
[< 90,45 >, < 60,30 >, < 90,45 >]										
0.01	SSE	7.8760e-27	1.2117e-26	1.8579e-26	3.5543e-26	3.2312e-26	5.4930e-26	3.2312e-26	6.4623e-26	1.6479e-25
0.1	SSE	2.7142e-25	4.6529e-25	1.1891e-24	1.0857e-24	1.0857e-24	1.8612e-24	1.6027e-24	1.1374e-24	1.7061e-24

Table A.8 Goodness of fit from Curve Fitting solution by interpolant with the method of thin-plate spline.

30 6, 9 9-node Lagrange Element  
Thickness 0.1

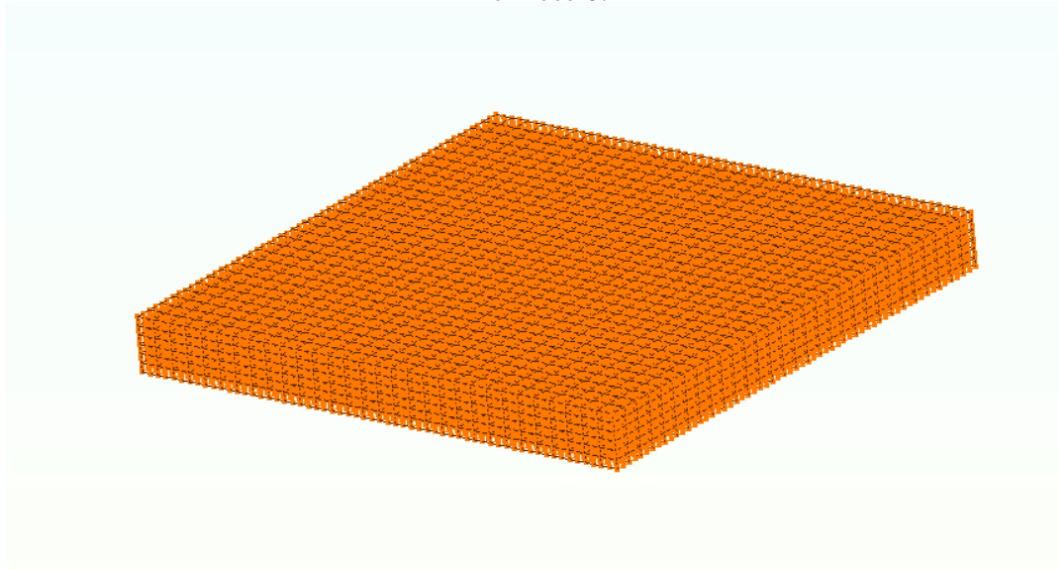


Fig. A.6 Meshed thick plate with 180 elements in cross-section.

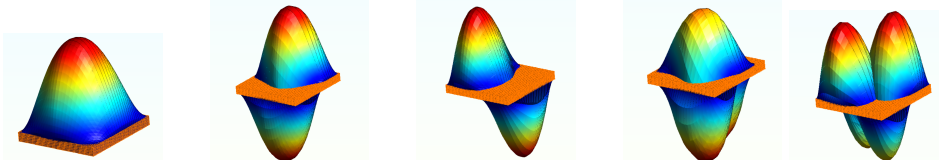


Fig. A.7 First 5 modal shapes of the CCCC 3-layer thick plate (Laminate a).

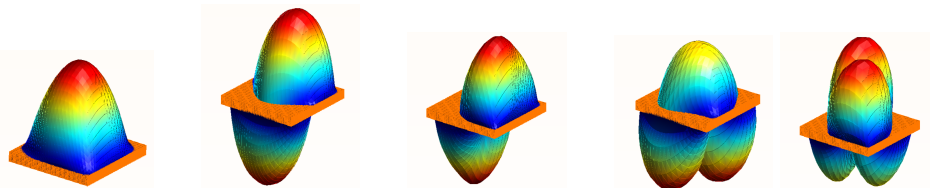


Fig. A.8 First 5 modal shapes of the CCCC 3-layer thick plate (Laminate b).

30 6, 9 9-node Lagrange Element  
Thickness 0.01

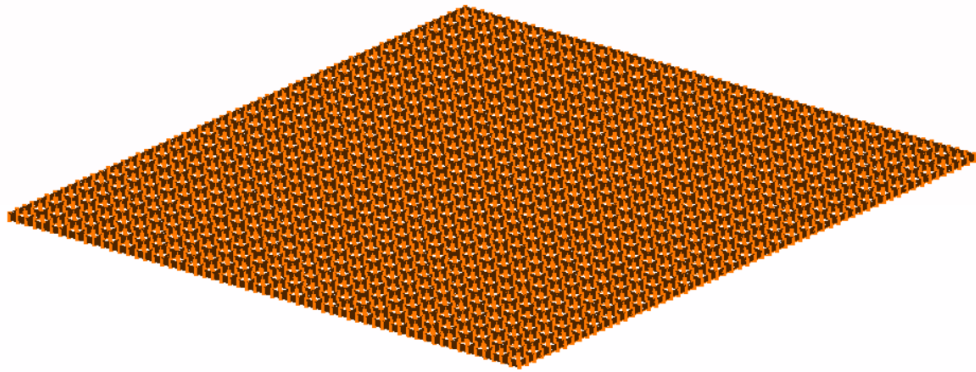


Fig. A.9 Meshed thick plate with 180 elements in cross-section.

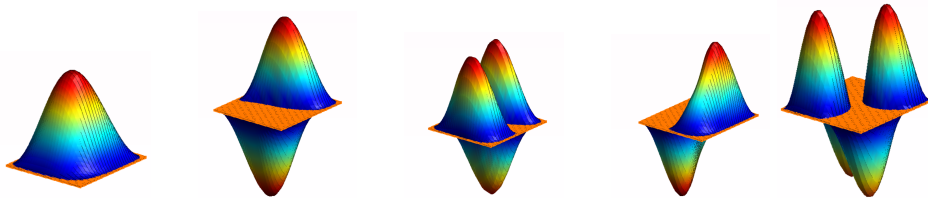


Fig. A.10 First 5 modal shapes of the CCCC 3-layer thick plate (Laminate a).

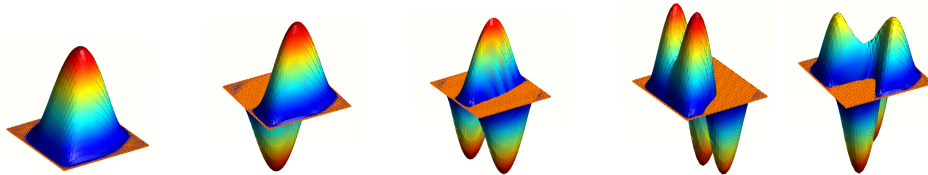


Fig. A.11 First 5 modal shapes of the CCCC 3-layer thick plate (Laminate b).

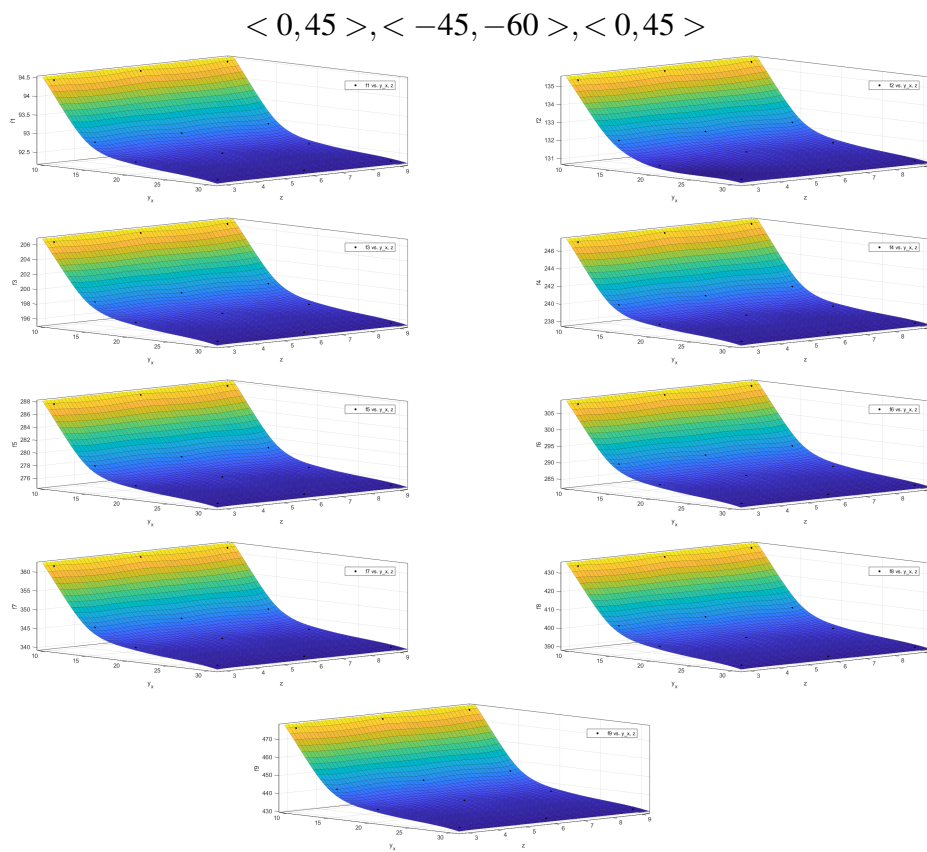


Fig. A.12 First 9 frequency modes in different number of beam elements (y and x) and nodes per thickness (z) in thin plate

$\langle 90, 45 \rangle, \langle 60, 30 \rangle, \langle 90, 45 \rangle$

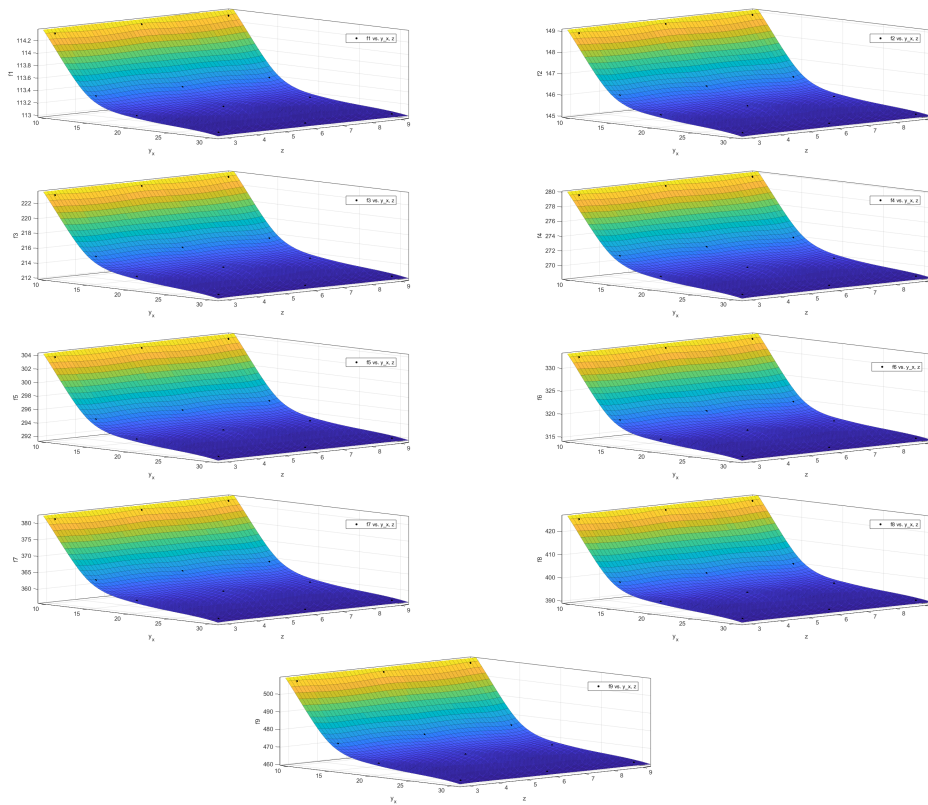


Fig. A.13 First 9 frequency modes in different number of beam elements (y and x) and nodes per thickness (z) in thin plate

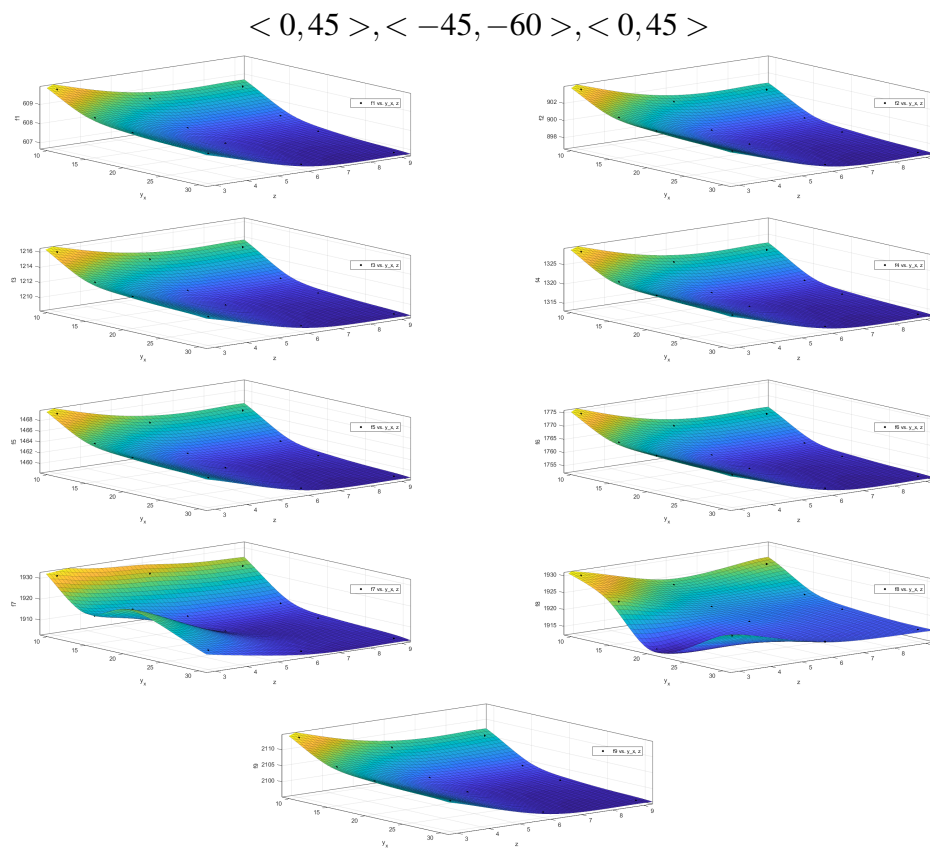


Fig. A.14 First 9 frequency modes in different number of beam elements (y and x) and nodes per thickness (z) in thick plate

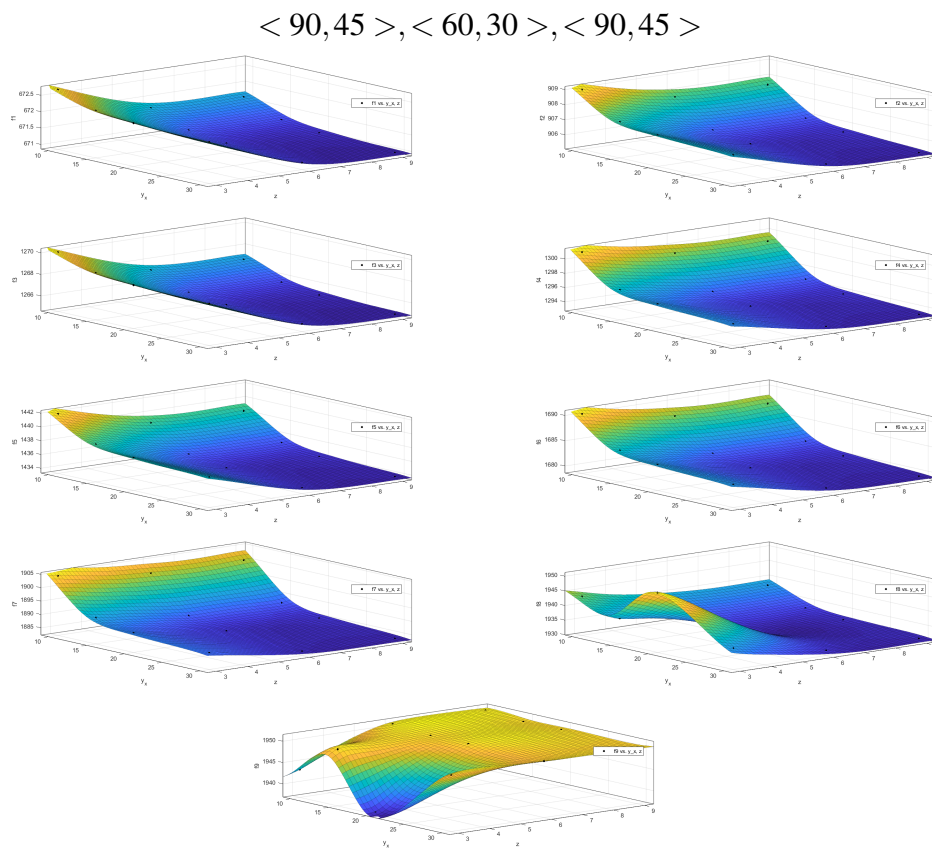


Fig. A.15 First 9 frequency modes in different number of beam elements (y and x) and nodes per thickness (z) in thick plate